Freie Universität Berlin

Institut für Geologische Wissenschaften

Evaluation of main controlling factors for the recent regional thermal field in Brandenburg (North German Basin)

Evaluierung von dominanten Kontrollfaktoren für das heutige regionale Temperaturfeld von Brandenburg (Norddeutsches Becken)

Kumulative Dissertation
zur Erlangung des Doktorgrades der Naturwissenschaften
“doctor rerum naturalium“
(Dr. rer. nat.)
in der Wissenschaftsdisziplin “Geologie“

eingereicht am
Fachbereich Geowissenschaften
der Freien Universität Berlin

von

Vera Noack

Berlin, Februar 2014

Erstgutachter: Prof. Dr. Michael Schneider
Freie Universität Berlin

Zweitgutachterin: Prof. Dr. Magdalena Scheck-Wenderoth
RWTH Aachen

Tag der Disputation: 20.06.2014

Preface

The present thesis received operational and financial support from the Helmholtz Centre Potsdam GFZ German Research Centre for Geosciences as the primary financier. As part of the GeoEn project it has been also funded by the German Federal Ministry of Education and Research in the program ‘‘Spitzenforschung in den neuen Ländern’’ (BMBFGrant03G767 A/B/C). The research activity was conducted in Section 4.4 Basin Analysis of the GFZ in collaboration with Freie Universität Berlin and Universität Potsdam.

The research activities contain contributions by other scientists, technicians and institutions:

- The primary database used for the compilation of datasets for the construction of the 3D structural model are provided by the geological survey of Landesamt für Bergbau, Geologie und Rohstoffe Brandenburg (LBGR)
- Data from previous models by Scheck and Bayer (1999); Scheck-Wenderoth and Lamarche (2005) and Maystrenko et al. (2010) have been integrated to construct a model being consistent in 3D
- Datasets have been complemented by the following data: structural data from published deep wells (Hoth et al., 1993), isolines of the base of Quaternary provided by the Landesamt für Umwelt, Naturschutz und Geologie Mecklenburg-Vorpommern, data of topography (ETOPO1: Amante und Eakins, 2009) and by well data provided by the Geological surveys of Brandenburg (LBGR) and Sachsen-Anhalt (LAGB)
- A large fraction of geophysical properties that have been assigned in the numerical simulations were derived from Norden and Förster (2006), Fuchs and Förster (2010) and Norden et al. (2008)
- Measured temperatures used to validate the model predictions are from Förster (2001) and Norden et al. (2008)

Table of Contents

List of Figures

List of Tables

Declaration of Originality

I hereby certify, as the author of this thesis, and as the main author of the publications involved, that the work presented in this thesis was composed by and originated entirely from me, except as acknowledged in both the text and the related reference list. The work was not submitted previously to any other institution.

Vera Noack

Acknowledgements

This PhD thesis summarizes results of a project that received financial support from the Helmholtz Centre Potsdam GFZ German Research Centre for Geosciences and has been also funded as part of the GeoEn project by the German Federal Ministry of Education and Research in the programme ‘‘Spitzenforschung in den neuen Ländern’’(BMBFGrant03G0671A/B/C). I would like to thank for this financial and operational support. Besides, the geological survey of Landesamt für Bergbau, Geologie und Rohstoffe Brandenburg provided the datasets on which this study is mainly based. In this context a huge thank to Dr. Werner Stackebrandt, Dr. Thomas Höding and Andreas Simon who supported the project with constant interest and fruitful discussions.

I wish to thank many people for their contribution to the studies behind the thesis.

First of all, I would like to thank Prof. Magdalena Scheck-Wenderoth, Prof. Asaf Pekdeger and Prof. Michael Schneider for giving me the chance to realize the thesis. As my supervisors, I would like to express my gratitude to Prof. Magdalena Scheck-Wenderoth and Prof. Michael Schneider. Thanks, Leni, for your continuous support, valuable advice and all your help making the outcome of the related studies better than they started out. A huge thank to Michael Schneider who took over the official supervision on behalf of the Freie Universität Berlin, and supported me with his constant interest and the necessary pressure to finish the thesis.

Without the members of section 4.4 this work would not have been possible. I want to thank Mauro Cacace as the assistant supervisor for his support that helped shape my understanding of physical principles related to this work. I am very grateful for technical, computational and operational support by Lew and Bo and for the pleasant working environment provided by Alex, Anna, Bo, Christina, Judith, Julia, Katja, Leni, Lew, Mauro, Yuriy, and Yvonne.

A special thank to Alex for the saving help on those days where non-scientific things apparently went continuously wrong.

Dear Yvonne, I will always remember our scientific discussions and small talks about our life after the thesis. I am glad for the nice time we spent together.

Without the patience and love of my family this thesis might still be unfinished. I thank Cassius, Nele and Helena for keeping me away from nightmares on bad days due to the warm home-coming feeling they always have given me.

Last but not least, I wish to thank my mother and Günter for their constant interest on the progress of the work and the support with scientific literature.

Summary

Sedimentary basins like the North German Basin host large amounts of energy and fresh-water resources, and have the potential to contribute to a climate friendly and sustainable energy supply. As a part of the North German Basin, the area of Brandenburg is of growing interest for geothermal utilization in Germany since the salt structures generated in the basin are known to be responsible for the existence of positive anomalies within the thermal field. Due to its special physical properties – i.e. lower density, high thermal conductivity – salt plays a prominent role within the geological units of the basin fill. The present-day configuration of the Zechstein salt is characterized by strong variations in thickness locally shaping salt pillows and mighty salt diapirs which also affect the geometry of the overburden. At the same time, the Permian Zechstein salt hydraulically decouples the overburden from deeper parts of the lithosphere as it is impermeable to fluid flow. In spite of these facts, the subsurface of the area of Brandenburg is not adequately known to identify potential areas for geothermal energy usage. Although the subsurface of the area has been explored by numerous wells and a few 2D maps of depth and thickness as well as temperature interpretations resulting from classical 2D interpolation for different layers, such information does not cover the subsurface consistently and does not account for the 3D nature of heat transport processes. Knowledge about the occurrence of different heat transport processes and about how they interact with the structural inventory is very important as these processes may influence the thermal state to different degrees. An increasing number of studies have been focused on a better assessment of the geothermal potential of Brandenburg in the recent years. These investigations are based on models that have limitations related to their horizontal size, their vertical resolution concerning the geological units, their applied 2D approach or the considered heat transport process. Despite of this, models of the configuration of important layers, which notably contribute to the heat budget and hence affect the temperature distribution on the basin-scale, are missing so far.

The present study aims to evaluate the 3D steady-state thermal field in Brandenburg. Therefore, a consistent 3D structural model of the basin fill has been developed that resolves the main stratigraphical units in Brandenburg which play an important role for the thermal field. This large-scale model covers an area of about 250 km (E-W) times 210 km (N-S) and has a horizontal resolution of 1 km. It encompasses a part of the basin centre of the North German Basin (NGB) in the north, whereas to the south the present-day south-eastern basin margin of the NGB is enclosed. Special emphasis has been put to evaluate the main controlling factors of the thermal field, as well as to understand the interaction between the deep geological structure and the shallower basin configuration and the related influence on the hydrothermal field with depth.

In the first part of the study the focus has been set on the construction of the 3D structural model based on a dataset of different origins. All individual layers of the basin fill were integrated considering their basin-affecting special characteristics, their depth position and thickness. First, calculations of the 3D thermal field have been carried out assuming heat conduction as the dominant transport mechanism to analyse the interaction between the structural configuration of the Zechstein salt and the overlying sediments as well as the interaction between the crustal parts of the model area and the basin fill. Therefore, the initial model includes a (simplified) homogeneous crust between the top of the crystalline basement and the Moho. The prediction of the thermal field reveals that on the one hand strong lateral and vertical variations in the temperature distribution result from local configurations of the highly conductive salt structures and their low conductive covering layers (local-scale anomalies), but on the other hand, the heat contribution of the highly conductive underlying crust affects also shallower parts of the thermal field (regional-scale anomalies). More precisely, the thermal anomalies are connected to the configuration of both the geological units in the basin and the deeper crust and their differences in dominant thermal properties.

In order to improve the knowledge about the role of the deeper lithosphere in shaping the shallower thermal field, a more appropriate, differentiated lithosphere has been tested in the second part of the study. Therefore, the focus has been set on a sensitivity analysis of 3D thermal models to the choice of different lower boundary conditions. By two alternative models, the influence of both basal heat flow at the Moho and 1300 °C at the lithosphere-asthenosphere boundary on the shallow thermal field are considered. Additionally, a sensitivity analysis to the choice of thermal properties for the geological layers reveals the effect of these parameters on the temperature predictions. The resultant lithospheric-scale model provides insights into the configuration of the deeper lithosphere and shows that shallow parts of the conductive thermal field are strongly controlled by this configuration. In particular, the influence of an intensely heat producing and highly conductive crystalline crust can be observed in the thermal signature above the Zechstein salt. Additionally, it has been shown that a thickened upper crust blanketed by a sufficiently thick overburden obviously slows down the transport of heat towards the surface – higher temperatures are predicted in the shallow thermal field in the basin centre compared with the surroundings, whereas a thinned upper crust produces less heat and thus leads to negative temperature anomalies at the same depth level. A comparison of the models shows clearly that the choice of boundary conditions and the assigned thermal properties have a specific influence on the temperature predictions. These results contribute suitable thermal boundary conditions and physically sound constraints for values of the rock thermal parameters to the following coupled fluid and heat transport investigations which are required since the shallow thermal field characteristics cannot be explained by heat transport through conduction alone.

Hence, the impact of fluid flow on the thermal field was the objective of the third part of the study to investigate how the main heat transport processes in the basin do interact and influence the thermal

field in Brandenburg. Therefore, based on the lithospheric-scale model a structural and hydrological model were built that represent three main aquifer complexes above the Zechstein salt those three being separated by the low permeable Middle Triassic Muschelkalk and the important Tertiary Rupelian-clay aquitard. The results of coupled fluid flow and heat transfer simulations show that the shallow thermal field down to 2000 m depth is strongly influenced by fluid flow driven by forced convective forces due to hydraulic pressure gradients. The depth influence of advective cooling is controlled by the depth of the shallowest aquitard and by communication pathways between the different aquifers. Free convective thermal anomalies induced by buoyancy forces due to density gradients occur only locally where the hydraulic pressure forces are weak and are controlled by the thickness and permeability of the permeable layers.

In summary, the results of the studies show that the structural setting of the geological units in the basin, therein particularly the Zechstein salt, and their differences in dominant physical properties play a prominent role for the basin-wide thermal field. Interaction between the constituting layers creates local thermal anomalies. The resultant local small-wavelength thermal signature may or may not be disturbed by the thermal heat input regulated by the deeper crust. Interaction of different heat transport processes is of great importance primarily for the shallow thermal field. The results of the studies indicate that conductive heat transport is the dominant heat transfer mechanism for the study area, whereas the thermal field in the shallow part of the basin is additionally influenced by forced convective heat transfer and related advective cooling within the permeable layers. Thereby, also the choice of the model boundary conditions influences the predictions for the thermal field strongly. Finally, it has been shown that large-scale models are able to predict the thermal field reasonably well. Besides, the investigations provide new insights on the interaction between geologic configuration, basin hydrodynamics and the thermal field as they could evolve in any other basin affected by salt tectonics.

Zusammenfassung

Sedimentäre Becken wie das Norddeutsche Becken beherbergen nicht nur große Mengen an Energie- und Frischwasserressourcen, sie haben auch ein großes Potential zu klimafreundlicher und nachhaltiger Energiebereitstellung beizutragen. Als ein Teil des Norddeutschen Beckens rückte Brandenburg in den letzten Jahren hinsichtlich geothermaler Nutzung zunehmend in den Focus wissenschaftlicher und industrieller Nutzung, da die Salzstrukturen im Untergrund bekanntermaßen verantwortlich sind für positive Anomalien innerhalb des thermischen Feldes. Aufgrund seiner speziellen physikalischen Eigenschaften – z.B. geringe Dichte, hohe thermische Leitfähigkeit – kommt Salz eine bedeutende Rolle innerhalb der geologischen Einheiten des Beckens zu. Die heutige Konfiguration des Permischen Zechsteinsalzes ist durch große Mächtigkeitsschwankungen geprägt. Lokal ausgebildete Salzstöcke und mächtige Salzdiapire beeinflussen auch die Geometrie des Deckgebirges. Gleichzeitig entkoppelt das Zechsteinsalz das Deckgebirge von tieferen Bereichen der Lithosphäre und ist undurchlässig für Fluide. Trotz dieser bekannten Fakten ist der Untergrund von Brandenburg noch nicht ausreichend bekannt um potentielle Gebiete für die geothermale Nutzung eingrenzen zu können. Obwohl Tiefen- und Mächtigkeitskarten sowie Temperaturkarten, die aus klassischen 2D Interpolationen einzelner Bohrungsdaten resultieren, einige geologische Schichten repräsentieren, ist nicht der gesamte Untergrund Brandenburgs mit seinem strukturellem Inventar konsistent erfasst. Somit kann die dreidimensionale Natur der Wärmetransportprozesse, die sich in der Temperaturverteilung im Becken widerspiegelt, auch nicht berücksichtigt werden. Kenntnisse über das Auftreten konkurrierender Wärmetransportmechanismen und deren Wechselwirkung mit den geologischen Strukturen im Becken sind wichtig, da sie möglicherweise auf unterschiedliche Weise das thermische Feld prägen. Eine zunehmende Anzahl von Studien beschäftigte sich in den vergangenen Jahren mit der genaueren Abschätzung des thermischen Potentials von Brandenburg. Diese Untersuchungen bieten lediglich Basiskenntnissee zur Bewertung der Temperaturverteilung, da die zugrunde liegenden Modelle durch ihre horizontale Größe, die vertikale Modellauflösung hinsichtlich der implementierten geologischen Schichten, des konzeptionellen Ansatzes oder der betrachteten Wärmetransportprozesse die Aussagen zum 3D thermischen Feld einschränken. Insbesondere sind wichtige geologische Schichten, die entscheidend zum Wärmebudget beitragen und somit einen starken Einfluss auf die Temperaturverteilung im Becken haben, nicht in den Modellen aufgelöst.

Die Studie befasst sich mit der Bewertung des rezenten thermischen Feldes in Brandenburg. Ein konsistentes 3D Strukturmodell der Beckenfüllung wurde entwickelt, dass bedeutende geologische Schichten Brandenburgs, die eine wichtige Rolle für die Temperaturverteilung im Beckenbereich spielen, auflöst. Das großskalige Modell umfasst ein Gebiet von 250 km (E-W) x 210 km (N-S) und

hat eine horizontale Modellauflösung von 1 km. Es umfasst einen Bereich des tiefen Norddeutschen Beckens im Norden, während im Süden der invertierte und hochgehobene Beckenrand erfasst ist. Im Rahmen der Untersuchungen kam der Evaluierung der Hauptkontrollfaktoren des Temperaturfeldes besondere Bedeutung zu, um Erkenntnisse über die Wechselwirkung zwischen tiefer geologischer Struktur und flacher Beckenkonfiguration und deren Einfluss auf das hydrothermische Feld in den verschiedenen Tiefen zu gewinnen.

Der erste Teil der Studie befasste sich mit der Erstellung des Strukturmodells auf der Basis unterschiedlicher Datensätze. Die geologischen Schichten des Modells der Beckenfüllung wurden anhand ihrer beckenspezifischen Charakteristika, ihrer Tiefenposition im Becken und ihrer Mächtigkeit interpretiert. Erste Berechnungen des thermischen Feldes unter der Annahme eines rein konduktiven Wärmetransports ermöglichten es, sowohl Aussagen zur Wechselwirkung zwischen der strukturellen Konfiguration des Zechsteinsalzes und der überlagernden Sedimente, als auch zwischen der Kruste und der Beckenfüllung zu treffen. Für diesen Ansatz wurde das Modell bis zur Moho durch eine homogene kristalline Kruste erweitert. Die Berechnungen des thermischen Feldes zeigen einerseits einen engen Zusammenhang zwischen lateralen und vertikalen Zonierungen in der Temperaturverteilung in Abhängigkeit zur lokalen Konfiguration des hochkonduktiven Zechsteinsalzes und den gering konduktiven überlagernden Schichten (lokale Temperaturanomalien). Andererseits modifiziert auch der Wärmeeintrag der unterlagernden hochkonduktiven Kruste das thermische Feld und bewirkt regionale Variationen der Temperaturverteilung. Insbesondere sind die lokalen thermischen Anomalien gebunden an die Geometrien der geologischen Schichten im Becken und deren unterschiedliche physikalische Eigenschaften.

Um den Einfluss der tieferen Lithosphäre auf die Temperaturverteilung im flachen thermischen Feld bewerten zu können, wurde im zweiten Teil der Studie eine realistischere, differenzierte Lithosphäre im Krustenbereich für das Strukturmodell entwickelt und mittels Sensitivitätsanalysen durch die Wahl unterschiedlicher unterer Modellrandbedingungen deren Einfluss auf die Temperaturverteilung getestet. Mit zwei alternativen Modellen wurden Berechnungen zur Temperaturverteilung im Becken durchgeführt, wobei einerseits ein basaler Wärmeflusses an der Moho und andererseits 1300 °C an der Lithophären-Asthenosphären-Grenze als untere Randbedingung vorgeschrieben wurden. Zusätzliche Sensitivitätsanalysen zur Wahl der thermischen Eigenschaften der geologischen Schichten zeigen darüber hinaus den Einfluss dieser Parameter auf die Temperaturverteilung.
Das entwickelte lithosphärenskalige Modell bildet die Konfiguration der tieferen Lithosphäre ab und zeigt wie diese Geometrien das flache konduktive Temperaturfeld kontrollieren. Insbesondere der Einfluss der wärmeproduzierenden und hoch konduktiven kristallinen Kruste ist im Temperaturbild des flachen thermischen Feldes zu erkennen. Dabei hat sich gezeigt, dass ein ausreichend mächtiges Deckgebirge über einer verdickten Oberkruste den Wärmeabtransport zur Oberfläche so verlangsamt, das im Vergleich zur Umgebung höhere Temperaturen für das flache Temperaturfeld berechnet

werden, während eine verdünnte Oberkruste weniger Wärme produziert und so negative Temperaturanomalien im gleichen Tiefenbereich hervorruft. Ein Vergleich der Modelle zeigt, dass die Wahl der Modellrandbedingungen und die zugewiesenen thermischen Eigenschaften einen spezifischen Einfluss auf die Temperaturvorhersagen haben. Insgesamt liefern diese Modellierungsergebnisse mit den geprüften Modellrandbedingungen und physikalisch validierten Werten der thermischen Eigenschaften eine Basis für die anschließend durchgeführten Berechnungen des gekoppelten Fluid -und Wärmetransports, die erforderlich sind, weil das beobachtete Temperaturfeld Hinweise auf den Einfluss von Fluidbewegung liefert.

Der dritte Teil der Studie befasste sich deshalb mit der Frage, wie die Hauptwärmetransportprozesse im flachen Becken interagieren und das thermische Feld beeinflussen. Basierend auf dem bereits entwickelten lithosphärenskaligen Strukturmodell wurde ein hydrogeologisches Modell aufgesetzt, das die drei Hauptaquiferekomplexe oberhalb des Zechsteinsalzes repräsentiert. Diese Aquiferkomplexe werden durch den gering durchlässigen Mitteltriassischen Muschelkalk und den Tertiären Rupelton, der eine wichtige Barriere zwischen dem oberen Trinkwasserleiter und den unteren Salzwasserhorizonten darstellt, getrennt. Die Ergebnisse zeigen, dass das flache Temperaturfeld bis in 2000 m Tiefe stark durch Fluidfluss beeinflusst wird, ausgelöst durch erzwungene thermische Konvektion infolge von hydraulischen Druckgradienten. Die Reichweite dieser advektiven Abkühlung wird dabei durch die Tiefe des flachsten Aquitards und durch kommunizierende Fluidpfade zwischen den verschiedenen Aquiferen kontrolliert. Auf freie Konvektion zurückzuführende thermische Anomalien, die durch Auftriebskräfte infolge von Dichtegradienten induziert werden, sind nur lokal auszumachen. Sie treten in Bereichen auf, in denen die topographieinduzierten Druckkräfte schwächer sind als die dichteinduzierten Auftriebskräfte. Diese Bereiche finden sich dort, wo große Mächtigkeiten der permeablen Aquifere vorliegen.

Die Ergebnisse der Studien zeigen, dass die strukturelle Ausbildung der geologischen Schichten im Becken im Zusammenhang mit ihren unterschiedlichen physikalischen Eigenschaften eine große Rolle für das thermische Feld spielt. Das Interagieren zwischen den beteiligten Schichten beeinflusst die Temperaturverteilung entscheidend. Im flachen Temperaturfeld ist darüber hinaus auch das Zusammenspiel zwischen den verschiedenen Wärmetransportprozessen von großer Bedeutung. Die Ergebnisse der thermischen Modellierungen zeigen außerdem, dass konduktiver Wärmetransport der dominante Wärmetransportmechanismus für das Untersuchungsgebiet ist, während das flache Temperaturfeld durch druckgetriebene Konvektion und induzierte advektive Abkühlung innerhalb der permeablen Schichten zusätzlich beeinflusst wird. Dabei ist auch die Wahl der Modellrandbedingungen für die Berechnungen des thermischen Feldes von Bedeutung. Es hat sich gezeigt, dass diese Modelle ein guter Ansatz sind, um das 3D Temperaturfeld hinreichend genau vorhersagen zu können. Die Untersuchungen liefern neue Erkenntnisse über das Zusammenwirken

zwischen geologischer Konfiguration, Beckenhydrodynamik und Temperaturfeld und sind generell auf sedimentäre Becken, die durch Salztektonik geprägt sind, übertragbar.

1 Introduction

Heat, generated and stored in the earth, is available in practically inexhaustible quantities. Due to the growing energy demand, the North German Basin and thus also the Brandenburg region have become of great interest with respect to scientific and economic research targeted at using the earth's heat to generate electricity. To produce electric power from a geothermal reservoir economically, a temperature minimum of 120 °C of the extracted hot water is required (Bruns et al. 2011). Typically, temperature increases with depth at a rate of 3 K/100 m. However, the geothermal gradient of the subsurface in Brandenburg is known to be somewhat higher and evidence suggests that regions of thermal anomalies exist with higher and lower temperatures than the average gradient would imply. To use the geothermal potential of the subsurface, knowledge about the occurrence of such positive thermal anomalies is required. Thereby, a fundamental problem is that their spatial distribution has not been adequately mapped so far. Large-scale regional considerations to assess the geothermal potential are based on simple approximations. Earliest approaches assessing the spatial characterisation of the thermal field are derived from temperature measurements in wells which have been intra- and extrapolated spatially. The resultant published temperature maps of Europe for different depths and maps of the surface heat flow density (Hurtig et al. 1992; Schellschmidt et al. 1999; Hurter and Haenel 2002; Agemar et al. 2012) provided large-scale concepts for the heat flow pattern. A more regional view on the thermal field was provided by Beer and Hurtig (1999) and Stackebrandt and Manhenke (2002) who presented temperature maps for the area of Brandenburg. Beer and Hurtig (1999) additionally described the interaction between sediments which are good and less good heat conductors. Their results point to diapirs of the Zechstein salt to efficiently transport heat to the surface whereas surrounding less conductive sediments inhibit vertical heat transport. These authors also show exemplarily for some wells how differences in the temperature gradient depend on lithology variation with depth. Generally, these investigations delivered strongly simplified temperature interpretations as the respective maps are based on 2D interpolation of temperatures for different depth levels and do not consider the 3D heterogeneity of thermal physical properties in the subsurface. Also, the information for single wells does not provide information related to the 3D nature of heat transport processes within the basin fill. Apart from that, the structural diversity of the subsurface of Brandenburg has not been interpreted in 3D so far. More precisely, only a few depth and thickness maps of geological units that represent the configuration of single stratigraphic layers are available (Stackebrandt and Manhenke 2002, 2010). To consider the variability of the structural features and their feedback on the thermal field according to differences in physical properties makes the construction of a consistent 3D structural model a pre-requisite to achieve a better assessment of the thermal field in Brandenburg.

In recent years numerical modelling has become a very important alternative to interpolation methods. First models that address parts of the area in Brandenburg focused on the relationship between structural setting and thermal field within the Northeast German Basin (Bayer et al. 1997; Scheck 1997; Ondrak et al.1998; Norden et al. 2008, 2012; Cacace et al. 2010). Although limited in their horizontal resolution of 4 km (Bayer et al. 1997; Scheck 1997; Cacace et al. 2010) or being two-dimensional (Norden et al. 2008), these models are able to predict the general trend of thermal anomalies within the basin fill. Apart from that, these studies tested the influence of different lower boundary conditions on the temperature distribution. Thereby, it was found that assuming a constant heat flow between 25 and 30 mW/m^2 at the level of the crust-mantle boundary (Moho) reproduces the observed heat flow trends best (Bayer et al. 1997; Scheck 1997). A deficit of these earlier 3D studies was that the crustal domain below the sediments was simplified as being homogeneous. In contrast, Norden et al. (2008) investigated the sensitivity of the thermal field in the NEGB with respect to different configurations of the lithosphere by means of 2D lithospheric models. Likewise, regional crustal-scale thermal models have investigated reasonable boundary conditions for local high resolution models used for the assessment of the geothermal production site Groß Schönebeck (Ollinger et al. 2010).

All these models reflect the influence on the thermal signature exerted by the structural heterogeneity in connection with the related variations of thermal properties. In particular, the configuration of the Zechstein salt plays a prominent role. One problem in earlier models is that they do not reasonably consider the heat input from the deeper mantle and from the radiogenic heat production provided by the deeper crust. Another limitation of earlier models relates to the heat transport mechanism considered. Although in the lithosphere heat is transported mainly by conduction (Fowler 1996), the shallow basin fill is characterized by porous layers where fluids may circulate in permeable areas. So far, the impact of heat transport by convection has been addressed mainly with 2D models of coupled heat and fluid transport (Magri 2005; Magri et al. 2008). A recent contribution has been focused on the main physical heat driving processes within the Northeast German Basin but was not available at the start of this thesis (Kaiser et al. 2011). Though this study has provided generic implications for basin-wide heat transport mechanisms, the related structural model shows limitations concerning its resolution. With a horizontal resolution of 4 km this model does not resolve the full structural detail of the existing salt structures. Furthermore, the vertical resolution of this model does not consider the hydraulically important Cenozoic Rupelian-clay which separates the Cenozoic fresh-water aquifer complex from the deeper Mesozoic saline aquifer complex.

However, basic knowledge as delivered by these previous models has greatly contributed to further develop the model approaches of this thesis. Basically, this study aims to clarify three main questions: (1) What are the main controlling mechanisms on the thermal field and (2) how intensively do they shape the thermal signature? (3) Which role does the geological structure play in affecting the thermal

field? Additionally, the thesis aims to arrive at a better characterisation of the present-day thermal field for the area of Brandenburg. Therefore, a basic assumption is to consider steady-state equilibrium between present geologic configuration, hydrodynamic conditions and the thermal field. To identify the active heat drivers of the region, the focus of the thesis is set on the influence of impacting factors on the 3D thermal field. As these factors are superposed, the complexity of the model approaches has been increased during the studies stepwise to quantify the contribution of individual factors.

1.1 Objectives of the Thesis

The motivation behind the thesis is based on two fundamental questions: (1) Is it possible to predict the regional thermal field adequately by means of thermal models which consider geological structures as well as physical processes and can these predictions be validated and considered as being more realistic than classical interpolation techniques? (2) Which heat transport processes should be considered at different model scales and depths and are there processes that can be neglected?
To clarify these fundamental questions, the thesis follows three main objectives:

- Construction of a three-dimensional structural model for the area of Brandenburg with improved horizontal and vertical resolution (compared to previous models) to adequately represent the geological complexity including salt structures

- Calculation of the present-day conductive thermal field

- Evaluation of the influence of coupled fluid and heat transport on the shallow thermal field

1.2 Synopsis of the Following Chapters

The synopsis provides both the main scientific contributions introduced by a condensed statement giving a general view on the following chapters and the link to the main objectives of the thesis. Chapters 2, 3 and 4 represent three papers published in peer-reviewed journals each.

Chapter 2: Assessment of the Present-Day Thermal Field (NE German Basin) – Inferences from 3D Modelling

The first part of this chapter focuses on the construction of a crustal-scale 3D structural model of the Brandenburg region and the configuration of its basin fill. In contrast to previous 3D structural models covering only parts of the region, the improved horizontal and vertical model resolution displays the structural features, especially the salt structures, in more detail for the whole Brandenburg area. Based on this model including a homogeneous crust, first calculations of the steady-state 3D conductive thermal field provide insights into the interaction between the structural configuration of both the Zechstein salt and the overburden as well as between the crust and the basin fill. To assess the potential influence of convective heat transport, the second part of this chapter provides a zoom-in on a specific location of Brandenburg corresponding to the in-situ geothermal laboratory Groß Schönebeck. As the first author, I was the main contributing author for this manuscript. I constructed

the 3D structural model of Brandenburg and conducted the connected numerical simulations, prepared the figures and wrote the text with minor contributions from my co-author Magdalena Scheck-Wenderoth. The second part of the chapter related to the local thermal field of Groß Schönebeck is a contribution written and based on studies by the second author Yvonne Cherubini. She also contributed in minor parts to the abstract, introduction and conclusions by addressing the Groß Schönebeck case study. Co-authors Lewerenz, Höding and Moeck have provided feed-back and constructive critics to the first draft of the manuscript with respect to technical (Lewerenz), data base-related (Höding) and structural aspects.

Published as:
Noack V, Cherubini Y, Scheck-Wenderoth M, Lewerenz B, Höding T, Simon A, Moeck I (2010) Assessment of the present-day thermal field (NE German Basin) - Inferences from 3D modelling. Chemie Der Erde - Geochemistry 70 (S3):47-62, http://www.sciencedirect.com/science/article/pii/S0009281910000425. The final publication is available at link.elsevier.com.

Chapter 3: Sensitivity of 3D Thermal Models to the Choice of Boundary Conditions and Thermal Properties: a Case Study for the Area of Brandenburg (NE German Basin)

For the studies related to this chapter a new database was used to construct a more realistic differentiated crust for a vertically improved lithosphere-scale 3D structural model. An innovative aspect of this chapter is that, by means of sensitivity studies, different configurations of the lithosphere and thus different lower boundary conditions for the thermal calculation, as well as variations in thermal properties were tested with respect to their influence on the resulting 3D conductive thermal field. Model validation is achieved by the comparison between modeled temperature predictions and temperature observations, thus suggesting that the steady-state thermal field in the Brandenburg area is mainly influenced by heat conduction. However, deviations between model predictions and observations, especially within the shallow thermal field, point to additional heat transport mechanisms apart from heat conduction. I am responsible for the whole content of this chapter, that however, has profited of advice from my co-authors. I extended the existing model to include the more complex configuration of the deeper lithosphere, carried out the sensitivity analyses and prepared all figures. The text was written by myself with minor contributions from the co-authors Magdalena Scheck-Wenderoth and Mauro Cacace, who also provided advice during the set up of the modelling.

Published as:
Noack V, Scheck-Wenderoth M, Cacace M (2012) Sensitivity of 3D thermal models to the choice of boundary conditions and thermal properties: a case study for the area of Brandenburg (NE German

Basin). Environ Earth Sci. 67 (6), 1695-1711, http://link.springer.com/article/10.1007/s12665-012-1614-2. The final publication is available at link.springer.com.

Chapter 4: Influence of Fluid Flow on the Regional Thermal Field: Results From 3D Numerical Modelling for the Area of Brandenburg (North German Basin)

This chapter focuses on the effect of fluid flow on the shallow thermal field above the Zechstein salt. To simulate the production of geothermal fluids (which could be a follow-up task posterior to the present study), relevant aquifers and aquitards need to be represented in the model to reproduce preferential pathways for fluid circulation. Therefore, a new database was compiled to implement the hydraulic barrier of the Rupelian-clay unit into the model, separating the shallow freshwater Quaternary complexes from the deep Mesozoic saline aquifers. In combination with the studies in chapter 3, the results from numerical simulations of coupled fluid flow and heat transfer provide a basic understanding of the influence of thermal and hydraulic boundary conditions in combination with effective average transport parameters for the basin-scale model of the subsurface of Brandenburg. In addition, the consideration of the regionally important Rupelian-clay aquitard offers new insights into the mechanisms of interchange between shallow freshwater complexes and saline brines from the deep aquifers. I am responsible for the whole content of this chapter. I carried out the numerical simulations with supporting advise from my co-authors. I have evaluated the results, prepared all figures and wrote the text.

Published as:

Noack V, Scheck-Wenderoth M, Cacace M, Schneider M (2013) Influence of fluid flow on the regional thermal field: results from 3D numerical modelling for the area of Brandenburg (North German Basin). Environ Earth Sci. 70 (8), 3523-3544, http://link.springer.com/article/10.1007%2Fs12665-013-2438-4 . The final publication is available at link.springer.com.

Chapter 5: Discussion

This chapter combines summaries and conclusions of the single chapters as they lead stepwise to final conclusions about capabilities and limitations of thermal model predictions. The interpretations of the results are then discussed in comparison with relevant studies of other regions and salt basins of similar inventory and with alternative modelling approaches. Another focus is set on the considered dynamic processes involved in heat transport in general as well as on temperature examination particularly for Europe.

Chapter 6: Limitations of the Method

Assumptions and simplifications which limit the model results are provided by this chapter.

Chapter 7: Conclusions and Best-Practice Workflow

This chapter includes the main results of the thesis and a suggested general workflow to adequately assess the regional thermal field in a sedimentary basin.

Chapter 8: References

The reference list combines references of all chapters.

Appendix 1: Governing Equations

Appendix 1 includes the governing equations related to chapter 2.

Appendix 2: List of Publications Related to this Thesis

Appendix 2 lists the publications arising from this thesis.

2 Assessment of the Present-Day Thermal Field (NE German Basin) – Inferences from 3D Modelling

Abstract

We use a refined 3D structural model based on an updated set of observations to assess the thermal field of Brandenburg. The crustal-scale model covers an area of about 250 km (E-W) times 210 km (N-S) located in the Northeast German Basin (NEGB). It integrates an improved representation of the salt structures and is used for detailed calculations of the 3D conductive thermal field with the Finite Element Method (FEM). A thick layer of mobilised salt (Zechstein, Upper Permian) controls the structural setting of the area. As salt has a considerably higher thermal conductivity than other sediments, it strongly influences heat transport and accordingly temperature distribution in the subsurface. The modelled temperature distribution with depth shows strong lateral variations. The lowest temperatures at each modelled depth level occur in the area of the southern basin margin, where a highly conductive crystalline crust comes close to the surface. In general, the highest temperatures are predicted in the north-western part of the model close to the basin centre, where rim syncline deposits around the salt domes cause insulating effects. The pattern of temperature distribution changes with depth. Closely beneath the salt, the temperature distribution shows a complementary pattern to the salt cover as cold spots reflect the cooling effect of highly conductive salt structures. The predicted temperatures at depths beneath 8 km suggest that the influence of the salt is not evident any more. Similar to the temperature distribution, the calculated surface heat flow shows strong lateral variations. Also with depth the variations in thermal properties due to lithology-dependent lateral heterogeneities provoke changing pattern of the heat flow. A comparison with published heat flow and temperature data shows that the model predictions are largely consistent with observations and indicates that conductive heat transport is the dominant mechanism of heat transfer. Local deviations between modelled and observed temperatures are in the range of ± 10° K and may be due to the convective heat transport. To assess the potential influence of convective heat transport we zoom in on a specific location of Brandenburg corresponding to the in-situ geothermal laboratory *Groß Schönebeck*. This local model is used to carry out 3D numerical simulations of coupled fluid flow and heat transfer processes. Our coupled models indicate that conduction is the dominant heat transfer mechanism below Middle Triassic strata. Above the Triassic Muschelkalk, the more than 3000 m of sediments with higher hydraulic conductivity promote the formation of convection cells. Here, especially high degrees of coupling result in remarkable convective heat transport.

2.1 Introduction

Being able to predict temperature distribution with depth in more detail is particularly relevant in the view of global climate change which requires exploration of geothermal energy as a timely strategy. As direct temperature information with depth can be obtained only by expensive drilling, which, in turn, provides only local information, methods to predict the temperature at different depths are needed. Numerical models considering both the structural setting of the subsurface as well as the physical processes controlling heat transfer are an option to assess and predict lateral and vertical variations of temperature distribution. Here we present new results from numerical modelling of the thermal field in the subsurface of Brandenburg, a federal state in north-eastern Germany. The modelled area comprises the southern part of the Northeast German Basin (NEGB, Scheck and Bayer 1999) a sub-basin of the Central European Basin System (CEBS), extending from the Southern North Sea to Poland (Littke et al. 2008).

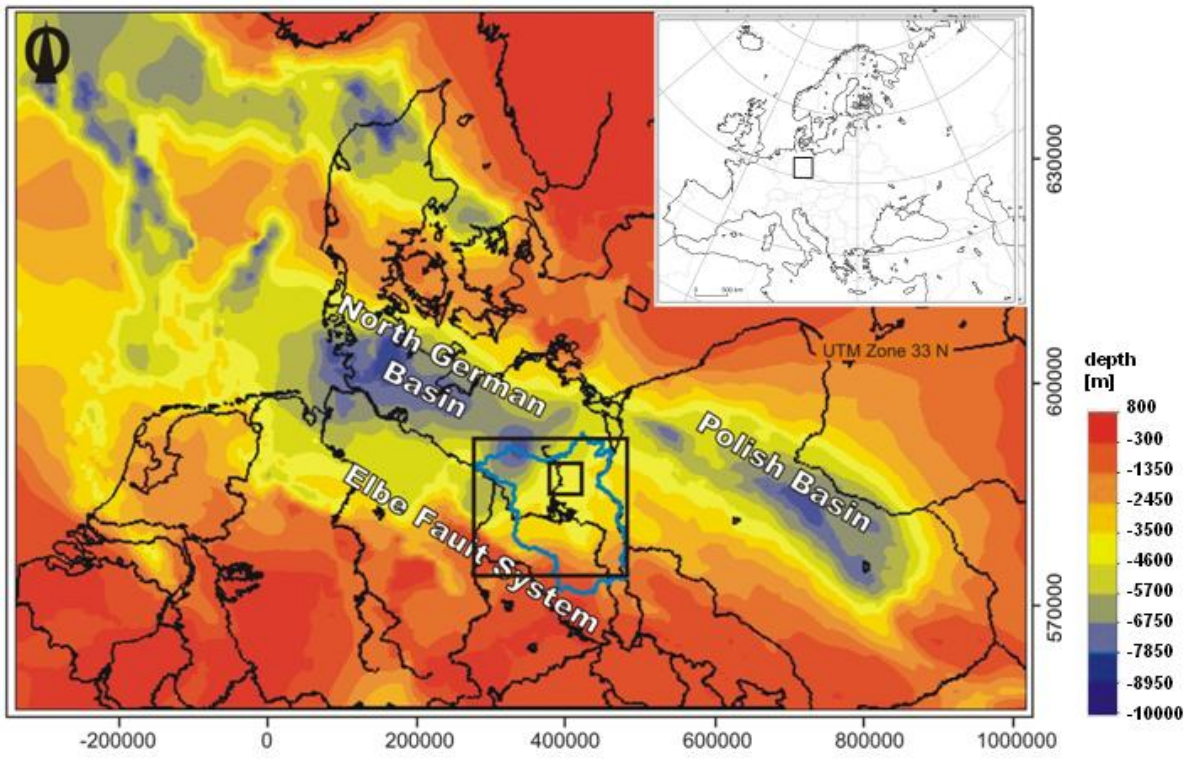

Figure 2.1 Location of study area in the south-eastern part of the Central European Basin System; depth to top pre-Permian (modified after Scheck-Wenderoth and Lamarche 2005). Large rectangle encloses the area covered by the 3D structural and thermal model of Brandenburg, small rectangle indicates the location of the model of the geothermal in-situ laboratory Groß Schönebeck, blue line – border of Brandenburg.

In the north, the study area encompasses a part of the basin centre of the NEGB whereas to the south, the present-day south-eastern basin margin of the NEGB is enclosed. There, the Permian to Cenozoic basin fill has been uplifted and partially eroded along the Elbe-Fault-System (Fig. 2.1). The Permian to Cenozoic basin fill of the NEGB is up to 8000 m thick and consists of Rotliegend clastics (Permian), a thick layer of strongly mobilised Zechstein salt (Permian) overlain by Mesozoic and Cenozoic sediments (Schwab 1985; Bayer et al. 1997; Scheck 1997). These overburden deposits are morphologically influenced by numerous salt structures which have developed since Early Triassic times in response to changing regional stress fields and differential loading (Scheck-Wenderoth et al. 2008b). Published temperature maps of Europe for different depths and maps of the surface heat flow density (Hurtig et al. 1992; Schellschmidt et al. 1999; Hurter and Haenel 2002) provided large-scale concepts for the heat flow pattern. For the study area of Brandenburg, Beer (1996) presented temperature measurements in deep wells and introduced a tentative empirical correction for temperature logs. However, Förster (1997) pointed out that measured borehole temperature data are often recorded shortly after drilling has ceased. Thus, these data do not reflect the equilibrium temperature and the corresponding values may be biased. Using a method to reliably correct borehole temperature data, Förster (2001) as well as Norden and Förster (2006) derived a new thermal database for the NEGB including measured temperatures and radiogenic heat production values measured on drill cores but also lithology-dependent thermal properties such as thermal conductivities. This led to new values of surface heat flow (Norden et al. 2008). The relationship between structural setting and thermal field within the NEGB has been also addressed in the last decade based on 3D simulations using Finite Element Methods. Models of the regional, crustal-scale 3D conductive thermal field of the NEGB have been compared with classical one-dimensional extrapolations (Bayer et al. 1997; Scheck 1997). These works assessed the influence of different lower boundary conditions and concluded that assuming a constant heat flow between 25 mW/m² and 30 mW/m² at the level of the crust-mantle boundary (Moho) reproduces the observed heat flow trends best. Moreover, these models described the decoupling effect of the Zechstein salt between a pre-Zechstein and post-Zechstein succession in the NEGB. This decoupling effect controls both, the structural setting of the overlying layers as well as temperature distribution and fluid flow. Ondrak et al. (1998) showed that regional crustal-scale thermal models can provide reasonable boundary conditions for local high resolution models as commonly used for the assessment of geothermal production sites. In addition to processes related to conductive heat transfer, the impact of heat transport by convection has been addressed mainly with 2D models of coupled heat and fluid transport (Magri 2005; Magri et al. 2008).

Previous studies were based on simplified model assumptions in terms of structural resolution so that they were able to reproduce the general pattern of the thermal field of the Northeast German Basin (Bayer et al. 1997; Ondrak et al. 1998; Norden et al. 2008). To describe dominant mechanisms of heat transport (Magri et al. 2008), their significance with respect to local anomalies such as required for

geothermal drilling remained limited. New data concerning both, the structural setting and thus also the spatial distribution of thermal properties, are meanwhile available for the area of Brandenburg and provide the opportunity to build a refined 3D structural model of the area as a base for more detailed temperature calculations. Accordingly, we present a new 3D structural model of the subsurface of Brandenburg characterised by an improved structural resolution compared to earlier models as it is based on a larger data base. For this model we calculate the crustal-scale 3D conductive thermal field and compare our results with available temperature data and published temperature depth maps.
Finally, we zoom in at a specific location in Brandenburg, where currently active experiments related to geothermal energy production are carried out. It corresponds to the in-situ geothermal laboratory Groß Schönebeck (Fig.2.1) located 40 km north of Berlin and is one of the key sites of geothermal exploration studies in the North German Basin. The in-situ laboratory is installed in a former gas exploration well and is utilised for the development of geothermal technologies necessary for electric power generation. For this geothermal site we present first attempts to model potential influences of convective heat transport in addition to conduction.

2.2 The 3D Structural Model of Brandenburg

2.2.1 Database

Several published datasets are available for the construction of a refined 3D structural model of Brandenburg (Tab. 2.1). The primary database consists of several depth and thickness maps as well as fault maps provided by the geological survey of Brandenburg (Landesamt für Bergbau, Geologie und Rohstoffe Brandenburg - LBGR) that partially are published in the Geological Atlas of Brandenburg (Stackebrandt and Manhenke 2002). In addition, data from former regional models were used to complement the marginal parts of the rectangular area covered by the model and to avoid boundary effects. Also for those units not differentiated further in the Geological Atlas of Brandenburg, data from previous models have been integrated. These previous models include a model of the Northeast German Basin with a horizontal resolution of 4 km (NEGB: Scheck and Bayer 1999), an earlier model of the entire Central European Basin System with a horizontal resolution of 8 km (CEBS1: Scheck-Wenderoth and Lamarche 2005) and a more recent model of the Central European Basin System with a horizontal resolution of 4 km (CEBS2: Maystrenko et al. 2010). These datasets have been complemented by data from published deep wells (Hoth et al. 1993) and by well data provided by the Geological Survey of Sachsen-Anhalt (Landesamt für Geologie und Bergwesen Sachsen-Anhalt - LAGB 2009).

Table 2.1 Input data for 3D structural modelling of Brandenburg: NEGB: 3D structural model of the Northeast German Basin (Scheck and Bayer 1999); CEBS1: 3D structural model of the Central European Basin System (Scheck-Wenderoth and Lamarche 2005); CEBS2: 3D structural model of the Central European Basin System (Maystrenko et al. 2010).

Stratigraphic Unit	Type of data	Horizontal resolution/scale	Reference
Topography	Grid data	1 Arc-minute	ETOPO1, Amante and Eakins (2009)
Quaternary	Scattered data	1:1.000.000	Stackebrandt and Manhenke (2002)
	Scattered data	1: 500.000	Landesamt für Umwelt, Naturschutz und Geologie Mecklenburg-Vorpommern (2002)
Tertiary	Grid data	NEGB: 4 km	Scheck and Bayer (1999)
	Grid data	CEBS1: 8 km	Scheck-Wenderoth & Lamarche, 2005
Upper Cretaceous	Scattered data	1:1.000.000	Stackebrandt and Manhenke (2002)
	Grid data	NEGB: 4 km	Scheck and Bayer (1999)
	Grid data	CEBS1: 8 km	Scheck-Wenderoth & Lamarche (2005)
Lower Cretaceous	Grid data	NEGB 4 km	Scheck and Bayer (1999)
Jurassic	Grid data	CEBS2: 4 km	Maystrenko et al. (2010)
	Grid data	NEGB 4 km	Scheck and Bayer (1999)
Keuper	Grid data	NEGB 4 km	Scheck and Bayer (1999)
Muschelkalk	Scattered data	1:1.000.000	Stackebrandt and Manhenke (2002)
	Grid data	NEGB 4 km	Scheck and Bayer (1999)
Buntsandstein	Grid data	NEGB 4 km	Scheck and Bayer (1999)
Zechstein	Scattered data	1:1.000.000	Stackebrandt and Manhenke (2002)
	Grid data	NEGB 4 km	Scheck and Bayer (1999)
	Grid data	CEBS1: 8 km	Scheck-Wenderoth & Lamarche (2005)
	Grid data	CEBS2: 4 km	Maystrenko et al. (2010)
Sedimentary Rotliegend	Scattered data	1:1.000.000	Stackebrandt and Manhenke (2002)
	Grid data	CEBS2: 4 km	Maystrenko et al. (2010)
Permo-Carboniferous Volcanics	Scattered data	1:1.000.000	Stackebrandt and Manhenke (2002)
	Grid data	CEBS2: 4 km	Maystrenko et al. (2010)

2.2.2 Model Construction

The first step in modelling is the interpolation of the compiled datasets into 2D grids using a minimum tension gridding technique and considering the trace of faults as interpolation barriers (Earth Vision, Dynamic Graphics Ltd., Version 8.0). Both depth and thickness data are interpolated to obtain the following stratigraphic units composing the 3D model from top to bottom: Quaternary, Tertiary, Upper Cretaceous, Lower Cretaceous, Jurassic, Triassic Keuper, Triassic Muschelkalk, Triassic Buntsandstein, Permian Zechstein, Permian Rotliegend and Permo-Carboniferous Volcanics (Fig. 2.2a). Subsequently, the 2D grids are integrated in a 3D structural model with the software Geological Modelling System (GMS developed at GFZ Potsdam). This part of the task proved to be more complex than expected, as numerous intersections and inconsistencies between the 2D grids have been encountered. These inconsistencies result from 2D interpolation and extrapolation of the available data to areas not covered by observations. The base of Quaternary and the base of Zechstein are chosen as

reference levels for the construction of the model as both horizons are very well-constrained by data. To create a model consistent in 3D that also integrates all available observation we follow a twofold strategy. In a first step the model is built from the topography downward to the base of the Lower Triassic Buntsandstein which also represents the top of the Upper Permian Zechstein salt, by calculating the thickness of each horizon resulting from the available datasets. Beginning with the first horizon, the Quaternary thickness is calculated as the difference between its two confining depth levels, the present topography (Fig. 2.2b) and the base Quaternary. This procedure is repeated for the other stratigraphic units of the model down to the Triassic Buntsandstein.

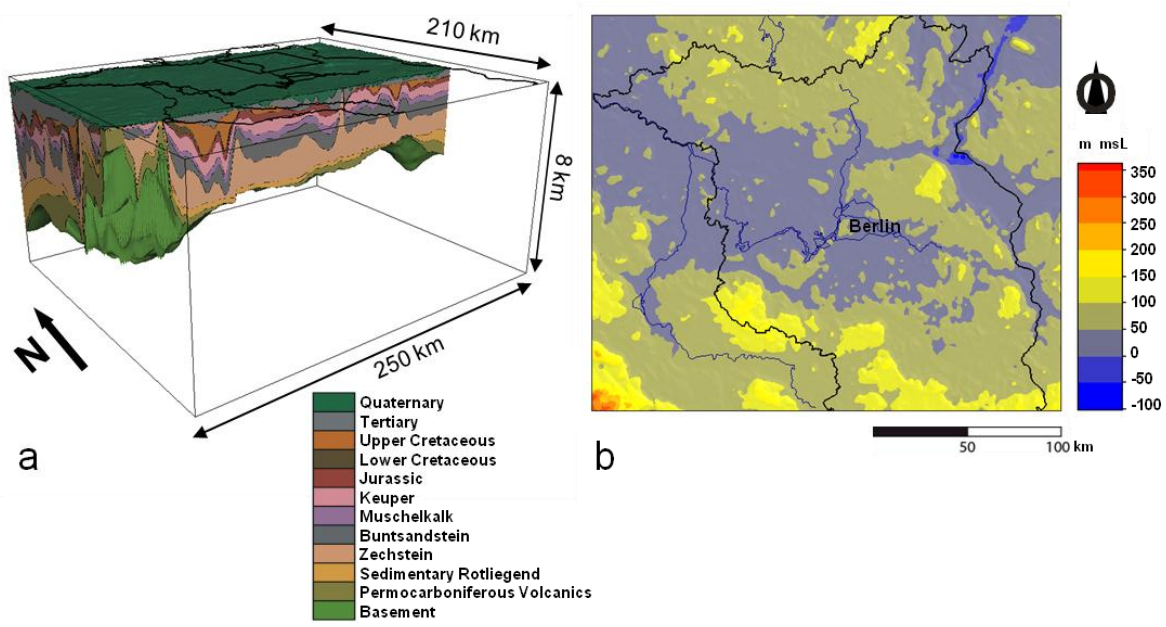

Figure 2.2a 3D view on the structural model of Brandenburg with colour key for the stratigraphic units differentiated in the model. The model is based on Gauss Krüger zone 4 coordinates. **b** present topography of the area; black line – border of Brandenburg, blue line – rivers.

In a second step we calculate the configuration for the Sedimentary Rotliegend and for the Permo-Carboniferous Volcanics by subtracting the respective thicknesses from the Base Zechstein, which also represents the top of the Rotliegend, downwards. The thickness of the Zechstein salt layer corresponds to the difference between the top Zechstein and the base Zechstein horizon. Finally, we complete the model downward adding a layer of pre-Permian crust obtained as the difference between the base of Permo-Carboniferous Volcanics and the depth of the crust-mantle boundary as compiled by Scheck-Wenderoth and Lamarche (2005). Spatially, the final model covers an area of 250 km in E-W direction and 210 km in N-S direction with a horizontal resolution of 1 km and a vertical resolution corresponding to the number of 11 layers resolved in the model (Fig. 2.2a). The detailed configuration of the 3D structural model is illustrated by isopach maps and maps of the base of each horizon (Figs. 2.3, 2.4 and 2.5)

2.2.3 Structural Setting

The lowermost unit of the basin fill consists of the **Permo-Carboniferous Volcanics**. In north-western Brandenburg the base of the Permo-Carboniferous Volcanics reaches depths of more than 8000 m (Fig. 2.3a), while in the east the base rises to about 3000 m depth below sea level. In the south, along the inverted southern margin of the basin, this surface is even partially above sea-level. The deepest part of this surface correlates with the location of the largest thicknesses of the Permo-Carboniferous Volcanics (Fig. 2.3b). Five zones of increased thickness are present in the northern domain of the model area (Fig. 2.3b) with largest values of up to 2000 m along a NE-SW oriented zone in north-western Brandenburg. Thicknesses of up to 1500 m are found in the north-eastern sector of the model domain. In the south of Brandenburg volcanics are absent (Stackebrandt and Manhenke 2002). Though, the composition of the volcanics varies, as rhyolites, andesites, ignimbrites and basalts were drilled (Hoth et al. 1993), the dominant lithology encountered is rhyolitic.

The base of the next-higher unit - the **Sedimentary Rotliegend** (Fig. 2.3c) - displays a deep structural low in the north-western part of Brandenburg where the respective surface descends with a smooth gradient to depths of more than 7000 m. In contrast, the geometry of this surface shows little change with respect to the underlying layer at the southern margin. Accordingly, the thickest Rotliegend deposits of up to 2000 m (Fig. 2.3d) are present in the north-western part of the model close to the basin centre whereas the Rotliegend thickness decreases to the south and east. In terms of lithology this layer consists predominantly of non-marine clastics and includes the major aquifer target for deep geothermal exploration at the in-situ laboratory Groß Schönebeck.

Above the Sedimentary Rotliegend, the base of the **Permian Zechstein** salt shows a similar structural pattern as the base Rotliegend, though in its deepest parts this surface reaches only about 5000 m (Fig. 2.3e). In contrast to the smooth pattern of the base Zechstein, the isopachs of this unit (Fig. 2.3f) display a highly differentiated structure. Accordingly, the structural pattern of the Zechstein thickness is characterised by numerous salt pillows and salt diapirs. The latter are piercing their cover layers to different levels and can reach vertical amplitudes of up to 4000 m.
Complementary, large areas are present where the post-depositional mobilisation results in almost complete removal of the salt. This is expressed by areas of close-to zero present-day thickness of the Zechstein in the north-western part of the study area. As this unit is mainly composed of rock salt, the impact of its structural setting on the lateral and vertical variations in temperature is huge because of its high thermal conductivity.

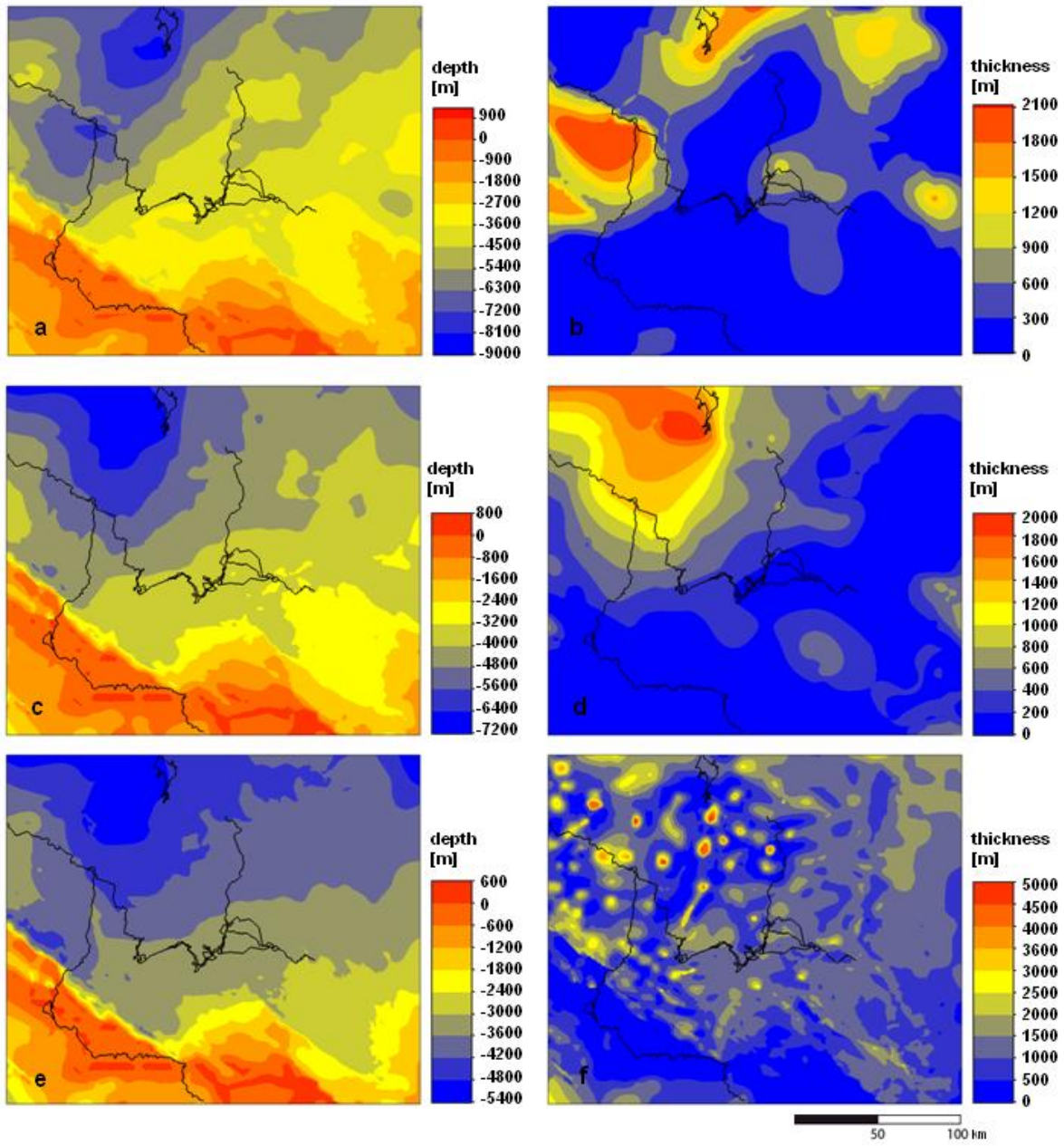

Figure 2.3 Isopachs and depths to the base of successive stratigraphic units in the 3D model: **a** base of Permo-Carboniferous volcanics; **b** isopachs of Permo-Carboniferous volcanics; **c** base of Permian Sedimentary Rotliegend; **d** isopachs of Permian Sedimentary Rotliegend; **e** base of Permian Zechstein salt; **f** isopachs of Permian Zechstein salt.

Basin reconstructions (Scheck et al. 2003b) indicate that the salt thickness distribution is following a similar pattern as the Permian Rotliegend and traces of this trend are visible in the general increase in thickness towards the north-west. Nevertheless, the dominant features of the present salt distribution are very steep thickness gradients. Present day salt structures are aligned along two types of structural axes: NNE-SSW trending axes in the central part of the model and NW-SE trending axes parallel to

the Elbe Fault System near the southern margin. This highly variable thickness distribution of the Zechstein salt causes corresponding gradients in the geometry of all cover layers. Accordingly, the base of the Triassic Buntsandstein (= Top Zechstein, Fig. 2.4a) mimics the pattern seen in the Zechstein isopachs - a phenomenon that is repeated in all depth maps of the layers above the salt.

The deepest parts of the Base of the **Triassic Buntsandstein** reach down to 3600 and 4200 m and, in the north-western part of the study area, where the underlying salt has been completely removed (compare with salt thickness in Fig. 2.3f), even down to 5000 m. A further consequence of salt movement is the overprinted thickness distribution of the cover layers where piercing by salt diapirs causes holes of zero thickness. This post-depositional piercing is obvious in the isopach map of the Buntsandstein (Fig. 2.4b), a unit dominantly composed of sandstones and siltstones. Similar to the thickness pattern observed for the Sedimentary Rotliegend, a general increase in thickness towards the north-western part of the model is visible with up to 1200 m of Buntsandstein. In the southern and eastern parts of Brandenburg, the Buntsandstein thickness decreases gradually to less than 200 m. Most of the thickness minima (blue spots of zero thickness) intersect this regional pattern without much local variations around salt diapirs, thus indicating post-depositional piercing.

The base of the **Triassic Muschelkalk** again mimics the topography of the Zechstein salt and, apart from salt structures, is located at depths between 3000 and 3500 m (Fig. 2.4c). As for the Buntsandstein, a long-wavelength pattern of continuously increasing thickness towards the north-western part of the model can be discerned, though the variation in thickness (Fig. 2.4d) covers a far smaller range between 300 and 400 m. In addition to the post-depositional thickness minima also local short-wavelength thickness maxima are present. An example of this phenomenon is a local thickness anomaly of more than 500 m in the proximity of the salt diapir Kleinmutz north of Berlin, that indicates syn-depositonal halokinetic movements resulting in salt withdrawal and early formation of a primary salt rim syncline.

The depth to the base of **Triassic Keuper** shows again a pattern similar to the top Zechstein and is located between 2800 and 3200 m (Fig. 2.4e). Contrarily, the thickness map of the Keuper (Fig. 2.4f) reveals a change in the location of the main depocentre compared to the underlying layers. In the NNE-SSW oriented Rheinsberg Trough the thickness of this unit mainly composed of continental clastics, locally attains up to 1400 m, whereas it decreases to less than 500 m in the other parts of the model. Seismic data (Scheck et al. 2003a) as well as reconstructions of the salt movements (Scheck et al. 2003b) indicate that the Rheinsberg Trough developed in response to salt withdrawal as a large elongated rim syncline perpendicular to regional E-W extension. Also, local smaller thickness maxima near salt structures point to syn-depositional formation of salt rim-synclines.

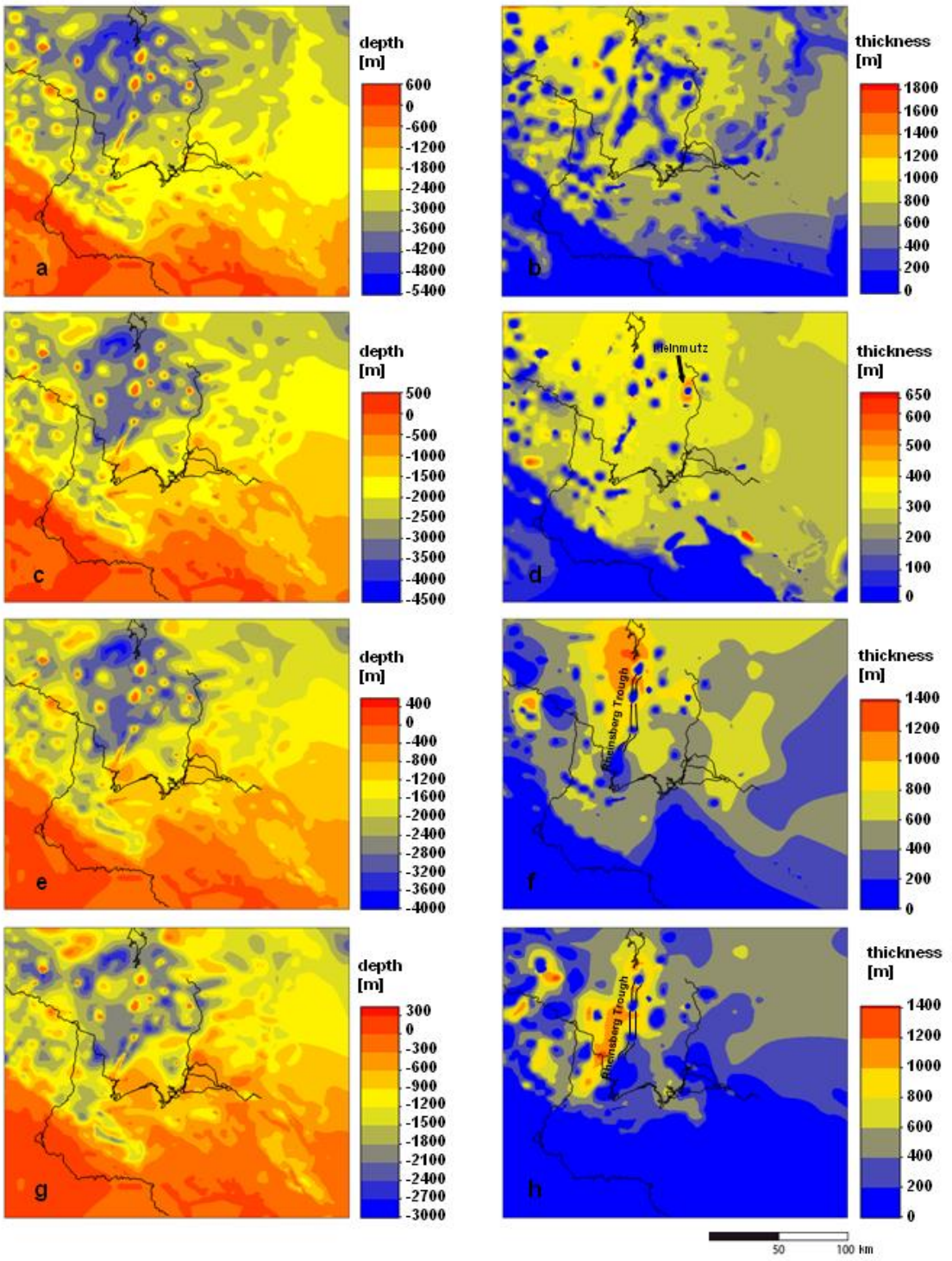

Figure 2.4 Isopachs and depths to the base of successive stratigraphic units in the 3D model: **a** base of Triassic Buntsandstein; **b** isopachs of Triassic Buntsandstein; **c** base of Triassic Muschelkalk; **d** isopachs of Triassic Muschelkalk; **e** base of Triassic Keuper; **f** isopach of Triassic Keuper; **g** base of Jurassic; **h** isopachs of Jurassic.

The base of the **Jurassic** (Fig. 2.4g) is modelled at depths between 900 and 3000 m with the deepest part in the Rheinsberg Trough. There, also the thickness of the Jurassic (Fig. 2.4h) is locally increased to up to 1400 m along a NNE-SSW trending axis. Beside this elongated thickness maximum also

smaller thickness maxima attest the formation of syn-depositional Jurassic rim synclines in response to coeval salt withdrawal.

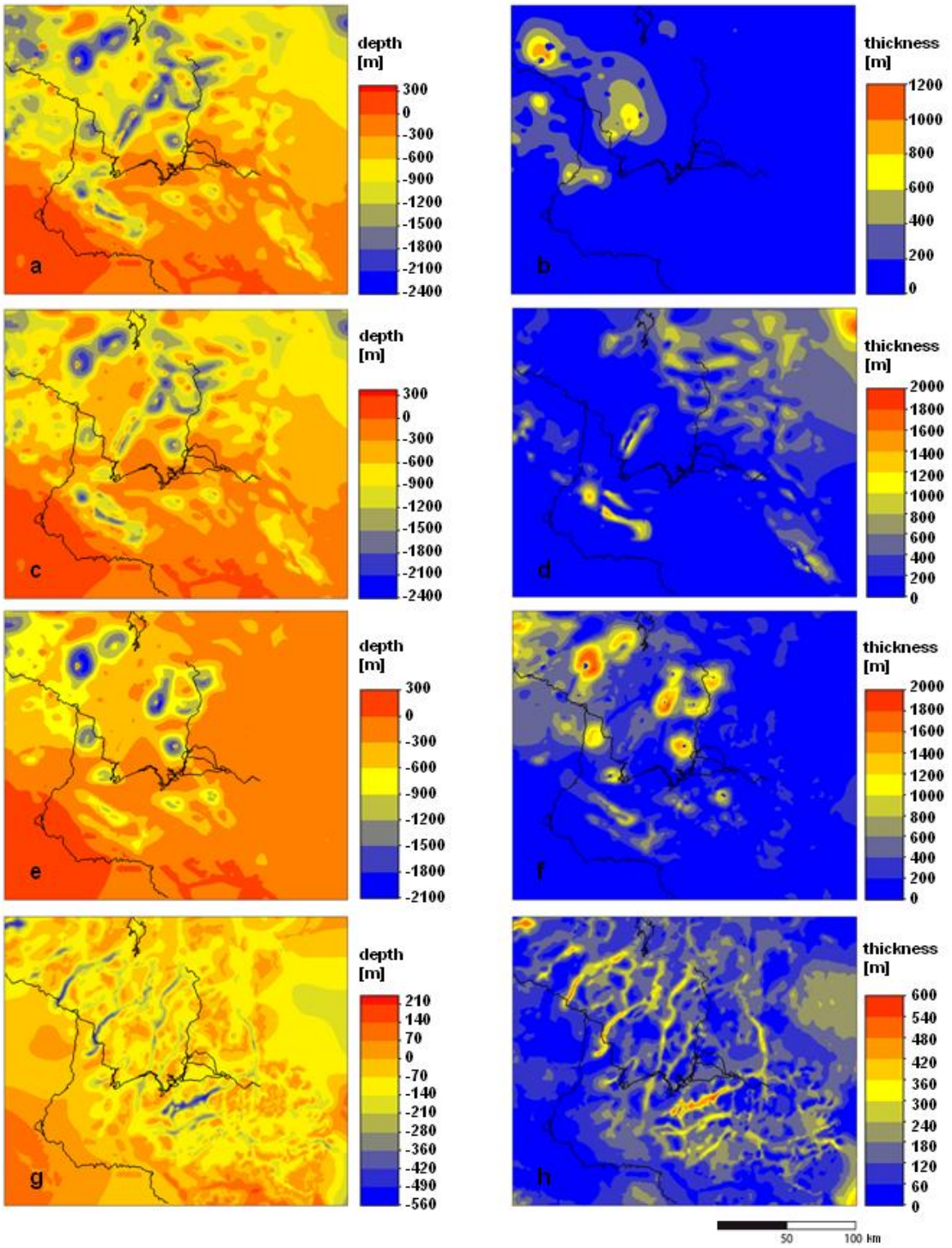

Figure 2.5a Base of Lower Cretaceous; **b** isopachs of Lower Cretaceous; **c** base of Upper Cretaceous; **d** isopachs of Upper Cretaceous; **e** base of Tertiary; **f** isopachs of Tertiary; **g** base of Quaternary; **h** isopachs of Quaternary.

The base of the **Lower Cretaceous** is up to 2400 m deep and, in contrast to the depth maps of the underlying horizons, is characterised by additional structural depressions indicating coeval formation of salt rim synclines (Fig. 2.5a). This is also exposed by the circular shape of thickness maxima of Lower Cretaceous deposits preserved only in the north-western part of Brandenburg and in the southern part of Mecklenburg (Fig. 2.5b). There, Lower Cretaceous clastic sediments attain a maximum thickness of up to 1000 m.

The base of the **Upper Cretaceous** reaches depths of more than 2000 m (Fig. 2.5c) and is generally similar to the base of the Lower Cretaceous. In contrast, the thickness distribution of the Upper Cretaceous chalk deposits (Fig. 2.5d) shows a pattern very different from the underlying layers. Localised maxima of up to 1400 m are present near salt structures of parallel orientation, both characterised by NW-SE oriented axes. Over the largest part of the model area no Upper Cretaceous is preserved, partially in consequence of post-depositional uplift and erosion in the Latest Cretaceous-Early Tertiary (Schwab 1985; Ziegler 1990; Scheck-Wenderoth et al. 2008a).

This erosional event is expressed as a regional unconformity in the sediment fill of the area, representing the base of the **Tertiary** clastic sediments. The depth to base Tertiary additionally bears the imprints of Cenozoic subsidence that had resumed after the phase of erosion (Scheck 1997). Within Cenozoic salt rim synclines, the base Tertiary is located at up to 2000 m depth (Fig. 2.5e) and rises to about 600 m depth in the areas apart from rim synclines. The isopach map of the Tertiary (Fig. 2.5f) displays a typical pattern of local salt rim synclines indicated by several circular thickness maxima of up to 2000 m near salt structures. Reduced sediment thicknesses (200 to 400 m) are identified in the south and the east of Brandenburg, some of which have been related to postdepositional erosion by subglacial channels (Stackebrandt et al. 2001).

The uppermost and youngest layer in the model is the **Quaternary**, the base of which (Fig. 2.5g) is structurally controlled by a number of northerly oriented and equally distributed subglacial channels (buried valleys) that locally may reach depths of more than 500 m. These channels were formed by subglacial erosion at the base of the inland ice where the advance caused hydrostatic overpressure in the area of water saturated sediments (Stackebrandt 2009). They are often filled with a variety of porous and permeable sediments and represent important water reservoirs (BURVAL Working Group 2009). The thickness map of the Quaternary (Fig. 2.5h) shows that up to 600 m sediments are present in these northerly trending channels whereas the Quaternary is less than 300 m thick outside the channels.

2.3 The 3D Conductive Thermal Model of Brandenburg

To assess the regional thermal field we calculate the steady-state 3D temperature distribution assuming heat conduction as the dominant transport mechanism. Therefore, we solve the three-dimensional steady-state heat conduction equation:

$$\mathrm{div}\,(\lambda\ \mathrm{grad}\ T) = -S \qquad (1)$$

with λ - thermal conductivity, T - temperature, S - radioactive heat production, numerically using a 3D FEM (Bayer et al. 1997). The solution of equation (1) depends on the thermal properties (λ and S) and on the choice of boundary conditions. A fixed temperature of 8°C, corresponding to the average surface temperature in the area, has been implemented as upper boundary condition. For the lower boundary, we choose a constant heat flow of 30 mW/m² at the Moho, following results of earlier work (Bayer et al. 1997). The lateral boundaries are considered closed. For temperature calculation, lithology-dependent physical properties are assigned to each stratigraphic unit of the model. According to equation (1) values for the thermal conductivities and for the heat production are the parameters required for the calculation of the 3D conductive thermal field. These are assigned to each layer assuming a uniform dominant lithology for each layer as detailed in Table 2.2.

Table 2.2 Input thermal properties for geothermal modelling after Bayer et al. (1997).

Stratigraphic Unit	Lithology	Heat conductivity [W/(m*K)]	Radiogenic heat production [W/m³]
Quaternary	Sand and Silt and Clay	1.50	0.7e-6
Tertiary	Sand and Silt and Clay	1.50	0.7e-6
Upper Cretaceous	Limestone (Chalk)	1.90	0.3e-6
Lower Cretaceous	Clays with Sand and Silt	2.00	1.40e-6
Jurassic	Clays with Sand and Silt and Marl	2.00	1.40e-6
Keuper	Clays with Marl and Gypsum	2.30	1.40e-6
Muschelkalk	Limestone	1.85	0.3e-6
Buntsandstein	Silts with Sand and Clay and Evaporite	2.00	1.00e-6
Zechstein	Rock salt	3.50	0.09e-6
Sedimentary Rotliegend	Clay-, Silt- and Sandstone	2.16	1.00e-6
Permo-Carboniferous Volcanics	Rhyolithe and Andesite	2.50	2.0e-6
Crust	Granite to Granodiorite	2.55	1.5e-6
Mantle	Peridotite	2.30	3.0e-7

2.3.1 Modelled Temperatures

The 3D structural model is illustrated along an E-W cross-section (Fig. 2.6a) down to 5000 m depth. As can be seen on the figure, one salt diapir pierces the up to 4000 m thick overburden. This diapir is bounded by salt rim synclines. Fig. 2.6b shows exemplarily the impact of the high thermal conductivity within the salt diapir on the temperature distribution down to 5000 m depth. The isotherms are bent convex upward above the diapir and convex downward below the structure. Highest temperatures are predicted below the salt rim synclines and correlate with the thickness maxima of the overburden sediments.

Figure 2.6c-f shows the calculated temperature distribution for selected depth levels. A feature common to all temperature depth maps is the strong lateral variation of predicted temperatures for a certain constant depth level. The temperature map at 2000 m depth (Fig. 2.6c) cuts Cenozoic sediments and salt structures within the model. The respective pattern of temperature distribution shows a strong spatial correlation with the thickness distribution of the Zechstein salt layer and the topography of the top salt surface (compare Fig. 2.3f and 2.4a). In general, calculated temperatures are higher above salt diapirs but lower within and below salt structures or areas of thick salt. This "chimney effect" is the result of the high thermal conductivity of the salt causing increased heat transfer and therefore enhanced cooling within the salt structure. In contrast, the surrounding low-conductive sediments have an insulating effect and cause heat storage. Therefore, higher temperatures are modelled where the low-conductive units are thick. Accordingly, the highest calculated temperatures at 2000 m depth vary between 90 °C and 100 °C, where the low-conductive sediments of Tertiary salt rim synclines attain their largest thickness in the north-western domain of the model area. In contrast, lower temperatures are predicted in areas where salt diapirs reach structural levels close to the surface and the cooling effect is most pronounced. In areas without prominent salt structures, temperatures generally attain 80 °C to 90 °C. The lowest temperatures of about 60 °C are calculated for the basin margin in the south.

The temperature distribution at 4000 m depth (Fig. 2.6d) shows highest temperatures between 145 °C and 160 °C in the northern domain of the model. This map cuts the model along a plane intersecting several salt structures in the western part of the study area where the highest temperatures are calculated. Increasing temperatures are predicted around salt domes due to the insulating effect of the surrounding rim syncline deposits. There, the enhanced lateral heat transfer from the salt structure is "captured" by the low-conductive sediments of the rim syncline. In the eastern part, this map cuts the model below the salt. Accordingly, the calculated temperatures are lower there and vary between 130 °C and 150 °C. The lowest temperatures of up to 100 °C have been calculated at the southern basin margin. This is related to the shallow position of the highly conductive crystalline crust in this domain, also causing a chimney effect.

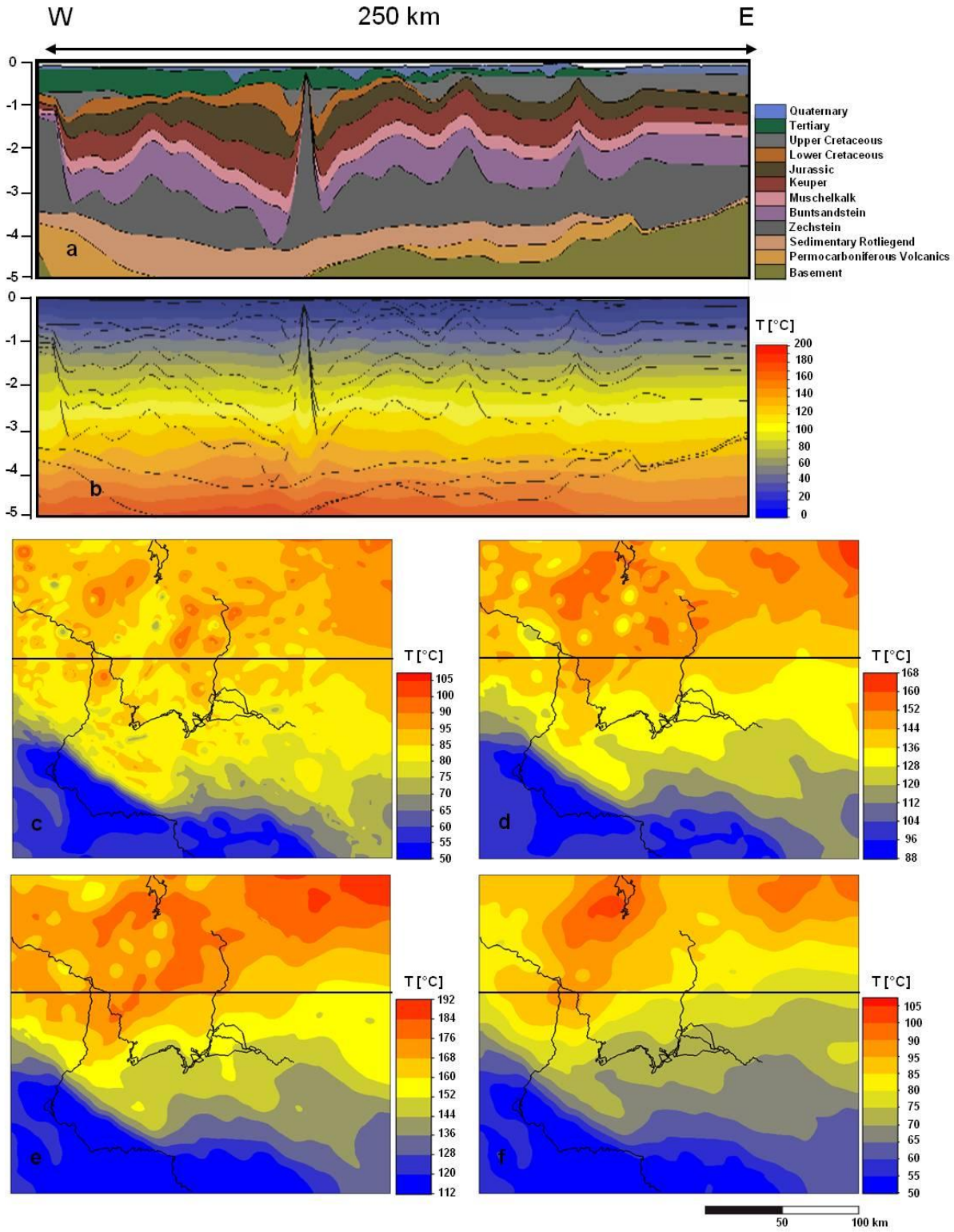

Figure 2.6a Cross section of the 3D structural model; **b** cross section of the 3D thermal model, vertical exaggeration 1:10; **c-f** Predicted temperature in °C extracted from the 3D conductive thermal model at the depth of **c** 2000 m; **d** 4000 m; **e** 5000 m; **f** 8000 m.

The pattern of temperature distribution changes with depth. At 5000 m depth (Fig. 2.6e) the spatial correlation between the pattern of temperature distribution and the salt thickness is only weekly expressed as circular cold spots beneath salt diapirs in the north-western part of the model. The long-wavelength trend of increasing temperatures from the southern margin (~110°C) towards the basin centre (up to 190°C) rather correlates with the cumulative thickness distribution of the post-salt deposits and reflects the blanketing effect and related heat storage due to the low conductivity of these layers.

At the depth of 8000 m (Fig. 2.6f) the temperature distribution shows only smooth, long wavelength variations. Domains of elevated temperatures between 230 °C and 270 °C correlate spatially with the superposed thickness maxima of the Permian Rotliegend sediments and the Permo-Carboniferous Volcanics (compare Fig. 2.3b and 2.3d). This indicates that these elevated temperatures are caused by the blanketing effect of the respective layers. In contrast, lower temperatures ranging between 170 °C and 200 °C, are calculated for areas where this surface cuts through the highly-conductive pre-Permian crust with the lowest values again occurring at the southern basin margin.

Like for the temperatures, also the lateral variations of heat flow predicted by the model are considerable. The calculated surface heat flow ranges between 80 mW/m² and 125 mW/m² close to salt domes and at the southern basin margin due to the enhanced heat transfer by the geological units with high thermal conductivities. Apart from salt structures predicted values of surface heat flow are lower and vary between 55 mW/m² and 75 mW/m². Likewise, calculated values of heat flow at deeper levels reflect the structural heterogeneities in the model. At 5000 metres depth, values of heat flow are generally lower, reaching 60 mW/m² to 90 mW/m² in the north-western, salt-influenced domain. Reduced heat flow values of 40 mW/m² to 50 mW/m² are characteristic for areas without large salt structures at this depth level.

2.3.2 Comparison with Published Data

Both, the predicted temperature range as well as the modelled surface heat flow are consistent with the general trend of published data, as for example depth-temperature maps derived from 2D interpolation of borehole measurements (Stackebrandt and Manhenke 2002) and the map of surface heat flow (Hurtig et al. 1992). In response to the improved structural resolution of our model concerning the distribution of the highly conductive Zechstein salt, we obtain a more pronounced lateral variation in predicted temperatures compared to published maps. The latter are mainly obtained by interpolation between data points of temperatures measured in wells and may not consistently consider the effects of single salt structures. To assess the consistence with the real measurements a local comparison is therefore required. This comparison is, however hampered by the small amount of published temperature measurements. Comparison between model results and measured temperatures available from literature (Förster 2001) shows that model predictions deviate from measured values by about 10° K. This deviation is in the same range as the standard deviation of corrected Bottom Hole Temperatures and temperature logs (Förster 2001). Possible reasons for the difference between predicted and measured temperatures could be related to both, (1) errors related to the observations or (2) oversimplifications in the model.

The measured BHT – temperatures may not represent equilibrium temperatures. This is indicated by the comparison of uncorrected and corrected BHT values. For corrected values the difference is smaller up to 5° K. Moreover, the difference between modelled and measured temperatures is in the same range as the difference between uncorrected and corrected temperatures (Förster 2001).
The model resolution on one hand and the assumption of laterally constant thermal properties in each layer may not correctly consider the local lithologies.

Future work therefore will focus on the sensitivity of the modelling results with respect to these effects. However, the added value of the model consists in the predictions considering physical principles as well as lateral variations due to the structural characteristics and lateral heterogeneity of physical properties.

2.4 The Geothermal In-Situ Laboratory Groß Schönebeck

To investigate the geothermal field and fluid regime at the Groß Schönebeck site three dimensional coupled fluid and heat transport simulations are carried out. These models enable to quantify the interaction of the different thermal rock properties and their feedback on the temperature and heat flow distribution related to the geological structures on a local scale. The Zechstein salt is of particular interest in this context because of its strong impact on the local geothermal field due to the high thermal conductivity of the salt. Furthermore the quasi-impervious salt decouples the overburden strata from the pre-Zechstein layers. In this regard we present first results from numerical simulations of the coupled heat and fluid transport for the Groß Schönebeck site, discuss the implications for the dominating processes affecting heat transport and the fluid regime but also the limits of smaller scale models.

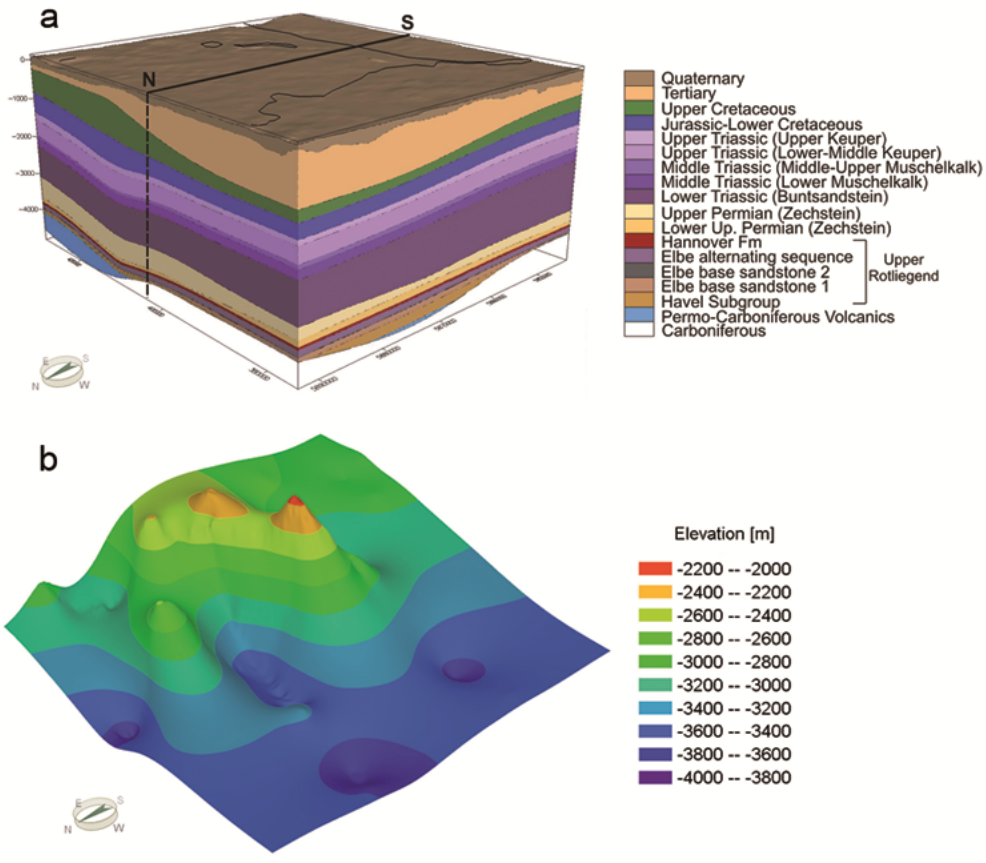

Figure 2.7a 3D geological model of the Groß Schönebeck site consisting of 18 layers from the Carboniferous to the Quaternary. The solid and dotted lines indicate the location of a representative cross-section which cuts the model from north to south. **b** Relief of the Top Zechstein Salt.

For the 3D coupled heat and fluid transport simulations a 3D structural model of the area Groß Schönebeck was available (Moeck et al. 2005) based on data from 15 wells with final depths greater than 4000 m and on six seismic profiles from former gas exploration (Ollinger et al. 2009). The site Groß Schönebeck is located at a NE-SW trending salt ridge which rises from - 4180 to - 2160 m (Fig. 2.7b) and has an average thickness of 700 m. This salt layer divides the sedimentary succession into a supra- and a subsalinar sequence.

From top to bottom, the suprasalinar sequence includes Cenozoic unconsolidated sands, clay and marly limestones, weakly consolidated sand- and siltstone of Cretaceous to Jurassic age, silt- and limestones of Triassic age and Upper Permian evaporites (Ollinger et al. 2009). The latter consist mainly of rock salt as well as of minor anhydrites and carbonates.

The sequence below the salt includes the Permian Upper Rotliegend deposits as well as Permo-Carboniferous Volcanics and Carboniferous rocks. Due to its role as the reservoir target zone, the Permian Upper Rotliegend is well characterised. Accordingly, the deposits are subdivided into the Hannover Formation with mainly mudstones and the Dethlingen Formation which is composed of fine- to coarse-grained sandstones. The Havel Subgroup contains sandstones and clast-supported conglomerates (Holl et al. 2005). Below, the layers consist of volcanic (andesitic) rocks of Late Carboniferous and Early Permian and Carboniferous foliated flyschoid sediments.

2.4.1 Method

For carrying out three-dimensional coupled heat and fluid transport simulations the Finite Element Method (FEM) is used. As a first step the geometry of the layers from the structural model (Moeck et al. 2005) is extracted and transferred into a format applicable for using the FEM. Additionally, the Cenozoic layer has been differentiated into a Quaternary and a Tertiary unit. Thus, the final geological model for the FEM simulations consists of 18 layers (Fig. 2.7a).
For solving the coupled fluid flow and heat transport equations we use the commercial software FEFLOW®. FEFLOW® is a software package for modelling fluid flow and transport processes in natural porous media based on the finite element technique. The governing three partial differential equations of thermal convection in a saturated porous media are based on Darcy`s law, energy and mass conservation laws, e.g. Nield and Bejan (2006). A detailed description of the equations can be found in Appendix 1.

The study area covers a surface of 55 km in E-W and 50 km in N-S direction. This square defines the horizontal extension of the finite element mesh and marks the superelement of the 3D model in

FEFLOW®. Within the superelement, a grid resolution of 250 x 220 grid points is assigned for constructing the finite element mesh representing a horizontal mesh resolution of 220 x 227 meters. The discretised superelement is a 2D surface slice which is multiplied according to the number of geological layers within the model. Each slice has the same mesh discretisation and consists of 54531 (249 x 219) rectangular elements.

To reproduce the geological structure, the z-elevations of the geological layers extracted from the structural model were assigned for each node of the 2D surface in a three dimensional space. The third dimension is entered by vertically connecting the nodes of corresponding elements within two slices.

Table 2.3 Thermal conductivities and radiogenic heat production used for the numerical simulations of the geothermal field for the Groß Schönebeck site; Thermal conductivities and radiogenic heat production for the Cenozoic to Upper Permian Zechstein after Norden and Förster (2006) and Norden et al. (2008); Data used for the Upper Rotliegend Formation to Late Carboniferous for thermal conductivities after Blöcher et al. 2010, for Carboniferous after Ollinger et al. (2009); Values for the radiogenic heat production of the Upper Rotliegend Formation to Carboniferous after Ollinger et al. (2009).

Stratigraphic Unit	Thermal conductivity $[Wm^{-1} K^{-1}]$	Radiogenic heat production $[10^{-7}Wm^{3}]$
Quaternary	1.5	9
Tertiary	1.5	9
Upper Cretaceous	1.9	6
Jurassic - Lower Cretaceous	2.0	15
Upper Triassic (Upper Keuper)	2.3	16
Upper Triassic (Middle - Upper Keuper)	2.3	16
Middle Triassic (Middle - Upper Muschelkalk)	1.85	10
Middle Triassic (Lower Muschelkalk)	1.85	10
Lower Triassic (Buntsandstein)	2.0	18
Upper Permian (Zechstein)	4.5	4
Lower Up. Permian(Zechstein)	4.5	4
Upper Rotliegend (Hannover Formation)	1.9	18
Upper Rotliegend (Elbe alternating sequence)	1.9	14
Upper Rotliegend (Elbe base sandstone 2)	2.9	14
Upper Rotliegend (Elbe base sandstone 1)	2.8	10
Upper Rotliegend (Havel Subgroup)	3.0	12
Permo-Carboniferous Volcanics	2.3	10
Carboniferous	2.7	20

Accordingly, the vertical resolution of the constructed 3D model is therefore a priori determined by the individual thickness of each geological layer. To avoid numerical instabilities, layers of large thickness have been subdivided into sub-layers of identical physical properties. The Lower Triassic Buntsandstein and the Upper Permian Zechstein are in each case subdivided into three layers of equal thicknesses whereas the Quaternary layer is differentiated into two units of equal thicknesses. At the

base of the model a plane is integrated at a constant depth of 5000 m. As a result, the final model consists of 23 layers which results in approximately one and a half million elements in total.

Physical parameters depending on the lithology of the respective geological unit are assigned for each layer. From the equations summarised in Appendix 1, it is obvious, that relevant physical properties influencing the results of simulation are thermal conductivities and radiogenic heat production rates (Tab. 2.3) as well as volumetric heat capacities, porosities and permeabilities (Tab. 2.4). Likewise, the results are depending on the applied initial and boundary conditions. We use a flow boundary condition equal to the topographic elevation to investigate the influence of the topography on the fluid system. A fixed constant temperature of 8 °C is assigned for the top thermal boundary representing the average surface air temperature in north-eastern Germany. For the bottom, a basal heat flux of 50 mWm^{-2} is applied. This value has been extracted from the large-scale thermal model of Brandenburg (Chapter 2.3) for the area in the vicinity of Groß Schönebeck. The lateral boundaries are closed to fluid and heat flow. As a starting point the initial temperature and pressure conditions are obtained from uncoupled steady-state heat transport and fluid flow simulations, respectively.

Table 2.4 Permeabilities, porosities and heat capacities assigned for the coupled heat and fluid transport simulations. Values for the Cenozoic to the Upper Permian Zechstein and for the Carboniferous after Magri (2005); Scheck (1997). Data used for the Upper Rotliegend Formation to Late Carboniferous after Blöcher et al. (2010).

Stratigraphic Unit	Permeability k [m²]	Porosity ε [%]	Rock heat capacity c^s [MJ/m^3K]
Quaternary	1.0E-12	23	3.15
Tertiary	1.0E-12	23	3.15
Upper Cretaceous	1.0E-13	10	2.4
Jurassic - Lower Cretaceous	1.0E-13	13	3.19
Upper Triassic (Upper Keuper)	1.0E-14	6	3.19
Upper Triassic (Middle - Upper Keuper)	1.0E-14	6	3.19
Middle Triassic (Middle - Upper Muschelkalk)	1.0E-18	~ 0	2.4
Middle Triassic (Lower Muschelkalk)	1.0E-18	~ 0	2.4
Lower Triassic (Buntsandstein)	1.0E-14	4	3.15
Upper Permian (Zechstein)	Impervious ~ 0	~ 0	1.81
Lower Up. Permian(Zechstein)	Impervious ~ 0	~ 0	1.81
Upper Rotliegend (Hannover Formation)	1.61E-16	1	2.4
Upper Rotliegend (Elbe alternating sequence)	6.44E-16	3	2.4
Upper Rotliegend (Elbe base sandstone 2)	1.29E-14	8	2.4
Upper Rotliegend (Elbe base sandstone 1)	2.58E-14	15	2.4
Upper Rotliegend (Havel Subgroup)	3.22E-16	0.1	2.6
Permo-Carboniferous Volcanics	3.22E-16	0.5	3.6
Carboniferous	Impervious ~ 0	~ 0	2.7

2.4.2 Results from Simulations of Coupled Heat and Fluid Transfer

Several fluid and heat transport simulations for the Groß Schönebeck model are carried out for 250000 years of simulation time to achieve stable numerical results. The main outcome of our simulations are illustrated along a representative cross-section (Fig. 2.8a) that straightly cuts the model from north to south and shows the impact of the salt structures on the thermal field more in detail.

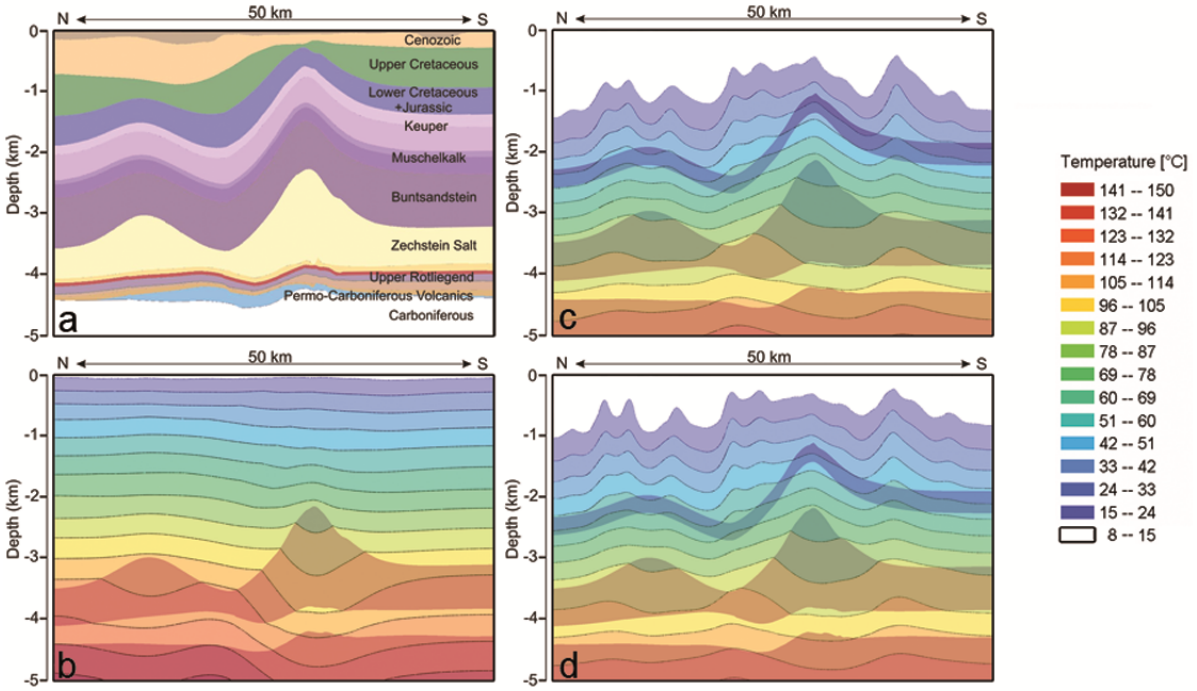

Figure 2.8 N-S cross-section illustrating simulation results, vertical exaggeration 1:7. **a** Representative cross-section cutting the model from north to south with focus on the Zechstein Salt structure. **b-d** Temperature distributions along the cross-section (**a**) after 250000 years of simulation time: for **b** the purely conductive model; **c** model in which the fluid density with a constant thermal expansion coefficient is included; **d** model in which the fluid viscosity taken as function of temperature is considered in addition to fluid density effects with a non-linear variable thermal expansion.

Starting from less coupled simulations, the degree of coupling is step-wise increased during the procedure of modelling. First, the simplest case means a purely conductive model, is calculated to assess the interaction between the different thermal properties and their feedback on the temperature field (Fig. 2.8b).

For this case, the temperature field displays in general nearly flat isotherms. This characteristic pattern reflects the diffusive nature of the conductive heat transfer where molecules transmit their kinetic energy by collision and no motion of the medium is involved. The isotherms are significantly disturbed only in the area of the Zechstein salt. Concave isotherms occur within the salt pillows whereas the isotherms above the salt show less pronounced convex shapes. These thermal anomalies are triggered by the high thermal conductivity of the salt compared to the surrounding sediments. Slightly higher temperatures can be observed where the thickness of the supra-salt sediments increases

to 3500 m. There, the low thermal conductivities result in insulating effects and an accumulation of heat.

Next, a simulation with one more degree of coupling was carried out in which the fluid density is taken into account as a function of temperature with a constant thermal expansion coefficient (Fig. 2.8c). The higher degree of coupling between the governing equations causes convection to take over a major role as a heat transfer mechanism. Convective heat transport is associated with the motion of a medium. When a fluid is heated, its density generally decreases because of thermal expansion and the heated fluid becomes buoyant compared to neighbouring areas of lower fluid temperatures. This leads to upward movement of the heated fluid and thus induces convection. In our model, convection can be observed above the calcareous Middle Triassic Muschelkalk. This unit acts like a quasi-impervious layer with much lower hydraulic permeabilities compared to the overburden sediments. As a consequence, the Muschelkalk layer hydraulically decouples the Lower Triassic Buntsandstein unit from younger strata which leads to the development of two aquifer systems with different hydro-dynamical characteristics.

In the system above the Triassic Muschelkalk, the sediments with higher hydraulic conductivity promote the formation of convection cells. Heated fluids tend to rise easier through the permeable sediments of the post-Muschelkalk succession. Furthermore, convective processes are additionally favoured by the large thickness (up to 3000 m) for the post-Muschelkalk deposits. On the contrary, conduction remains the dominant heat transfer mechanism below the Muschelkalk as indicated by rather flat isotherms of a shape similar to the conductive case. The temperature distribution above the salt domes displays the “chimney effect” which carries away the heat upwards due to the high thermal conductivity of the salt.

One higher degree of coupling between the governing equations involves the fluid density as a function of temperature with a variable thermal expansion coefficient β. In FEFLOW® this relationship is approximated by a 6th order polynomial, meaning that β takes the role of a function being dependent on the temperature which defines a non-linear variable thermal expansion valid for 0-100 °C (Diersch 2002). For increasing the coupling both variable thermal fluid expansion and fluid compressibility within the state equation of density (Eq. 7) are considered by means of approximated coefficients for a wide range of pressures ρ_{sat} with $\rho_{sat}<\rho\leq100$ MPa and for temperatures below 350 °C ($0\leq T\leq350$°C) (Magri 2005). Applying these two approaches for the thermal expansion coefficient during the simulation caused only small variations in the temperature distribution compared to the less coupled model assuming a constant thermal expansion coefficient (Fig. 2.8c).
Significant differences are observed for the temperature field only if fluid viscosity effects are additionally taken into account (Fig. 2.8d). These results refer to calculations adopting the highest

grade of coupling presented where the fluid viscosity taken as function of temperature is considered in addition to fluid density effects with a non-linear variable thermal expansion. A general increase in temperature leads to a decrease in viscosity which subsequently enforces the convective flow. As a result the convection cells above the Muschelkalk unit are clearly more pronounced and reach higher up to the Quaternary layer. In greater depths conduction is again the dominant heat transfer process. The salt induces curved long-wavelength isotherms within the Buntsandstein which reflect the conductive heat regime in this area.

In summary, the 3D numerical simulations of coupled fluid flow and heat transfer processes of the Groß Schönebeck site confirm the strong impact of the Upper Permian Zechstein salt. The latter disturbs the regional temperature field as indicated by strongly curved isotherms within and above the salt structures. Rather flat isotherms show that heat tends to be dominantly transferred by conduction below the impermeable Middle Triassic Muschelkalk deposits. Though the Buntsandstein and the different Rotliegend units are characterised by reasonable permeabilities, their thickness is obviously too small to allow the development of convection cells. Consequently, the coupled models suggest that conduction is an important heat transfer mechanism in regions below the Middle Triassic strata in the subsurface of northern Germany.

In contrast, convection affects heat transport within the up to 3000 m thick, permeable sediments above the Muschelkalk. The integration of fluid density effects causes the formation of convection cells providing a heat transfer mechanism at shallower levels. Considering a variable expansion coefficient, however, does not influence the heat and fluid transport processes strongly. By contrast, temperature dependencies of the fluid viscosity considerably affect the geothermal field. The minor influence of a variable thermal expansion coefficient on the heat and fluid transport could be related to the fact that the absolute temperatures are still too low to cause sufficient thermal expansion in the individual post-Muschelkalk layers.

As a final word of caution we would like to include remarks concerning the limitations of the method. Sources of uncertainty that may be quantified in future studies include: (1) the chosen lateral boundary conditions for the fluid flow and heat transport and (2) the ratio between the vertical to the lateral extent of the model.

2.5 Conclusions

The refined 3D structural model of Brandenburg visualises the 3D configuration of the subsurface including an improved representation of the salt structures. This model can be evaluated to assess the structural heterogeneities and their relevance for the thermal field in the area but also to analyse changes in subsidence dynamics and related halokinetic processes. The 3D distribution of dominant physical properties assigned in the model can be used as a base for process-oriented modelling of subsurface heat transport. Our preliminary models indicate considerable lateral variations of both temperature and heat flow for any depth level which implies two major conclusions:

(1) Geothermal exploration can take advantage of such models that provide a cheap and rapid method aiding in the selection of a drilling location, and (2) the assumption of a constant heat flow or a constant temperature at the base of local, reservoir-scale thermal models may not be appropriate in areas where short wavelength variations of these parameters are present. These results are, however, preliminary and need to go through further testing. In particular, geological units in nature are not laterally uniform as simplified in our approach. Therefore, the sensitivity of the results with respect to laterally changing lithologies and associated physical properties needs to be studied to evaluate the potential thermal effects of these variations.

Our results further demonstrate that combining large-scale regional models with local scale models of a geothermal production site is useful. For the Groß Schönebeck site the 3D numerical simulations of coupled fluid flow and heat transfer processes confirm the strong impact of the Upper Permian Zechstein salt. The outcomes indicate a relevant influence of convective heat transport in the upper 3000 m, where a critical thickness of permeable sediments is achieved. Increasing the degree of coupling has little effect on the temperature range in the upper 3000 m as temperature induced density-differences are too small to impose buoyancy of the fluid. Stronger differences in the temperature distribution are only observed when considering the temperature-dependence of fluid viscosity. However, sources of uncertainty may also be given by the ratio between the vertical and the lateral extent of the model and the chosen lateral boundary conditions for fluid flow and heat transport. Our studies suggest that especially high degrees of coupling result in remarkable convective heat transport. How far this result is valid for other geothermal sites remains uncertain. To assess the sensitivity of the results, further studies are required.

Acknowledgements

We thank our colleagues from the geological surveys of Landesamt für Bergbau, Geologie und Rohstoffe Brandenburg, Landesamt für Geologie und Bergwesen Sachsen-Anhalt and Landesamt für Umwelt, Naturschutz und Geologie Mecklenburg-Vorpommern for providing additional well data and for helpful discussions. Mauro Cacace supported us with valuable advices about the physical principles behind the applied simulation methods. The project received financial support from the project GeoEn of BMBF and from Helmholtz Centre Potsdam GFZ German Research Centre for Geosciences. This paper was greatly improved by the comments of three reviewers: R. Kirsch, S. Mazur and K. Obst. This work is part of GeoEn and has been funded by the German Federal Ministry of Education and Research in the programme ‘‘Spitzenforschung in den neuen Ländern’’ (BMBFGrant03G0671A/B/C).

3 Sensitivity of 3D Thermal Models to the Choice of Boundary Conditions and Thermal Properties: a Case Study for the Area of Brandenburg (NE German Basin)

Abstract

Based on newly available data of both, the structural setting and thermal properties, we compare 3D thermal models for the area of Brandenburg, located in the Northeast German Basin (NEGB), to assess the sensitivity of our model results. The structural complexity of the basin fill is given by the configuration of the Zechstein salt with salt diapirs and salt pillows. This special configuration is very relevant for the thermal calculations because salt has a distinctly higher thermal conductivity than other sediments.

We calculate the temperature by using a FEMethod to solve the steady state heat conduction equation in 3D. Based on this approach we evaluate the sensitivity of the steady-state conductive thermal field with respect to different lithospheric configurations and to the assigned thermal properties. We compare three different thermal models: (a) a crustal-scale model including a homogeneous crust, (b) a new lithosphere-scale model including a differentiated crust and (c) a crustal-scale model with a stepwise variation of measured thermal properties. The comparison with measured temperatures from different structural locations of the basin shows a good fit to the temperature predictions for the first two models, whereas the third model is distinctly colder. This indicates that effective thermal conductivities may be different from values determined by measurements on rock samples. The results suggest that conduction is the main heat transport mechanism in the Brandenburg area.

3.1 Introduction

Large-scale 3D thermal models are useful in the planning state of geothermal production sites, as they provide comprehensive information about structural heterogeneities and their relevance for the thermal field in potential exploitation areas.

We present new results from 3D thermal modelling in the area of Brandenburg in north-eastern Germany (Fig. 3.1a) based on a recently published structural model (Noack et al. 2010) of the basin fill with an improved representation of the salt structures.

The study area is located in the south-eastern part of the Northeast German Basin (NEGB) within the Central European Basin System. As the formation of the basin started with extensive volcanism in the Late Carboniferous/Early Permian the lowermost geological unit of the basin fill is composed of volcanic rocks (Benek et al. 1996).

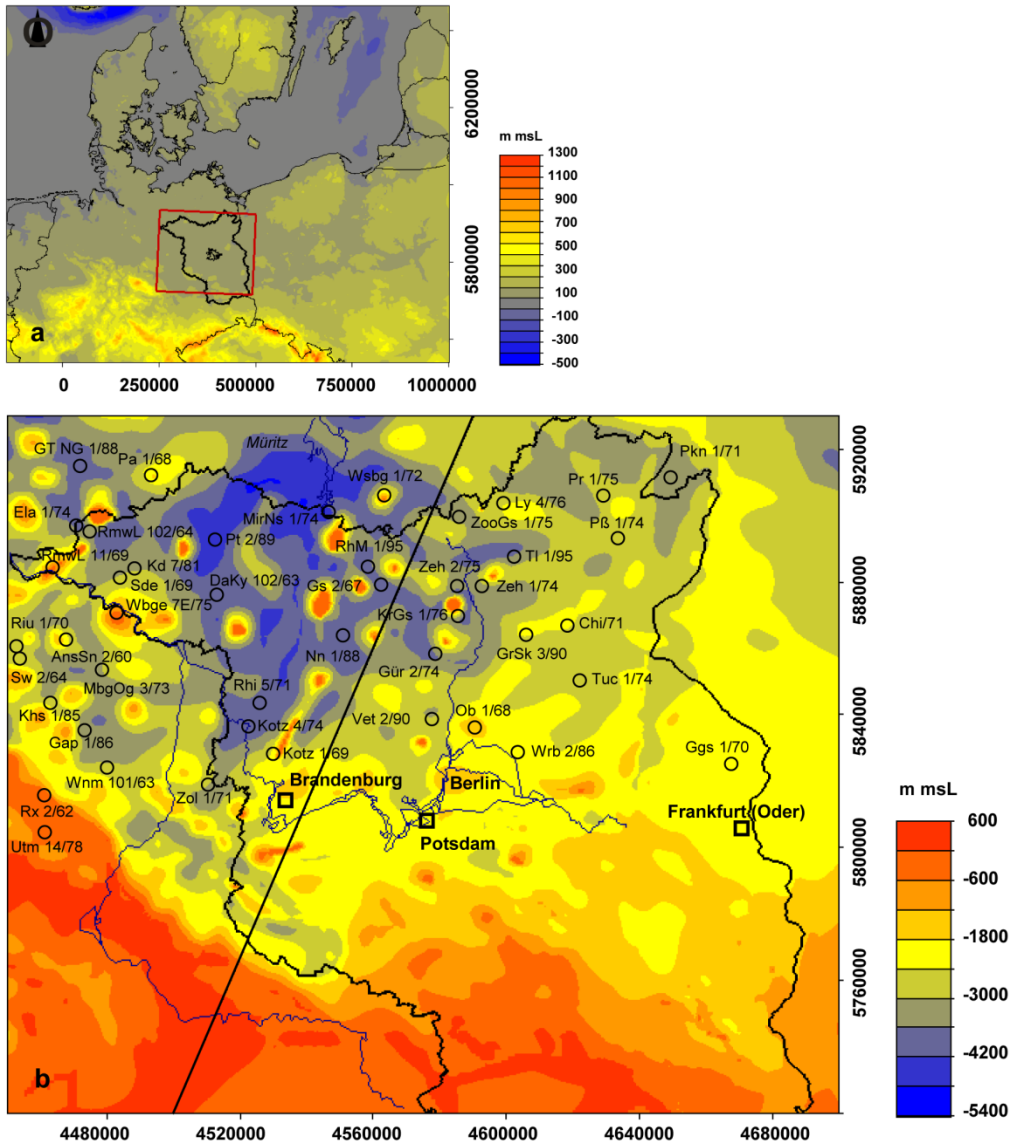

Figure 3.1a Location of study area with topography in UTM Zone 33N (ETOPO1, after Amante and Eakins (2009) of Central Europe. Large red rectangle encloses the area covered by the 3D thermal models of Brandenburg, black line delineates the border of Brandenburg. **b** Top of the Zechstein salt for the model area with location of wells where measured temperatures are available. Coordinates are Gauss Krüger zone 4. Black line indicates the location of a representative, NNE-SSW orientated cross section which cuts major geological structures across the model.

Above the volcanic rocks, the Permian to Cenozoic sediment fill attains a thickness of up to 8000 m in the central part of the NEGB (Schwab 1985; Scheck and Bayer 1999). The structural setting in the basin is mainly influenced by a layer of strongly mobilised Upper Permian Zechstein salt.

Reconstructions of the initial thickness of the Zechstein salt indicate the highest thickness of up to 2500 m in the north-western basin centre, but halokinetic movements generated local structures such as salt pillows and salt diapirs, where much larger thicknesses occur (Scheck et al. 2003b). Also, the deep structure of the basin is differentiated, as the sediments are underlain by crustal domains that have different consolidation ages (Maystrenko and Scheck-Wenderoth 2011).

Accordingly, the structural setting of the modelled area in Brandenburg is highly complex (Fig. 3.1b). In the northwest, the area comprises a part of the basin centre of the NEGB, where the base of the Permian-Cenozoic basin fill reaches depths of more than 8000 m (Noack et al. 2010). In the south, the inverted southern margin of the basin is included, where the crystalline crust comes close to the surface. In the basin area, the structural setting is mainly determined by the configuration of the Zechstein salt, which is characterized by numerous salt pillows and diapirs, surrounded by areas where the salt has been withdrawn. Diapirs piercing their overburden reach structural amplitudes of up to 4500 m (Noack et al. 2010). These salt structures are surrounded by salt rim synclines of various Mesozoic and Cenozoic ages. The largest of these rim synclines are of Tertiary age and filled with up to 2000 m thick clastic sediments (Noack et al. 2010).

The geothermal field of the NEGB and thus also the area of Brandenburg have been investigated with different focus and on different scales during the last 50 years. Initial studies of the surface heat flow density in the area of Brandenburg have already been carried out by Schössler and Schwarzlose (1959). These studies were followed by investigations on the relationship between the thermal field and the deep structural setting in northern Germany (e.g. Hurtig 1975; Hurtig and Oelsner 1979). Maps of the surface heat flow density and temperature maps at different depths have been provided by Hurtig et al. (1992) for entire Europe. According to these maps, a large positive anomaly in heat flow stretches from Poland to the river Elbe, crossing the area of Berlin. Also published temperature maps at 1000 m depth and 2000 m depth indicate high temperature anomalies related to areas in the north-west and south-west of Brandenburg. These published maps of temperature and heat flow were based on interpretations of corrected temperatures, measured by continuous thermal logging in wells. Beer (1996) presented a temperature map covering the area of Brandenburg and proposed a tentative empirical correction method for temperature measurements, later improved by Förster (2001). In this way, a new thermal database for the NEGB was provided, additionally including data of both thermal conductivity and radiogenic heat production determined on drill cores and well-logs (Norden and Förster 2006; Norden et al. 2008; Fuchs and Förster 2010).
Already Ollinger et al. (2010) pointed out that calculations of the thermal field are most sensitive to the variations in thermal conductivity. They conclude this from sensitivity analyses for thermal conductivities in the sedimentary layers assuming a constant basal heat flow of 60 m mW/m² for the geothermal site Groß Schönebeck in NE Germany.

In addition, the relationship between the structural setting and the thermal field within the NEGB has been investigated by large-scale thermal models based on 3D Finite Element simulations (Bayer et al. 1997; Scheck 1997). Assuming a homogeneous crust down to 30 km depth and a heat flow of 25 mW/m² as lower boundary condition at the base of the crust, these models were able to reproduce the generalized pattern of the temperature distribution in the temperature maps published earlier (Hurtig et al. 1992). These works focussed on the effect of alternative lower boundary conditions. They compared the resulting thermal field for a fixed temperature of 600 °C and a fixed heat flow of 25 mW/m² at the crust-mantle boundary (Moho). Concerning the structural setting of the basin fill these models also included the Zechstein salt, though with a limited horizontal resolution of 4 km (Bayer et al. 1997; Scheck 1997; Ondrak et al. 1998). However, these models already demonstrated that the salt structures control the short-wavelength pattern of heat flow as well as of the temperature distribution. In the shallow part of the basin, a more recent 3 D thermal model with an improved resolution of 1 km has assessed this influence for the present-day thermal field of Brandenburg (Noack et al. 2010). The improved representation of the salt structures allowed to evaluate the influence of structural heterogeneities on the temperature distribution. Due to the specific configuration of the salt diapirs and their surrounding clastic sediments and carbonates a phenomenon in the temperature distribution can be observed which is known as "chimney effect". This effect occurs due to the interaction between the thermally highly conductive Zechtsein salt and the low conductive clastic rocks. Thereby, the highly conductive salt efficiently transports the heat to the surface within the salt diapirs, whereas the neighbouring lower conductive clastics and carbonates act as insulating layers. This leads to cooling effects within and below the salt. In contrast, the thick low conductive sediments act as a thermal blanket and cause the storage of heat below. The result is a very characteristic temperature distribution around the salt structures. Compared to the neighbouring insulating layers, the 3D thermal model predicts higher temperatures at the same depth in the top region of the diapirs and lower temperatures within and below. This modelling result is confirmed by observed temperatures as for example at the diapir Kootzen in Brandenburg (Beer and Hurtig 1999).

Other studies focussed on the base of the lithosphere-asthenosphere boundary (LAB) as lower boundary condition. It is generally assumed that the base of the lithosphere is represented by the 1300 °C isotherm, at which partial melting of peridotite occurs (Turcotte and Schubert 2002). To constrain the depth and geometry of the LAB Cacace and Scheck-Wenderoth (2010) tested different seismological models. Maystrenko and Scheck-Wenderoth (2011) developed a lithospheric configuration for the entire Central European Basin System that is consistent with temperature and gravity observations. Apart from that, Norden et al. (2008) investigated the sensitivity of the thermal field in the NEGB with respect to different configurations of the lithosphere. All these earlier studies provided basic results to investigate the main controlling factors on the 3D thermal field.

Newly available data of both, the structural setting of the deeper lithosphere of Brandenburg and of thermal rock properties measured in wells of the NEGB, enabled us to better constrain thermal models. The new aspects of this paper concern the validation of earlier models in that we address the sensitivity of our results with regard to specific controlling factors of the 3D conductive field. These are the lithosphere configuration and the chosen boundary conditions, as well as the chosen thermal properties of the geological units. Thus, this approach permits to estimate to which degree specific assumptions for the configuration of the deeper lithosphere and as well as for the thermal properties influence the pattern of the conductive thermal field. Moreover, we address the thermal interaction between different crustal configurations and the sedimentary overburden and their effects on heat transport within the basin. Besides of this our systematic analysis reveals if the assumption of dominantly conductive heat transport is generally valid or if areas exist where this assumption is inconsistent with observations.

We focus on the 3D conductive thermal field using a Finite Element Method (FEM) and assume steady-state conditions for the model area. To evaluate the sensitivity of our 3D conductive thermal model with respect to different parameters, we run a series of simulations of which we present 3 different thermal models as end member scenarios. Thereby, the configuration of the lithosphere is the first parameter addressed, followed by an evaluation of the influence of different thermal properties. To validate our model results we compare modelled temperatures with temperatures observed in 45 wells (Fig. 3.1b).

3.2 Method

Assuming that heat moves predominantly by conduction through the lithosphere (Fowler 1996), we assess the regional thermal field by solving the three-dimensional equation of heat conduction (Bayer et al. 1997). Ignoring temperature and pressure dependence of the coefficients, the principle equation is:

$$c\rho(\delta T/\delta t) = \mathrm{div}(\lambda \mathrm{grad} T) + S$$

(where c is heat capacity, ρ is density, T is temperature, λ is thermal conductivity, gradT is the temperature gradient, t is time, and S is radiogenic heat production). Furthermore, we assume an equilibrium situation for the model area and calculate the temperature by solving numerically the conductive heat equation for steady-state conditions ($\delta T/\delta t = 0$):

$$0 = \mathrm{div}\,(\lambda\ \mathrm{grad}\ T) + S$$

using a 3D FEM (Bayer et al. 1997). Thus, the temperature distribution does not depend on heat capacitiy and density, but is sensitive to the values of the thermal parameters thermal conductivity (λ) and radiogenic heat production (S) as well as to the choice of boundary conditions. In consequence of the stationary approach the system of linear equations is solved iteratively until the stationary solution is achieved. The FEM is based on the conjugated gradient solver with an iteration limit of 1.e-5. The model units are discretized as deformed 8-noded prisms with a grid resolution of 1 km and 250 x 210 grid points in horizontal direction. The vertical length of the elements corresponds to the thickness of the layers. For the temperature calculations we use the software Geological Modelling System (GMS, developed at GFZ Potsdam, Bayer et al. 1997).

As upper boundary condition we assign a fixed temperature of 8 °C at the surface, which corresponds to the average annual surface temperature in the area. The lateral boundaries are considered closed. We use the 3D structural model of Brandenburg (Noack et al. 2010) as a starting point for the calculations of the temperature field. This model comprises an area of 250 km x 210 km horizontally with a horizontal resolution of 1 km and extends downward to the top Pre-Permian surface. The vertical resolution of the model is defined by the number of layers resolved in the model. The model integrates 11 layers of the basin fill (Fig. 3.2a) consisting from top to bottom of: Quaternary, Tertiary, Upper Cretaceous, Lower Cretaceous, Jurassic, Triassic Keuper, Triassic Muschelkalk, Triassic Buntsandstein, Permian Zechstein, Permian Rotliegend (post-volcanic) and Permo-Carboniferous Volcanics.

As mentioned above, the structural setting in the basin fill is controlled by the distribution of the Zechstein salt. This concerns both the configuration of the highly irregular top salt surface as well as of the base of the salt. At the south-western basin margin, the pre-Zechstein basement is uplifted by about 5 km south of the Gardelegen fault (Scheck-Wenderoth et al. 2008). Apart from this area, the base of the Zechstein salt is a comparatively flat surface, which reaches up to 5000 m depth in its deepest part in the north-west (Fig. 3.2b). This north-western part of the model is characterized by the most mature salt diapirs and by areas of close-to zero present-day thickness of the salt where salt has been removed (Fig. 3.2c). The structural configuration of the basin fill is the same for all thermal models in this study.

For the temperature calculation, we assign lithology-dependent physical properties constant to each stratigraphic unit of the model depending on the dominant lithology of the respective units (Tab. 3.1).

The thermal model 1 reaches downward to the crust-mantle boundary (Moho) and integrates a homogeneous layer for the Pre-Permian crust. For this model a basal heat flow of 30 mW/m² at the Moho is adopted as lower boundary condition following earlier studies (Noack et al. 2010).

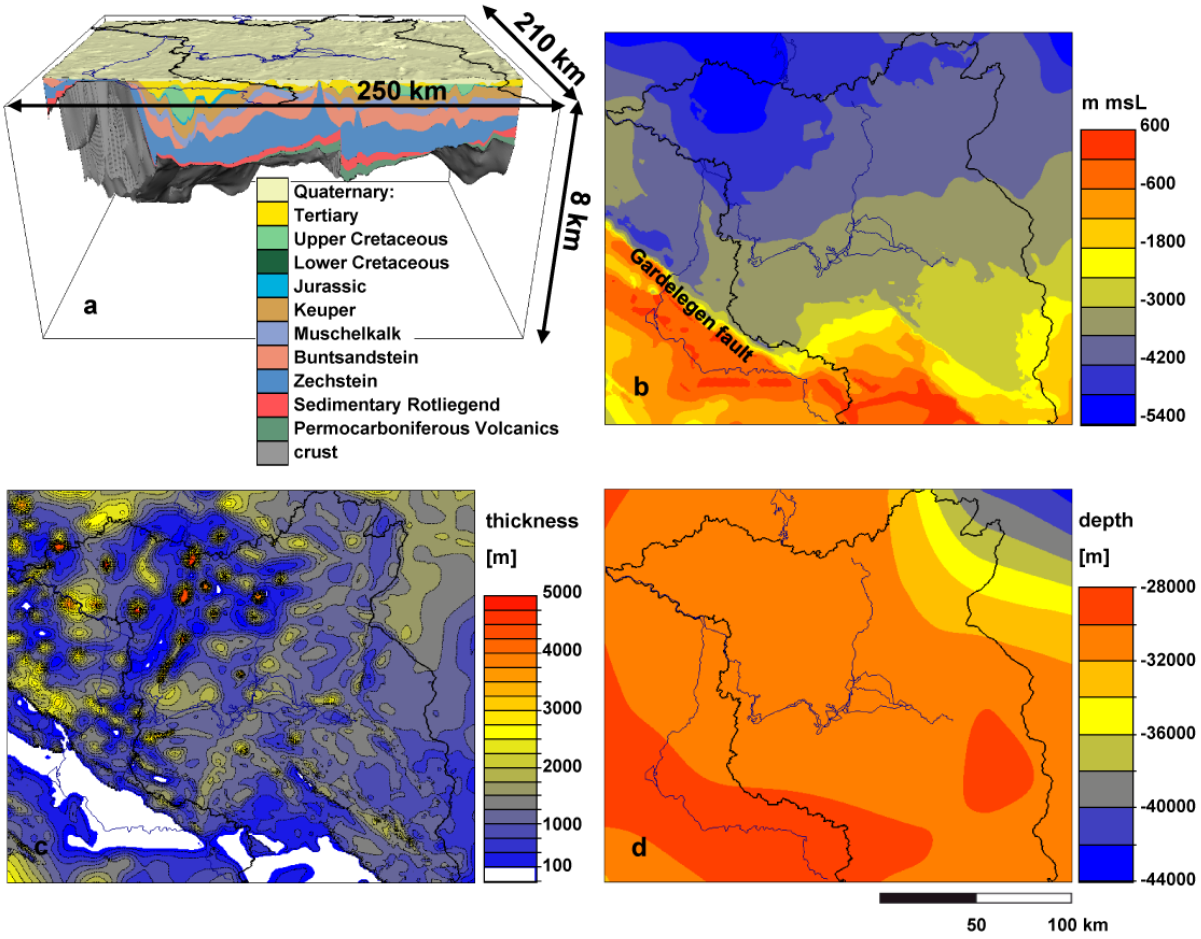

Figure 3.2a 3D view on the structural configuration of the Permian to Cenozoic basin fill with colour key for the stratigraphic units differentiated in the model. **b** Base of Permian Zechstein salt (modified after Noack et al. 2010). **c** Thickness of Permian Zechstein salt (modified after Noack et al. 2010). **d** Depth of the crust-mantle boundary of the crustal-scale thermal model.

For the new thermal model 2 we change the lower boundary condition by extending the model downward to the lithosphere-asthenosphere boundary (LAB) and by considering a differentiated crust. Here a fixed temperature of 1300 °C is assumed as lower boundary condition at the base of the LAB (Turcotte and Schubert 2002; Scheck-Wenderoth and Maystrenko 2008). For both models we assign the same thermal properties after Bayer et al. (1997) for the Permian to Cenozoic units. In thermal model 3 we use the same configuration of the crust and thus the same lower boundary condition of 30 mW/m² at the Moho as used for model 1, but assign measured thermal properties after Norden and Förster (2006); Norden et al. (2008) and Fuchs and Förster (2010) for the respective units.

Table 3.1 Assigned physical properties for geothermal modelling: for the lithological characteristics dominant lithology is mentioned first. Values for the thermal properties are assigned following earlier studies for model 1 and model 2 after Bayer et al. 1997. Measured values used for model 3: (a) radiogenic heat production and thermal conductivity data after Norden and Förster (2006), (b) thermal conductivity data after Fuchs and Förster (2010) and (c) after Norden et al. (2008); additional input thermal properties used for the differentiated lower lithosphere of model 2; thermal properties for the Pre-Permian after Bayer et al. 1997; for the upper crust and the lower crust after Norden et al. (2008) and for the lithospheric mantle after Scheck-Wenderoth and Maystrenko (2008).

Stratigraphic Unit	Lithology	λ [W/(m K)] Model 1, 2	S [W/m³] Model 1, 2	λ [W/(m K)] Model 3	S [W/m³] Model 3
Quaternary	Sand, Silt and Clay	1.50	0.70e-6	1.80[c]	0.9e-6[a]
Tertiary	Sand, Silt and Clay	1.50	0.70e-6	1.80[c]	0.9e-6[a]
Upper Cretaceous	Limestone (Chalk)	1.90	0.30e-6	3.04[b]	0.6e-6[a]
Lower Cretaceous	Clays with Sand and Silt	2.00	1.40e-6	2.71[b]	1.5e-6[a]
Jurassic	Clays with Sand, Silt and Marl	2.00	1.40e-6	2.71[b]	1.5e-6[a]
Keuper	Clays with Marl and Gypsum	2.30	1.40e-6	2.35[b]	1.6e-6[a]
Muschelkalk	Limestone	1.85	0.3e-6	2.30[b]	1.0e-6[a]
Buntsandstein	Silts with Sand, Clay and Evaporite	2.00	1.00e-6	2.58[b]	1.8e-6[a]
Zechstein	Evaporites	3.50	0.09e-6	4.50[c]	0.4e-6[a]
Sedimentary Rotliegend	Clay-, Silt- & Sandstone	2.16	1.00e-6	3.30[a]	1.4e-6[a]
Permo-Carboniferous Volcanics	Rhyolithe and Andesite	2.50	2.0e-6	2.50[a]	2.6e-6[a]

Stratigraphic Unit	Lithology	λ [W/(m K)] Model 1, 3	S [W/m³] Model 1, 3
Crustal Configuration			
Homogenous	Granite to Granodiorite	2.55	1.5e-6

Stratigraphic Unit	Lithology	λ [W/(m K)] Model 2	S [W/m³] Model 2
Differentitated			
Praepermian	Strongly compacted clastics	2.65	1.5e-6
Upper Crust	Granite to Granodiorite	3.10 (2.70)	2.5e-6 (2.0)
Lower Crust	Gabbro	2.70 (2.30)	0.8e-6 (0.6)
Lithospheric mantle	Peridotite	3.95	0.03e-6

Table 3.2 Summary of the characteristics for the calculated models.

Model	Thermal properties of sediments	Crustal structure	Boundary conditions	
1	After Bayer et al., 1997	Homogenous	Moho	30 mW/m²
2	After Bayer et al., 1997	Differentiated	LAB	1300 °C
3	Measured thermal properties	Homogenous	Moho	30 mW/m²

The models differ according to the characteristics presented in Table 3.2. As mentioned before, we use the same structural configuration of the basin fill for all models. Likewise, the upper boundary is fixed for all models with an average annual surface temperature of 8 °C at the surface. Because of that, model 2 differs from model 1 and model 3 in both their lower boundary condition and their composition of the lithosphere.

To validate our model results a database including 84 temperature measurements (Tables 3.3, 3.4) is available for the area of Brandenburg (Förster 2001 and Norden et al. 2008). This database offers (1) temperatures at total depth from the equilibrium temperature logs, (2) temperatures corrected at total depth of perturbed temperature logs and (3) corrected Bottom-Hole Temperatures. As can be seen in Tables 3.3 and 3.4, the temperatures originate from different wells and reach various depths and stratigraphic levels. Figure 3.1b shows the lateral distribution of these wells displayed on the top of the salt surface and illustrates their position with respect to different structural elements across the model area. Some of the measurements have been made within the deepest part of the basin in the north-west, but also in areas where the salt has partly been removed. Moreover, observations were also available at the basin margins in the south-west and in the east.

3.3 Results

3.3.1 Different Configurations of the Lithosphere

For the lithosphere below the Paleozoic to Cenozoic deposits we test two different configurations. In model 1 the Pre-Permian crust is defined by a homogeneous layer of granitic to granodioritic composition (Tab. 1) which is limited downward by the Moho. The shallowest position for the Moho is observed at ~ 30 km depth at the south-western basin margin (Fig. 3.2d), where the sub-Permian is thickest and comes close to the surface. From there, the Moho descends gently northward across the basin. In the north-eastern edge of the model the Moho deepens considerably to 40 km depth. The crust itself is characterized by a very large volume with a higher thermal conductivity and a higher radiogenic heat production than the sediments and thus also mimics the heat input of the crystalline crust (Tab. 3.1).

For model 2 newly available data describing the configuration of the deeper lithosphere in the area permitted to define a more realistic lithosphere-scale model (Maystrenko and Scheck-Wenderoth 2011). The latter is based on deep seismic experiments and constrained by 3D gravity modelling. Accordingly, the depth level of both an improved Moho and the lithosphere-asthenosphere boundary (LAB) are integrated.

Table 3.3 Observed temperatures in wells used for model validation: T at total depth (TD) of temperature log, for perturbed logs corrected temperature at TD of log and corrected bottom-hole temperatures after Förster (2001).

Well	TD of log/ depth of BHT [m]	T at TD of log [°C]	Tcorr. at TD of log [°C]	BHT corr. [± 3 °C]	BHT corr. [± 10 °C]	T of model 2 [°C]
AnsSn/Arendsee 2/60	1500	69.8				77
Chi/Chorin 1/71	3800	144.3	147			146
DaKy/Dannenwalde 102/63	1250	49.8				60
Ela/Eldena 1/74	5150	169.8	181			190
Gap/Garlipp 1/86	4580	149.7	156			169
Ggs/Gorgast 1/70	3250	120.8	124			129
Gs/Gransee 2/67	5050	181.9				186
Gür/Grüneberg 2/74	4100	157	161			165
Khs/Kahrstedt 1/85	2300	105				104
Kd/Karstädt 7/81	900	43.4	45			49
Kotz/Kotzen 1/69	4450	144.4	150			159
Kotz/Kotzen 4/74	5500	172.6	181			198
KrGs/Kraatz 1/76	4350	162	168			169
Ly/Lychen 4/76	4700	154.7	163			167
MbgOg/Meseberg 3/73	4100	148	151			149
MbgOg/Meseberg 3/73	4950				173	177
MirNs/Mirow 1/74	4400	149.2	154			148
MirNs/Mirow 1/74	6040				205	193
MirNs/Mirow 1/74	6820				233	214
Nn/Neuruppin 1/88	2081	78.9				94
GT NG/Neustadt-Glewe 1/88	2284	100.5				98
Ob/Oranienburg 1/68	4200	124	132			156
Pa/Parchim 1/68	6150	188	200			195
Pkn/Penkun 1/71	4100	142.6	144			154
Pkn/Penkun 1/71	5500				189	195
Pß/Polßen 1/74	4000	143.4	152			148
Pr/Prenzlau 1/75	4400	151.5	160			159
Pt/Pritzwalk 2/89	2145	81.1				95
RmwL/Rambow 102/64	1950	80				88
RmwL/Rambow 11A/69	4250	139.8				160
RhM/Rheinsberg 1/95	1600	66.1				75
Rhi/Rhinow 5/71	5200	179	182			188
Riu/Riebau 1/70	3500	149.5				139
Rx/Roxförde 2/62	2850	97	113			114
Sw/Salzwedel 2/64	3650	142.6	147			144
Sde/Schilde 1/69	2400	109.5	111			103
Tl/Templin 1/95	1652	69.3				82
Tuc/Tuchen 1/74	4250	139.8	147			167
Utm/Uthmöden 14/78	790			35		40
Utm/Uthmöden 14/78	950			40		45
Vet/Velten 2/90	1650	64.5				82
Wrb/Wartenberg 2/86	1749	71.9				88
Wsbg/Wesenberg 1/72	4250	145.5	149			147
Wsbg/Wesenberg 1/72	5093			184		174
Wbge/Wittenberge 7E/75	5200	171.2	181			172
Wnm/Wittenmoor 101/63	550	28.2				35
Zeh/Zehdenick 2/75	3650	139				146
Zeh/Zehdenick 1/74	4250	159.5	162			170
Zol/Zollchow 1/71	4100	149.8	161			158
ZooGs/Zootzen 1/75	5000	165	173			177

Table 3.4 Observed temperatures in wells used for model validation after Norden et al. (2008).

Well	Depth [m]	Temperature [°C]	Quality	T of model 2 [°C]
GrSk/Groß Schönebeck 3/90	2800	119.9	unperturbed	121
	3770	135.1	unperturbed	144
	4230	148.6	unperturbed	160
	4286	150.8	unperturbed	162
Gs/Gransee 2/76	4100	156.8	unperturbed	159
	4150	157.9	unperturbed	160
	4200	159	unperturbed	162
	4600	170	unperturbed	174
	4650	171.1	unperturbed	175
	4750	173.2	unperturbed	178
	4800	174.8	unperturbed	180
	5000	181	unperturbed	185
RmwL/Rambow 11/A 69	500	36.2	unperturbed	45
	750	42.3	unperturbed	52
	1700	67.6	unperturbed	79
	1950	75.2	unperturbed	86
	3200	107.3	unperturbed	122
	3450	113	unperturbed	129
	3500	114.3	unperturbed	131
Chi/Chorin 1/71	2900	126.6	slightly perturbed	123
	3650	139.8	slightly perturbed	141
Sw/Salzwedel 2/64	2850	122.6	slightly perturbed	123
	3000	126.5	slightly perturbed	126
	3150	129.2	slightly perturbed	129
	3250	131.1	slightly perturbed	131
	3350	133	slightly perturbed	134
Gap/Garlipp 1/86	3400	125	corrected	135
	3800	131	corrected	145
	3850	131.7	corrected	147
	4150	138.2	corrected	156
	4200	139.2	corrected	158
	4350	142.2	corrected	162
	4400	143.7	corrected	163
	4500	149.7	corrected	166

Moreover, the crystalline crust is differentiated into a layer of Pre-Permian sediments, an upper layer of silicic composition and a lower layer of mafic composition. Thus, the new lithosphere-scale structural model integrates additional layers for the Pre-Permian, the upper crust, the lower crust and the upper mantle downward to the LAB. For the refined lithospheric part we assign in the same way thermal properties (Tab. 3.1) corresponding to their main lithologies. These are taken for the upper crust and the lower crust after Norden et al. (2008); for the Pre-Permian after Scheck (1997) and for the lithospheric mantle after Hofmeister (1999) and Scheck-Wenderoth and Maystrenko (2008). According to its granitic composition the thermal conductivity of the upper crust is distinctly higher than that of the sediments. Additionally the radiogenic heat production is nearly three times higher

than that for the lower crust. This crustal contribution in concert with the crustal configuration strongly controls the heat input from the crust. The thickness of the upper crust in model 2 (Fig. 3.3a) increases rapidly from less than 6 km in the north-western part of the model to ~ 24 km in the south-east. The largest thickness (up to 30 km) is reached at the basin margin in the south-west. This configuration is important for the temperature calculation as the granites of the upper crust produce large amounts of radiogenic heat (Tab. 3.1).

A complementary pattern to the thickness of the upper crust is visible for the underlying lower crust (Fig. 3.3b). The lower crust is thickest (with up to 20 km) in the north-western part of the model, whereas the thickness of this layer decreases to less than 4 km to the south and the east.

Similar to model 1 the shallowest position for the new Moho is observed at ~ 30 km depth at the south-western basin margin (Fig. 3.3c). Towards the basin the Moho descends in a NNW-SSE oriented depression, rises up and descends again in the north-eastern edge of the model.

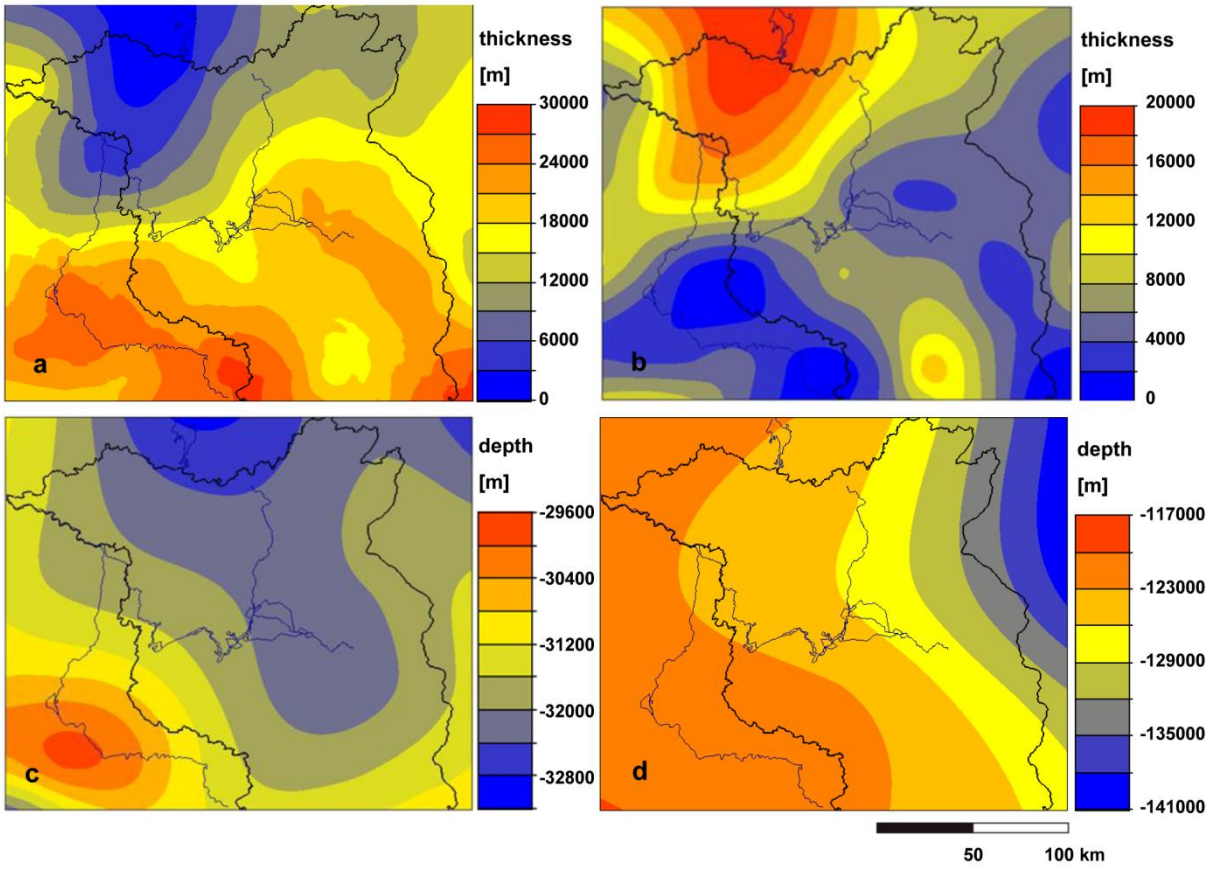

Figure 3.3a Thickness of Upper crust. **b** Thickness of lower crust. **c** Depth of the crust-mantle boundary of the lithosphere-scale thermal model. **d** Depth of lithosphere-asthenosphere boundary of the lithosphere-scale thermal model.

The LAB as the lowermost boundary of the model reaches a depth of ~120 km in the western part, and descends with a gentle gradient to ~ 140 km in the north-eastern part (Fig. 3.3d) of the model. The lithosphere mantle is assumed to consist of peridotite and accordingly is characterized by a lower radiogenic heat production than the crust, but also a relatively high thermal conductivity (Tab.3.1).

To estimate how far these two different configurations of the deeper lithosphere and thus different conditions for the basal heat input, affect the model results we run a sensitivity analysis for both the crustal-scale model 1 and the lithosphere-scale model 2 using thermal properties after Bayer et al. 1997 and compare their results. Since the thermal properties vary within a certain range and no measurements within the deeper lithosphere are possible, we run sensitivity analyses to estimate the influence of these variations for the crystalline rocks (Table 3.1, minimum end member values in brackets). A comparison between the crustal-scale model 1 and the lithosphere-scale model 2 allows us to test, how far it is justified to apply a crustal-scale boundary condition, as it is the case if we use a constant heat flow of 30 mW/m² at the Moho.

The crustal-scale structural model that corresponds to models 1 is illustrated along a representative SSW-NNE oriented cross section (see Fig. 3.1b) down to 30 km depth (Fig. 3.4a). In the southwest the cross section cuts the inverted southern basin margin and continues further through the basin centre along the salt structures to the NNE. Aside the legend shows the thermal conductivities that have been assigned to each layer for model 1. Fig. 3.4b visualizes the temperature distribution obtained for model 1 from the basin margin to the salt structures of the basin centre.

The isotherms are bent downward below the basin margin and upward at the basin centre, as can be seen below the 5 km depth level. This observation is even more distinct in a zoom in on the basin fill (Fig. 3.4c and Fig. 3.4d). These figures illustrate the impact of both the high thermal conductivity of the salt diapirs and the crust on the temperature distribution down to 5 km depth. The temperatures at the 5km depth level vary laterally across the basin and decrease towards the basin margin in the southwest by about 50 °C. Highest temperatures are predicted at 2 km depth in the proximity of the most significant diapir in the basin centre, where the thickness maxima of the clastic overburden are largest above the salt diapirs. There, additional structural complexity comes from the salt rim synclines which are filled with up to 2000 m weakly consolidated low conductive Tertiary clastics (Noack et al. 2010). Lowest temperatures occur at the basin margin, where the highly conductive crust comes close to the surface and no significant sedimentary cover is present. Consequently, heat can efficiently escape in these areas.

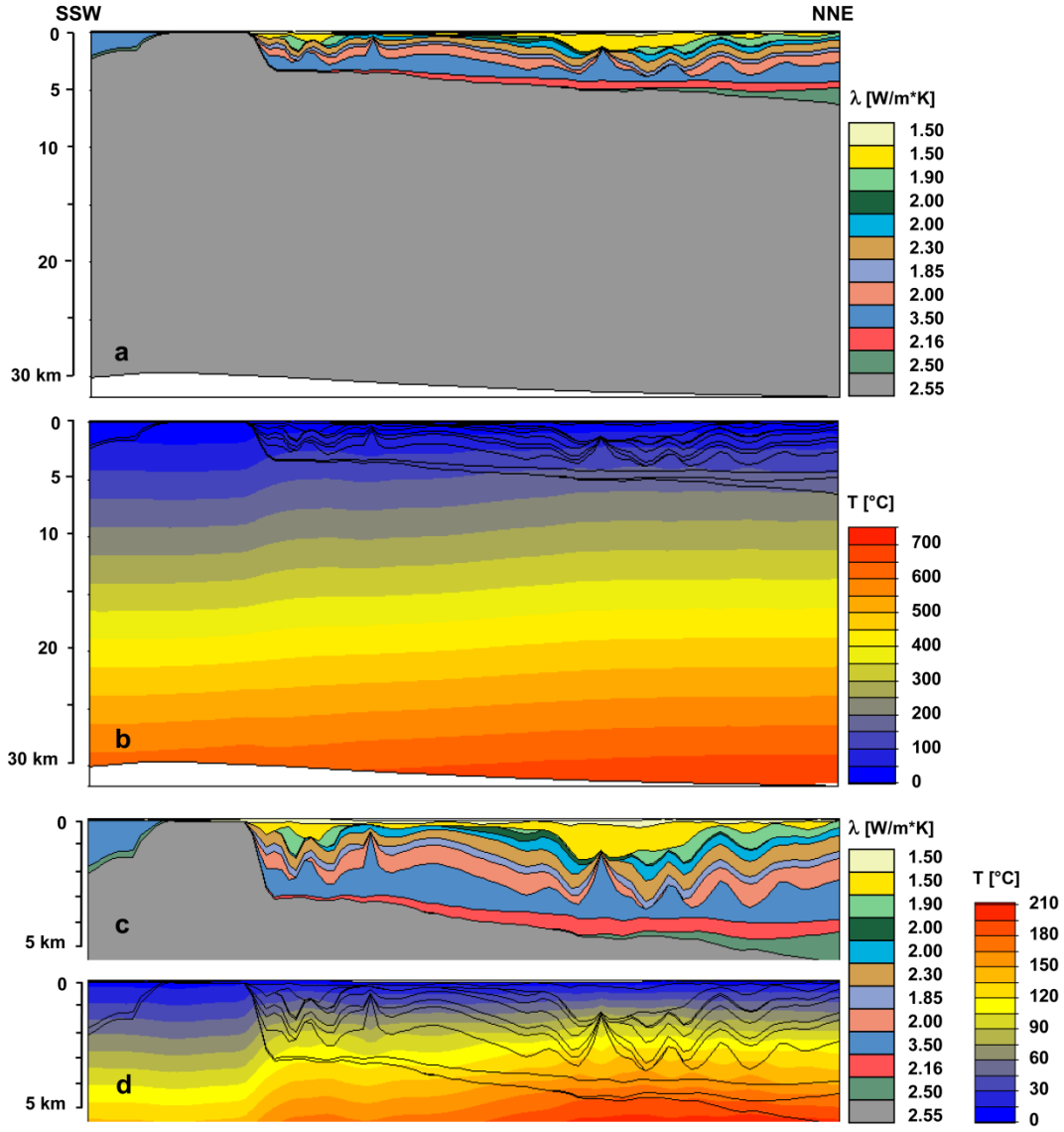

Figure 3.4a NNE-SSW oriented cross section through the 3D crustal-scale structural model with colour key for the assigned thermal conductivities. **b** Modelled temperatures along the same cross section for thermal model 1. **c** Zoom in to the shallow part of the cross section down to 5 km. **d** Zoom in on modelled temperatures in (b).

The lithosphere-scale structural model 2 is displayed in Fig. 3.5a down to the LAB along the same cross section as in Fig. 3.4. The scale bar of the legend shows in addition to the basin fill the conductivities for the refined crystalline crust and the mantle used in model 2. The configuration of the upper crust displays a thickening towards the basin margin in the SSW, whereas the thinning of the upper crust in the NNW is accompanied by a thickening of the lower crust (Fig. 3.5a). The base of the 1300 °C isotherm, acting as the lower boundary, is shallowest in the SW and varies according to Fig. 3.5b. The 1300 °C isotherm is bent convex upward within the crustal thickening and bent softly downward towards the basin centre.

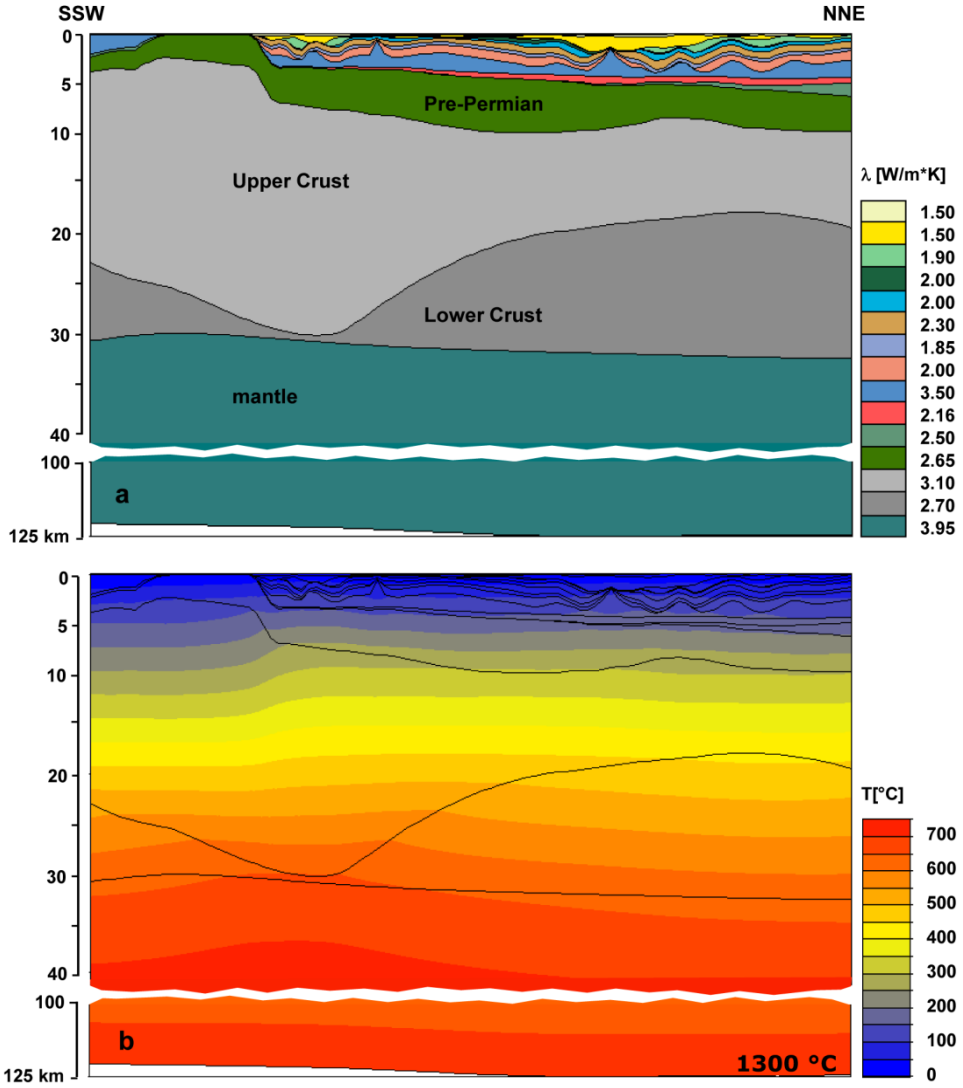

Figure 3.5a NNE-SSW oriented cross section through the 3D lithosphere-scale structural model with colour key for the assigned thermal conductivities. **b** Modelled temperatures along the same cross section for thermal model 2.

At the southern basin margin, where the upper crust is thickest and closest to the surface, no relevant insulating sediments overlying the crust are present. This configuration causes a mega chimney effect due to the very high thermal conductivity of the upper crust. In other words, the efficient heat transport to the surface leads to a loss of heat which is reflected by lower temperatures predicted down to about 20 km depth. In contrast, the increasing thickness of the overlying sediments towards the basin centre causes the storage of the heat below and hence increased temperatures in these areas.

Fig. 3.6 shows the calculated temperature distribution for selected depth levels of both models, the crustal-scale 3D model 1 (a1-c1) and the lithosphere-scale model 2 (a2-c2). A comparison of all temperature maps shows a strong lateral variation of predicted temperatures across the study area with lower temperatures towards the southern basin margin and higher temperatures in the basin area. This

lateral variation in temperatures is controlled by the position and configuration of the underlying crust in interaction with the configuration of the Zechstein salt and the sediments.

The temperature maps at 3000 m depth (Fig. 3.6a1 and 3.6a2) cut the southern basin margin, Mesozoic sediments and salt structures within the basin area. The pattern of the temperature distribution is characterized by both a long-wavelength trend of increasing temperatures from the southern basin margin towards the basin centre and a short-wavelength trend in the deeper basin area. The long-wavelength pattern is caused by the interaction between the configuration of the crust and the sediments. The short-wavelength pattern results from the interaction between the configuration of the Zechstein salt and the overlying sediments. The latter is similar for both models.

Due to the high thermal conductivity of the crust, lowest temperatures of up to 70 °C have been calculated at the southern basin margin for model 1. The temperatures increase towards the basin centre to up to 140 °C according to the cumulative thickness of the post-salt deposits which provoke a thermal blanketing effect in response to their low conductivity. Highest temperatures are predicted in the areas adjacent to the salt diapirs, where the surrounding low conductive sediments also cause thermal blanketing and the storage of the heat below.

For model 2, the configuration of the crust plays an important role for the temperature distribution. The reason is a higher heat input generated by the granites of the upper crust. Accordingly, a larger volume of upper crust contributes a larger amount of radiogenic heat. As almost the entire southern area of model 2 is characterized by an increased thickness of the upper crust, higher temperatures are also predicted in areas devoid of salt structures (Fig. 3.6a2). Apart from that, larger areas of increased temperatures are predicted around salt diapirs in the northern model area, triggered by the heat input of the thick underlying upper crust. Like in model 1, the lowest temperatures are predicted at the southern basin margin, but their range between 100 °C and 120 °C is distinctly warmer (by around 40 °C) compared with model 1. Although the highest temperatures predicted for both models are in the same range (around 140 °C), the comparison between both models indicates clearly that model 1 predicts lower temperatures than model 2 in those areas where the upper crust is thick.

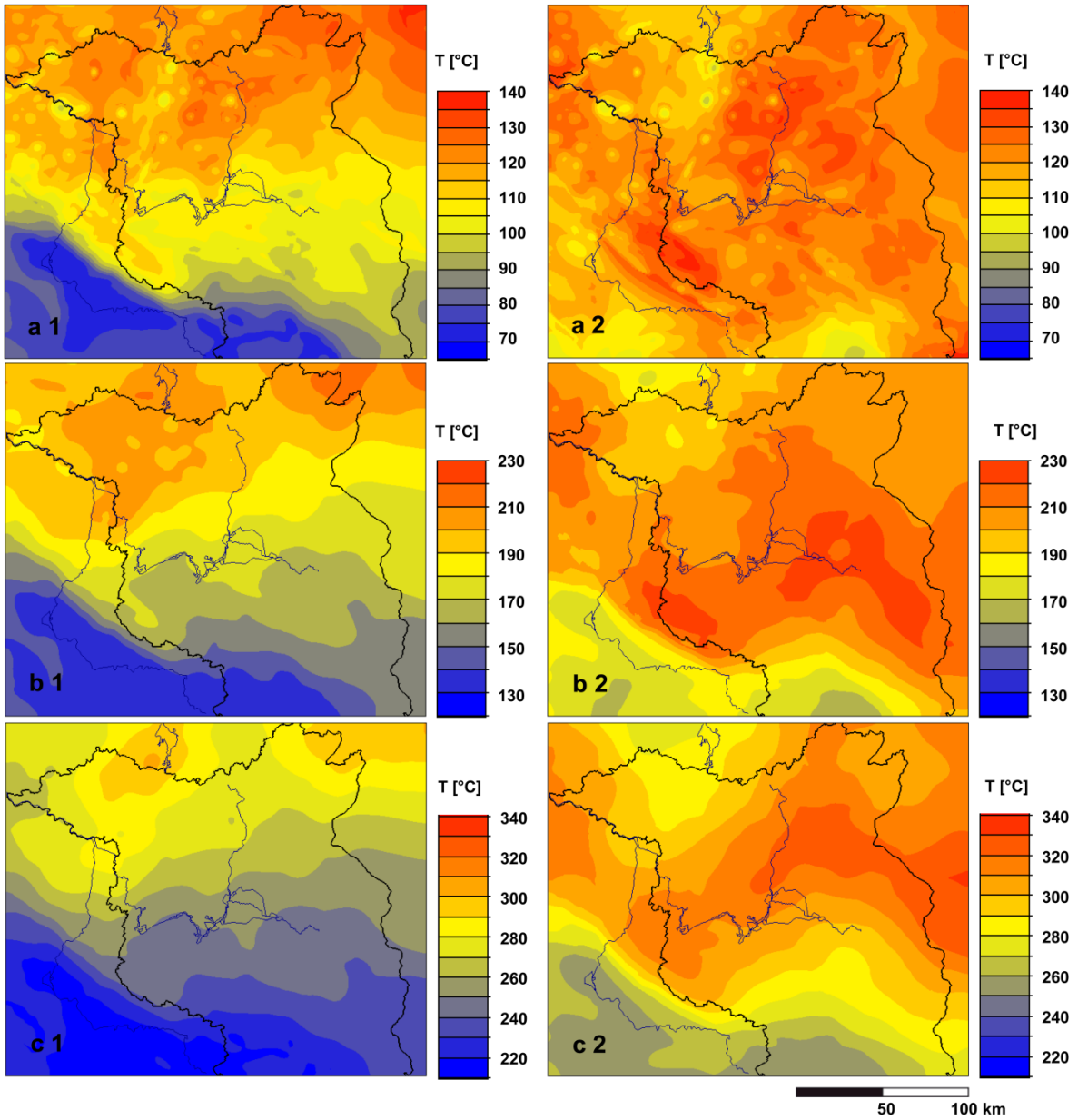

Figure 3.6 Predicted temperatures in °C extracted from the 3D conductive thermal models: for model 1 (**a1 - c1**) and model 2 (**a2 - c2**) at the depth of 3000 m (**a**), at 6000 m (**b**) and at 10000 m (**c**).

The temperature maps at 6000 m depth (Fig. 3.6b1 – 3.6b2) cut Pre-Permian crust below the salt structures in the north-western part of the model. For both models the pattern in the temperature distribution changes with increasing depth. In particular, the spatial correlation between the pattern of the temperature distribution and the thickness of the salt is only weakly expressed by a few cold spots beneath the most mature diapirs. In contrast, a more pronounced long-wavelength trend of the temperature pattern points to the increasing influence of the underlying crust. For model 1, the long-wavelength trend of increasing temperatures from the southern basin margin towards the basin centre correlates with the thickness distribution of the post-salt deposits. Accordingly, lowest temperatures of

up to 150 °C are predicted at the southern basin margin and highest temperatures of up to 210 °C are predicted for the basin centre in the northern model area (Fig. 3.6b1). For model 2, the long-wavelength trend of increasing temperatures (Fig. 3.6b2) additionally correlates with the thickness maxima of the upper crust (see Fig. 3.5a). In the north-western area, where the upper crust is thinnest, lower temperatures are predicted (180 - 200 °C) than in model 1 where the crust is homogeneous. Towards the southern and eastern area the large thickness of the upper crust leads to a drastic increase in temperatures to up to 230 °C in model 2. In all temperature-depth maps, the lowest temperatures have been calculated for both models at the southern basin margin. There the highly conductive crust is thickest and not covered by low conductive sediments. The lowest temperatures predicted for model 2 are warmer (160-190 °C) than those predicted for model 1 (~150 °C) in response to the higher value of radiogenic heat production assigned to the upper crust in model 2.

At the depth of 10000 m (Fig. 3.6c1 – 3.6c2), the influence of the salt structures is not evident any more in both models. The correlation between the sediments and the underlying crust is now expressed in a smooth long-wavelength pattern of the temperature distribution. But similar to the temperature pattern at 6000 m depth, the temperature distribution differs. For model 1 the temperature distribution is clearly influenced by the thickness of the post-salt deposits, whereas the temperature pattern of model 2 suggests an additional influence of the underlying crust. Again, lowest temperatures occur at the basin margin for both models. For the model 1 the lowest temperatures vary between 210 and 230 °C, whereas for the model 2, temperatures between 250 and 270 °C are predicted. In response to the largest cumulative thickness of the overburden, the highest temperatures of up to 300 °C have been modelled for model 1 in the northern model area. For model 2 the highest temperatures of up to 330 °C clearly correlate spatially with the thickest upper crust in combination with a thick sediment fill.

To evaluate the results from the crustal-scale model 1 as well as the lithosphere-scale model 2, we test the validity of the models. Therefore, we extract the temperatures of both models for the respective coordinates and depths, where observed temperatures are available (Tab. 3.3 and 3.4). The comparison between temperature predictions of model 1 (blue line) and model 2 (green line) with observed temperatures (red triangles) shows that both models reproduce observed temperatures well (Fig. 3.7a). Although the amount of temperature data is limited and thus also the statistical significance, the scatter of temperatures derived from different structural elements at different depth confirms this finding.
Nevertheless, model results indicate that model 1 is colder than model 2. For shallower depths (up to 2 km) the predicted temperatures of model 1 and model 2 overestimate the observed temperatures slightly. This indicates that the chosen thermal conductivities are either too large or cooling due to moving groundwater may occur. Between 2 and 5 km, the wider scatter of observed temperatures (84 temperatures from 45 wells) reflects the larger variety of structural levels in which these values have been measured. Nevertheless, in this depth interval, the deviation between model predictions and

observations is small for model 1, and larger for model 2. For model 1 80 % of the model predictions show deviation smaller than 10 K from observations, whereas for model 2 only 65 % stay within this range. Thereby, distinctly overestimated temperatures deviate in the range between 10° and 20°C for model 2 (Tab. 3.3 and 3.4). This comparison is only valid down to 7 km, as no temperatures were available below this depth level.

3.3.2 Sensitivity with Respect to Thermal Properties

A wide range of values for rock properties is measured in wells of the NEGB due to the natural petrophysical heterogeneity of rocks (Čermák et al. 1982, Norden and Förster 2006). As described before, the first dataset includes parameter values after Bayer et al. (1997) for the layers of the basin fill, in particular average values of thermal conductivity. To consider the range of lithological variation we test a second dataset, which we assign to the crustal-scale model 3. This dataset includes recently measured properties on rocks taken from wells of the NEGB (Tab. 3.1).

Values for radiogenic heat production of the units for the basin fill are based on data determined by log analysis or drill cores by Norden and Förster (2006). Thermal conductivities of the Quaternary and Tertiary units and the Zechstein salt are assigned according to a study of Norden et al. (2008). For the Mesozoic strata (Upper Cretaceous - Buntsandstein) we use average bulk thermal conductivities calculated from a thermal conductivity profile of the well Stralsund 1/85 by Fuchs and Förster (2010). Thermal conductivities for the Sedimentary Rotliegend and the Permo-Carboniferous Volcanics are based on data determined on drill cores from Norden and Förster (2006).
The comparison of both datasets, as illustrated in Table 3.1, reveals that the measured values for the thermal conductivities exceed the ones used by Bayer et al. (1997). This is especially the case for the Upper Cretaceous, the Lower Cretaceous and the Jurassic, where measured values are one third higher than the conductivities after Bayer et al. 1997. Likewise, the thermal conductivity for the Zechstein salt is about 1W/m*K higher. In contrast, the measured values for the radiogenic heat production show rather small differences between the two datasets. Since these thermal properties are valuable real observations we run several simulations for model 3 using the same homogeneous configuration of the crust as used for model 1 but varied thermal conductivities to assess the influence on the modelling results.
Modelling results for model 3 show that predicted temperatures do not reproduce the observed temperatures in wells in a similar manner like model 1 and model 2 (Fig. 3.7a). Although, for the upper 2 km the model fits the observed data better than models 1 and 2, the predicted temperatures are lower than observed for depth levels between 2 km and 7 km. Between 5 and 7 km depth this

mismatch reaches up to about 40 K. This difference between model prediction and observation is 30 K larger compared to model 1.

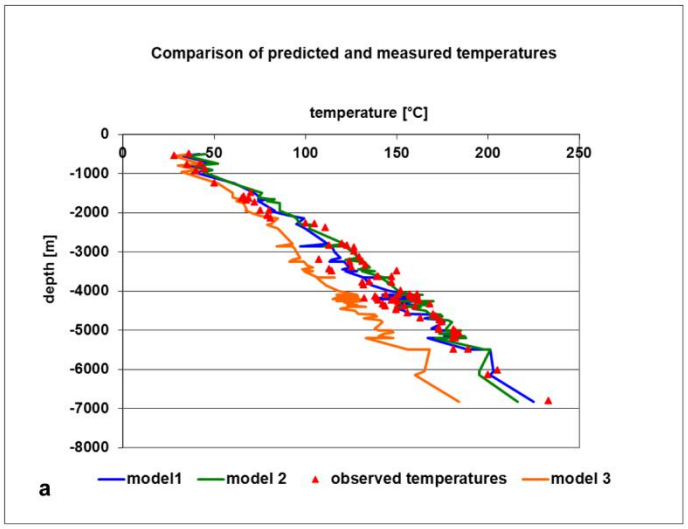

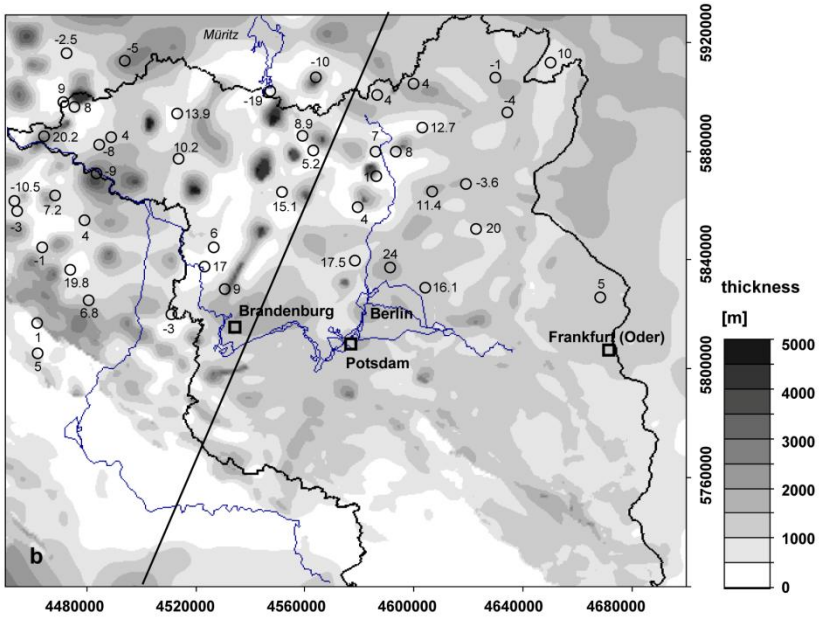

Figure 3.7a Comparison of measured and predicted temperatures: for model 1, model 2 and model 3. **b** Largest difference between observed and modeled temperatures for the wells of model 2 superimposed on the isopach map of the Zechstein salt.

A stepwise variation of thermal properties for the upper crust (λ to 3.3 W/m*K and S to 3.0e-6 W/m³) and for the Permo-Carboniferous Volcanics (S to 3.4e-6 W/m³) within a reasonable range, leads to an increase in temperatures, but is not sufficient to reproduce the observations. Likewise, increasing the heat flow to 35-40 mW/m² as suggested by Norden et al. (2008) leads to generally higher temperatures but these are still too low to reproduce the observations.

3.4 Discussion

The comparison between predicted and measured temperatures (Förster, 2001) of the different thermal models shows that using thermal parameters after Bayer et al. 1997 as adopted for the crustal-scale model 1 and the lithosphere-scale model 2 leads to comparatively small deviations between predicted and observed temperatures. A larger misfit between model predictions and observations occurs in the upper 2 km for both models (Tab. 3.3 and 3.4, Fig. 3.7b). Possible reasons for this deviation could be related to limitations in model resolution as connected to extrapolations in areas where no structural data were available. This is especially the case for locations in the periphery of the model.
Likewise, simplified model assumptions such as laterally uniform geological units do not consider the heterogeneity of depositional sequences, both vertically and laterally. This also could result in erroneous predictions in areas where such lithological heterogeneities are present.
Furthermore, the observed temperatures of the shallow temperature field above the Zechstein salt may be additionally influenced by cooling effects due to moving groundwater in the permeable layers.
How far the temperatures predicted for the southern part of the model are valid remains uncertain as no temperature observations covering this area were available.
For the temperature field between 2 and 5 km depth, the deviation between model prediction and observation is small for model 1 and partly larger for model 2 (Tab. 3.3 and 3.4, Fig. 3.7b). To figure out the reason for this larger deviation we compare the temperature predictions of model 1 (Fig. 3.8a) and model 2 (Fig. 3.8b) with the thickness map of the upper crust. The comparison reveals that model 2 predicts much higher temperatures compared with model 1 in the region of the model area where the upper crust is thickened. This is the case in the east at the south-western basin margin, where the predicted temperatures in model 1 are too cold, whereas model 2 overcomes the misfit with the observations. However, the higher heat input from the thickened upper crust also results in partly too high temperatures that deviate from observations by about 20 K (Fig. 3.8b) in the eastern part of the model area. The overestimation of temperatures could result from an overestimation of the radiogenic heat production in the upper crust as no spatial variations in crustal composition are resolved in the model. How far the overestimation is caused by the assumption of a purely conductive heat transport, needs to be tested further, as studies of coupled fluid and heat flow in the NEGB give more than indications for the presence of a convective fluid system in the subsurface (Cacace and Scheck-Wenderoth 2010). Likewise, the cooler observations in these areas could be related to cooling effects occurring due to forced convective processes as described by Kaiser et al. (2011).

Nevertheless, our studies show that the average values of thermal conductivity as used in model 1 and model 2 reproduce observed temperatures reasonably well. This indicates that the chosen values may

represent “effective” thermal conductivities that are different from real conductivities measured on the rock samples. The temperatures predicted by model 3 remain distinctly colder than in models 1 and 2. This is not surprising as most values of the thermal conductivities are larger for the sedimentary units in this model. A stepwise variation of thermal properties has shown that the shallow temperature predictions are not very sensitive to changes in radiogenic heat production, but highly sensitive to changes in the thermal conductivities of the respective sedimentary layers. Thus, the large deviation between observed and predicted temperatures below 2 km for model 3 seems to be related to the very high thermal conductivities assigned. This effect implies three conclusions:

(1) The assumption of a uniform horizontal distribution of conductivities does not reflect the heterogeneity of the respective layers. These conclusions were also discussed in the studies of Ollinger et al. (2010), who obtain a better fit with observed temperatures by assuming a non-uniform horizontal distribution of conductivities and by calculating optimized conductivities for individual wells.

(2) The possible influence of heat transport processes due to deep circulating fluids is not sufficiently taken into account. Cacace and Scheck-Wenderoth (2010) assume that positive heat flow anomalies at the surface, resolved in the study of Norden et al. (2008), could result from deep circulating fluids transporting heat from the basement to the surface. This assumption is confirmed by studies of Kaiser et al. (2011) who show that the formation of thermal convective cells leads to positive small-wavelength thermal anomalies in certain areas within the NEGB. Such phenomena could also explain the underestimated temperatures predicted by model 3.

(3) The simple vertical model resolution which is defined by the number of layers resolved in the model may not account for vertical anisotropy. The latter may exist in response to the presence of thin intercalated layers of reduced thermal conductivity. Such deposits may be responsible for increased temperatures due to the storage of the heat below these layers. Studies from Mottaghy et al. (2011) on a small scale model reveal the strong sensitivity of the temperature field to thermal conductivity by means of the upper and lower limit of temperature profiles resulting from varying thermal conductivities.

(4) Furthermore, our approach does not take into account the possible influence of faults which may provide pathways for an upward migration of warm fluids within the model area. Lampe and Person (2002) showed in their studies on advective cooling within the Upper Rhinegraben (Germany) that fault-related factors can play a major role in determining the geothermal regime. Moreover, Yousafzai et al. (2010) indicate in their studies on the Himalayan foreland basin that hydrochemical signatures of groundwater samples such as water and reservoir temperatures calculated for spring waters point to origin from deep horizons. They suggest that the remarkable proximity of thermal and hydrochemical anomalies to major faults are caused by waters ascending along these faults from greater depth. Likewise, the rise of deep high-salinity groundwater along tectonic fracture zones has been described for the western area of Apennine ridge by Petitta et al. 2011. There these ascending saline brines mix with shallow groundwater in Quaternary deposits filling depressed areas.

(5) The assigned thermal conductivities for the Mesozoic layers have been derived from only one location, which may not be representative for the entire basin.

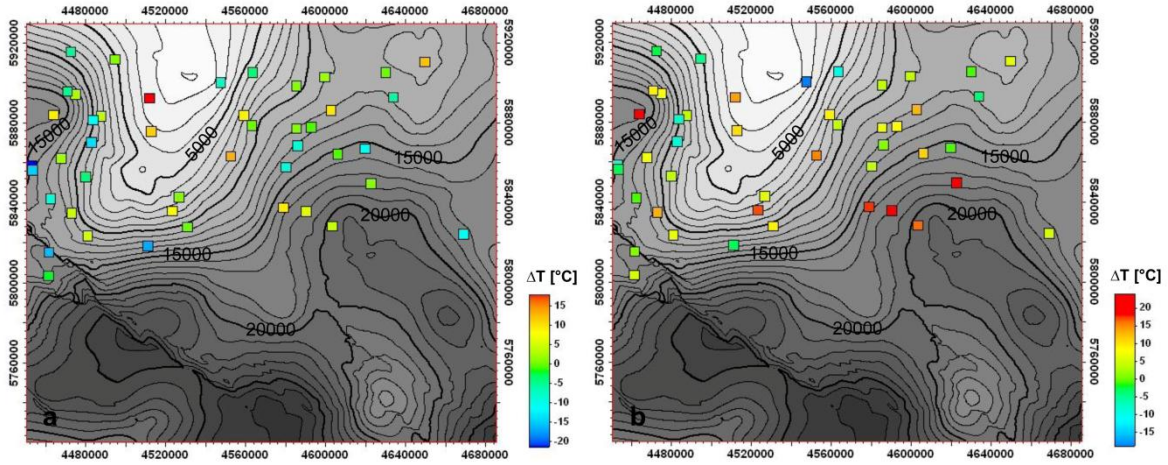

Figure 3.8 Thickness of the upper crust for the model area with location of wells where measured temperatures are available. Coordinates are Gauss Krüger zone 4. Coloured squares represent difference between temperatures and predictions for **a** the crustal-scale model 1 and **b** the lithosphere-scale model 2.

The use of measured thermal properties for the crustal-scale model 3 resulted in a large deviation between predicted and observed temperatures. The reason for this strong deviation of predicted temperatures could be related to the assumption of a homogeneous crust producing insufficient heat in certain areas of model 3. Therefore, in a stepwise variation, we have tested how much heat would be required at the level of the crust-mantle boundary to match the data. Our studies show that only a rather high heat flow of 50 mW/m² would reproduce the observed temperatures for the model with measured properties. Such a high heat flow at the Moho is in conflict with the general consensus (Huenges 2010). Accordingly, the heat flow from the mantle should vary in the range of 20 – 40 mW/m², where no anomalous hot zones at the base of the European crust are suggested. In addition, more recent results (Cacace et al. 2010) indicate that the heat flow at the Moho cannot be assumed to be laterally uniform. Nevertheless, our results suggest that there may be more heat entering the crust at its base than considered in model 3. An alternative way of increasing the heat input from the crust and mantle would be a differentiated crust as considered in model 2 in concert with a larger temperature at the lithosphere asthenosphere boundary. Sensitivity analyses testing these scenarios proved that neither using a crustal differentiation, nor increasing the basal temperature to 1400 °C were sufficient to reproduce the observations.

3.5 Conclusions

We show that the choice of both different configurations of the lithosphere and thus different lower boundary conditions, as well as of different thermal properties strongly influence the results of 3D thermal modelling. For the lower boundary of the models we test two different model configurations, a fixed heat flow at the Moho and an isothermal boundary of 1300 °C at the LAB. Both, the 3D crustal-scale model as well as the 3D lithosphere-scale model of the steady-state conductive thermal field are able to reproduce observed temperatures, which indicates that conductive transport is the dominant mechanism of heat transfer on a basin scale.

Under the simplified assumption of a homogeneous crust, the crustal-scale model 1 using a constant heat flow of 30 mW/m² at the Moho leads to temperature predictions which largely reproduce observed temperatures. The more appropriate lithosphere-scale model 2 generates higher temperatures than model 1 due to its differentiated lithosphere and the related heat input at the base of the Permian to Cenozoic deposits. Although model 2 partly overestimates the temperature observations, the results are considered to be more realistic, since the model is consistent with temperature, deep seismic and gravity observations. Obviously the chosen thermal parameters (Bayer et al. 1997) for the stratigraphic layers resolved in the model represent reasonable average values. However, these values may not correspond to the specific thermal properties measured on rock samples of these units.

Model 3 shows a less good correlation between predicted and observed temperatures below 2 km depth. Although below 2 km depth the trend of the temperature distribution is similar to those of models 1 and 2, model 3 predicts colder temperatures compared with the observations. Moreover, the increase in temperatures predicted by model 3 using the differentiated lithosphere, does not overcome the misfit with the observations.

In summary, our results suggest that the thermal regime in the Brandenburg area is mainly influenced by heat conduction, but there are also indications for the presence of moving fluids in restricted areas. The predicted temperature distribution itself is strongly controlled by two major influencing factors: (1) Configuration of the lithosphere and the chosen lower thermal boundary condition. (2) The effective thermal properties which according to our results are characterized by smaller values than those determined on rock samples.

Acknowledgements

We thank our colleagues from the geological surveys of Landesamt für Bergbau, Geologie und Rohstoffe Brandenburg for providing the main data to construct the refined 3D structural model of the basin fill and for fruitful discussions. Landesamt für Geologie und Bergwesen Sachsen-Anhalt and Landesamt für Umwelt, Naturschutz und Geologie Mecklenburg-Vorpommern kindly provided additional well data to improve the database at the border of the structural model. The project received financial support from the Helmholtz Centre Potsdam GFZ German Research Centre for Geosciences. This work is part of GeoEn and has partly been funded by the German Federal Ministry of Education and Research in the programme ‘‘Spitzenforschung in den neuen Ländern’’ (BMBFGrant03G0671A/B/C). The authors wish to thank the anonymous reviewers for the very thorough and most helpful review. We are grateful for valuable comments from the editorial team.

4 Influence of Fluid Flow on the Regional Thermal Field: Results From 3D Numerical Modelling for the Area of Brandenburg (North German Basin)

Abstract

We analyse the effect of fluid flow on the recent thermal field for the Brandenburg region (North German Basin) which is strongly affected by salt structures. The basin fill is modified by a thick layer of mobilized salt (Zechstein, Upper Permian) that decouples the overburden from deeper parts of the lithosphere and is responsible for thermal anomalies since salt has a distinctly higher thermal conductivity than the surrounding sediments and is impermeable to fluid flow.

Numerical simulations of coupled fluid flow and heat transfer are carried out to investigate the influence of fluid flow on the shallow temperature field above the Zechstein salt, based on the finite element method. A comparison of results from conductive and coupled modelling reveals that the temperature field down to the low permeable Triassic Muschelkalk is influenced by fluids, where the shallow low permeable Tertiary Rupelian-clay is absent. Overall cooling is induced by forced convective forces the depth range of which is controlled by the communication pathways between the different aquifers. Moreover buoyancy induced effects are found in response to temperature dependent differences in the fluid density where forced convective forces are weak. The range of influence is controlled by the thickness and the permeability of the permeable strata above the Triassic Muschelkalk. With increasing depth, thermal conduction mainly controls the short-wavelength pattern of the temperature distribution whereas the long-wavelength pattern results from interaction between the highly conductive crust and low conductive sediments. Our results provide generic implications for basins affected by salt tectonics.

4.1 Introduction

Geothermal energy is one of the major sources of renewable energy, which is available in practically inexhaustible quantities. To keep low production costs, its exploitation is limited to areas with favourable hydrogeological and thermal conditions. Amongst other physical parameters, geothermal reservoirs are characterized by increased temperatures of their rocks – petrothermal applications - and fluids – hydrothermal applications - at accessible depth. Information about the temperature distribution with depth for regional exploration is easily obtained by large scale 3D numerical models.

The advantage of the latter is given by their capability of combining direct information on the structural setting of the subsurface with physical processes controlling fluid and heat transport. Since such models are consistent with respect to the 3D geology and the physics involved they may be used to detect prospective areas for geothermal energy usage as they deliver local information about the subsurface temperature distribution.

In this study we focus on 3D models of coupled fluid flow and heat transport processes to analyse the influence of fluid flow on the temperature distribution in the area of Brandenburg. Numerical efforts presented in this study benefit from previous geological and thermal modelling focussing on the steady-state conductive thermal field of the region (Noack et al. 2010, 2012). These studies provided essential information on the 3D regional hydrogeology of the study area comprising relevant major aquifers and aquitards of interest. At the same time, the results from 3D lithospheric scale conductive simulations contribute to the present modelling efforts in terms of suitable thermal boundary conditions and physically sounded constraints for values of rock thermal parameters needed for the modelling investigations – thermal conductivity and heat production rates.

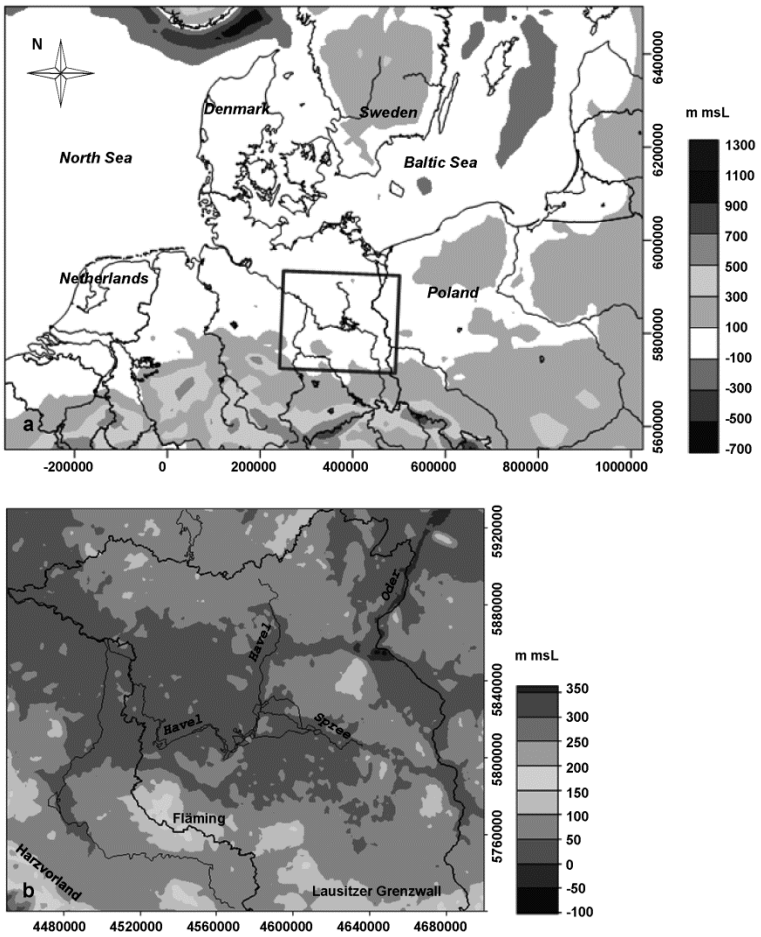

Figure 4.1a Location of study area with topography, coast lines and rivers in UTM Zone 33N (ETOPO1, after Amante and Eakins 2009) of Central Europe. Large rectangle encloses the area covered by the 3D numerical models of Brandenburg. **b** Present topography of the model area in Gauss Krüger zone 4 coordinates; thick line-border of Brandenburg, small line-rivers (modified after Noack et al. 2010).

Brandenburg belongs to the south-eastern part of the North German Basin (NGB). The NGB covers an area ranging from the Baltic Sea in the north across flat lowland terrains to higher terrains of the Harz Mountains in the southwest and to plateaus as the Fläming High and Lausitzer Grenzwall in the south (Fig. 4.1a, 4.1b). Thus, the study area encompasses a part of the basin centre in the north, whereas to the south the present-day south-eastern margin is enclosed, where crystalline crust reaches close to the surface. Starting with Permo-Carboniferous volcanic rocks the basin fill is represented by up to 8000 m thick Permian to Cenozoic sediments (Scheck and Bayer 1999). A very special feature amongst these sediments is a thick layer of mobilized Zechstein salt (up to 4500 m) which is accountable for structural diversity. The primary horizontal stratification of the Post-Zechstein sediments is strongly modified where diapirs, salt pillows and areas of salt withdrawal define the structural pattern of the overburden as it is the case in the north-western region of Brandenburg (Fig. 4.2a). This spatial structural configuration of the basin fill is very important for the regional temperature field since rock salt has a distinctly higher thermal conductivity than surrounding sediments and is also impermeable to fluid flow. Consequently, the Zechstein salt acts both as a conductive "heat chimney" (Noack et al. 2010, 2012) and as a hydraulic decoupling horizon between the Pre-Permian and the Mesozoic-Cenozoic strata (Kaiser et al. 2011). The latter are characterized by two further low permeable sediment complexes, the Tertiary Rupelian-clay aquitard and the Middle Triassic Muschelkalk aquitard. These two aquitards divide the Post-Permian strata into three main aquifer systems: the Lower Triassic Buntsandstein, the Upper Triassic Keuper to early Tertiary Pre-Rupelian-clay and the late Tertiary to Quaternary Post-Rupelian aquifer complex. The combined effects of both the variable thermal and fluid properties and the structural configuration of the basin fill will likely exert a first order control on the temperature distribution at shallow depths in the basin. In addition, the structural configuration of the deeper lithosphere interacts concurrently with the basin fill controlling the regional temperature trend (Cacace et al. 2010; Noack et al. 2012). In particular, the influence of a highly heat producing and highly conductive crystalline crust can be observed in the thermal signature above the Zechstein salt (Noack et al. 2012).

As stated above, the region of Brandenburg is a part of the larger NGB which is considered as one of the three major target sedimentary basin settings for geothermal utilization in Germany. As a matter of fact, in the last decades this region has become of growing interest for geothermal exploration and an increasing number of studies have been focused on a better assessment of its geothermal potential (Beer and Hurtig 1999; Ondrak et al. 1998; Norden and Förster 2006; Norden et al. 2008; Ollinger et al. 2010; Noack et al. 2010, 2012; Norden et al. 2012). Academic research has benefited from a relative large database of measured temperature that became available in recent years from different wells across the area (Förster 2001; Norden et al. 2008). Generally, such information has been processed by classical 2D interpolation algorithm resulting in published temperature maps (Schulz et al. 2007; Stackebrandt and Manhenke 2010). Unfortunately, being limited in their approach to planar

interpolations these maps might only offer a restricted understanding of the 3D regional thermal field. At the same time, information about causative processes and their thermal manifestation in the subsurface remains at least speculative. To improve the current knowledge about the temperature distribution in the subsurface of Brandenburg and the relevant active processes at depths, investigations of the regional temperature field have focussed on different issues in recent years. 3D thermal models that describe the structural configurations of the basin fill and its interaction with the conductive thermal field were built based on 3D Finite Element simulations on a regional scale (Bayer et al. 1997; Ondrak et al. 1998 and Noack et al. 2010). These models partially also consider deeper parts of the lithosphere – i.e. crustal heat contribution to the thermal budget. Controlling factors of the 3D conductive field such as specific assumptions for the configuration of the deeper lithosphere and the chosen boundary conditions as well as the influence of variation in thermal rock properties have been analysed among others by Bayer et al. 1997; Vosteen et al. 2004; Norden et al. 2008; Ollinger et al. 2010; Noack et al. 2012; Norden et al. 2012. These models were able to reproduce the first order trends of surface heat flow or temperatures as deduced from available observations derived from numerous wells. However, local inconsistencies were also found in all these studies indicating that the assumption of a purely conductive thermal regime may not be valid locally. Local misfits between simulated and observed subsurface temperatures point to additional heat transfer mechanisms acting in the subsurface. In this context, results from 3D conductive modelling in the area of Brandenburg show a thermal field which is mainly influenced by heat conduction, but also pointed to the influence of moving fluids and its capability to affect the shallow temperature field above the Zechstein salt (Noack et. al. 2012). Similar findings have been also described for different basin settings worldwide (Deming 1994; Garven 1995; Person et al. 1996; Smith and Chapman 1983).

With the focus of the Brandenburg region, a systematic 3D analysis of different heat transfer mechanisms has been carried out by Kaiser et al. (2011). In their study, Kaiser and co-workers showed that the presence of fluids may distort a background conductive temperature profile, provided that rock permeability and aquifer thickness is sufficiently large for groundwater flow to be significant. This study pointed to the prominent role played by the permeability file and its variation within the basin to affect the groundwater flow file and temperature distribution. Indeed, permeability and permeability heterogeneity and anisotropy among and within geologic units can have a large impact on heat and mass transport (Manning and Ingebritsen 1999; Ledru and Frottier 2010). This has also been demonstrated by Lampe and Person (2002) who varied fault zone permeability in their 2D numerical studies on advective cooling within the Upper Rhinegraben (Germany) to determine possible fluid pathways and the effects of circulating groundwater on the thermal field in the subsurface of the graben.

Numerical simulations of coupled fluid flow, heat and mass transport have already been carried out for the NEGB (e.g. Magri et al. 2005a, b; Kaiser et al. 2011). The respective results derived from 2D and

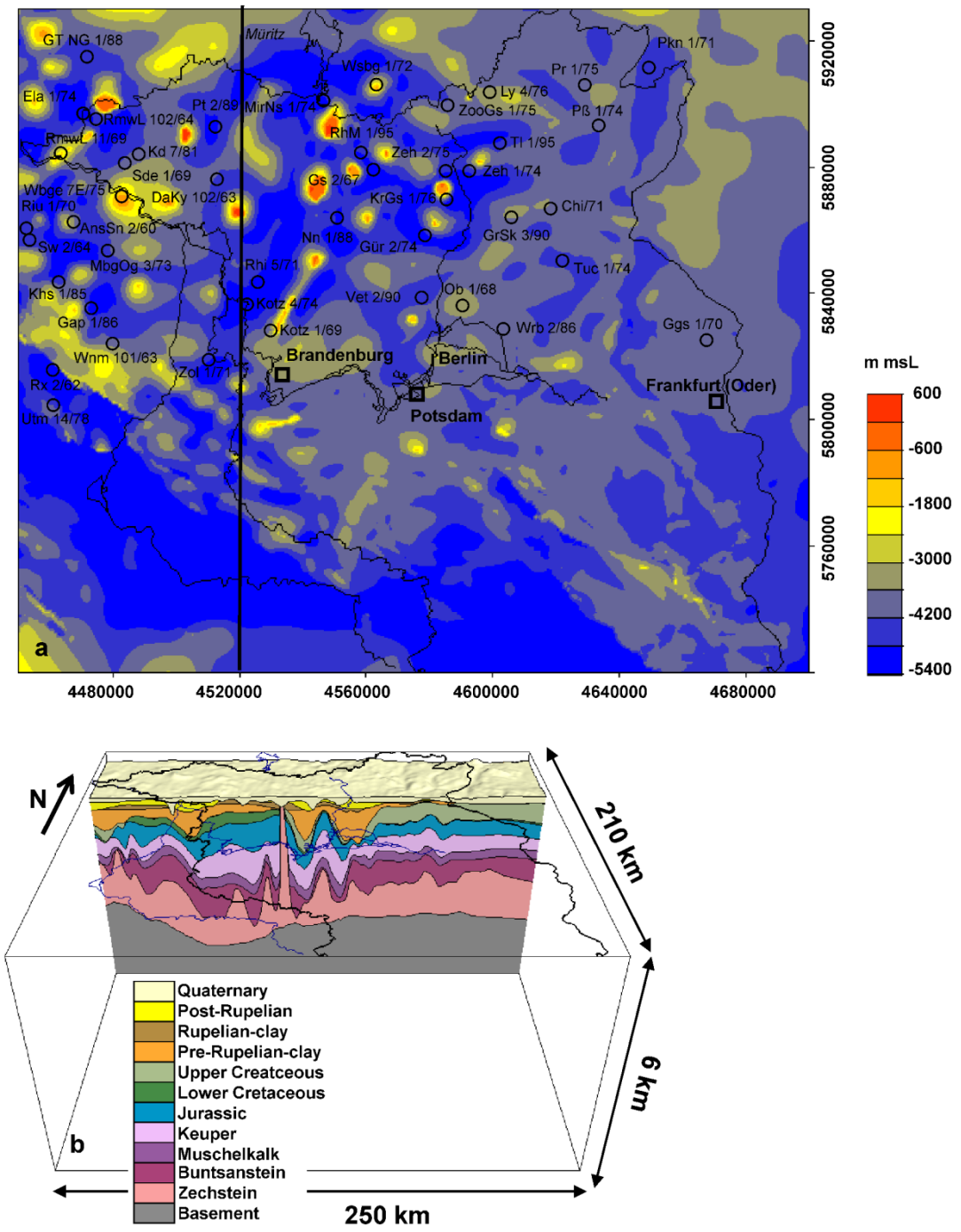

Figure 4.2a Thickness of the Zechstein salt for the model area with location of wells where measured temperatures are available. Coordinates are Gauss Krüger zone 4. Black line delineates the border of Brandenburg. Black line crossing the model from N to S indicates the location of a representative cross section which cuts major structural elements (modified after Noack et al. 2010). **b** 3D view on the structural configuration of the thermal models with colour key for the stratigraphic units differentiated.

3D approaches indicate that upward flow of dissolved halite is induced by the geothermal gradient. Based on 2D thermohaline modelling studies Magri et al. (2008) propose that thermally induced convective heat transport can cause transport of salty water to the surface. Besides, geochemical

analyses also indicate that formation water may have been replaced by geologically younger waters (Tesmer et al. 2005; Möller et al. 2008). More recently, Cacace et al. (2010) and Kaiser et al. (2011) have revisited the question of main heat driving processes by means of 3D numerical simulations within the NEGB and partially challenged the findings from earlier 2D studies. According to these 3D modelling studies advection of heat by topography driven fluid flow (forced convection) should be regarded as the major process affecting the shallow temperature field in addition to conductive heat transport. In addition, these studies have shown that the process of topography driven fluid flow is only locally overwhelmed by density driven upward fluid flow (free convection) where the hydrogeological setting of the subsurface is characterized by small gradients in hydraulic head. Also the geometry of both the salt and the low permeable Muschelkalk (Middle Triassic) in interaction with the thickness and permeability of the shallower aquifers are of decisive influence for the shallow temperature field and the stability of convective thermal processes. Additionally, results from 3D coupled fluid and heat transport simulations at the geothermal production site Groß Schönebeck indicate a relevant influence of convective heat transport in the upper 3000 m, where a critical thickness of permeable sediments is achieved (Noack et al. 2010).

Summarising, the results from previous studies aiming to identify main heat drivers showed that conductive heat transport should be regarded as the main heat transport mechanism within the basin, but advection by moving fluids triggered by topography driven fluid flow may also be an important process affecting above all the shallow temperature field. In addition, the thermal field may be locally influenced by free convective heat transport. All these earlier modelling studies were rather systematic in nature and based on a limited stratigraphic resolution of the subsurface. In particular these models did not resolve an important shallow aquitard, the low permeable formation of the Tertiary Rupelian-clay. The only approximation of the shallower Cenozoic aquifer system and its connectivity to deeper levels is based on 2D thermohaline simulations (Magri et al. 2008) that do not account for the 3D nature of transport processes and for a local 3D thermohaline study by Kaiser et al. (2013) therefore limited in its characteristic length.

Newly available data concerning the top and the base of the Rupelian-clay in Brandenburg enable to include this important hydraulic barrier separating the freshwater complexes from deep saline aquifers within the study area and thus to address the potential impact of this geological unit on the 3D thermal field. By integration of this layer into a vertically refined model we investigate the influence of moving fluids on the regional thermal field by means of 3D Finite Element simulations and additionally evaluate the effects of heterogeneity in permeability within the aquifer systems. Thereby, we focus on the groundwater flow and thermal field above the Zechstein salt since previous studies indicate a hydraulic decoupling at this depth level between the Supra- and Sub-salt units. To analyse the influence of the moving fluids we compare results from a purely conductive model with model

scenarios from numerical simulations of coupled fluid flow and heat transfer. We validate the resulting model temperatures by comparison with temperatures observed in 44 wells (Fig. 4.2a, Tables 4.3, 4.4).

Consequently, the first model considers a purely conductive heat transfer. For the second model we vary the heat transport process by additionally introducing heat transfer by the liquid medium (Kaiser et al. 2011). Accordingly, the model scenarios for coupled fluid and heat transport take into account heat conduction as well as pressure and density driven groundwater flow. With these scenarios for the coupled model we analyse to which degree variations in aquifer thickness and permeability control the regional thermal field. Thus, the study reveals where moving fluids decisively control heat transport and provides insights into the interaction between thermal and hydraulic properties within the geological layers above the Zechstein salt.

4.2 Methods

4.2.1 Hydrogeological Model

To carry out 3D coupled fluid and heat transport simulations we use the 3D structural model of the sedimentary sequence as outlined in (Noack et al. 2010). The model includes the main stratigraphic units of the basin fill corresponding to Permian to Cenozoic sediments (Noack et al. 2010). Beginning with the Zechstein salt at the base of the new model up to the Quaternary at the top, these sediments correspond to eight geological layers. These are from top to bottom: Quaternary, Upper Cretaceous, Lower Cretaceous, Jurassic, Upper Triassic Keuper, Middle Triassic Muschelkalk, Lower Triassic Buntsandstein and Permian Zechstein. Apart from the Upper Cretaceous limestones, the Middle Triassic Muschelkalk carbonates and the Zechstein evaporites, the remaining layers represent mainly clastic deposits. With respect to their physical properties two low permeable sediment complexes are included in the model in addition to an impervious basement that limits the model downward, - the Zechstein salt and the Middle Triassic Muschelkalk. A further naturally impervious unit, which acts as a hydraulic barrier separating the shallow freshwater Quaternary complexes from the deep Mesozoic saline aquifers, is the Tertiary Rupelian-clay. To take this important sedimentary layer into account, we divided the Tertiary unit of the structural model into three sub-units, the Post-Rupelian late Tertiary to Quaternary aquifer system, the late Tertiary Rupelian-clay aquitard and the early Tertiary Pre-Rupelian-clay aquifer. The required data to construct top and base of the Rupelian-clay are provided by the geological survey of Brandenburg (Landesamt für Bergbau, Geologie und Rohstoffe Brandenburg-LBGR). Accordingly, a map of the top of the Rupelian-clay obtained from a compiled dataset including discontinuities mapped in the aquitard thickness distribution, -i.e. Rupelian-windows (Stackebrandt and Manhenke 2010) has been supplemented by data from wells (Landesamt für

Bergbau, Geologie und Rohstoffe Brandenburg). For the construction of the base of the Rupelian-clay less dense data coverage was available. Both surfaces including areas of zero thickness have been mapped. Taking these three layers into account the final model consists of eleven layers for the basin fill ranging from the Quaternary to the Zechstein salt (Fig. 4.2b). Like in earlier models and maps (Bayer et al. 1997; Stackebrandt and Manhenke 2002; Noack et al. 2010, 2012), the thickness and distribution of the sediments within the basin fill are strongly influenced by the structural configuration of the Zechstein salt.

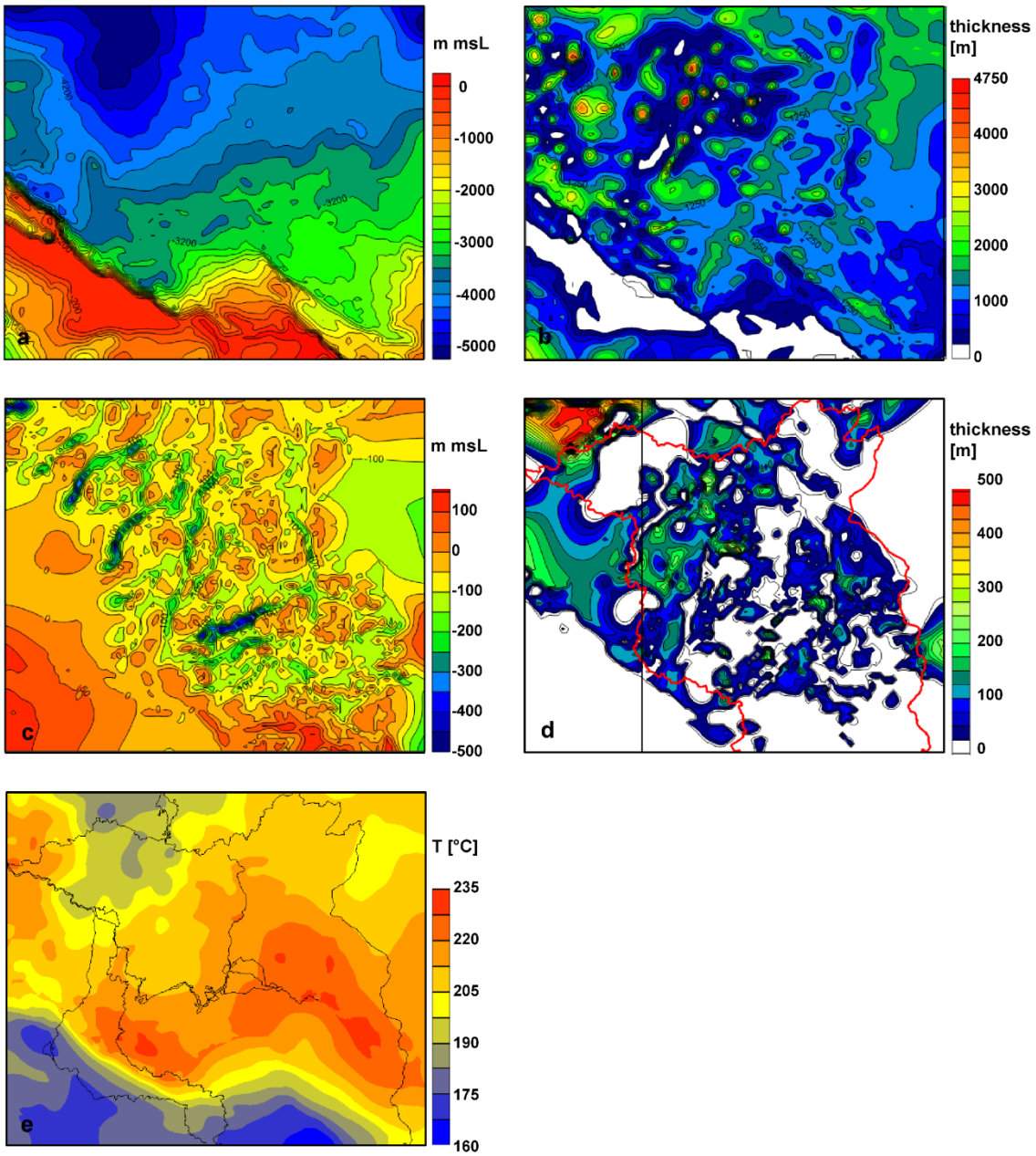

Figure 4.3a Base of Permian Zechstein salt (modified after Noack et al. 2010). **b** Thickness of Permian Zechstein salt (modified after Noack et al. 2010). **c** Base of Quaternary (modified after Noack et al. 2010). **d** Thickness of Rupelian-clay. e Non-constant temperature distribution adopted as lower boundary condition.

While the base of the Zechstein salt is represented by a relatively flat surface (Fig. 4.3a), the salt surface is highly differentiated following the topography of salt pillows and diapirs as well as of areas of salt withdrawal.

This structural diversity is also reflected in the configuration of the overlying deposits. Salt diapirs may attain a local thickness of up to 4500 m (Fig. 4.3b). Especially where diapirs pierce their overburden, the surrounding post-salt sediments are irregularly shaped and may be discontinuous. Additionally, the rise of major diapirs created accommodation space in areas where the salt has been removed. This led to the formation of surrounding salt rim synclines during Mesozoic and Cenozoic times. The latter are filled with up to 2000 m thick sediments.

Additional structural features that determine the structural configuration of the post-salt deposits are Quaternary channels cutting through the Rupelian-clay aquitard (Fig. 4.3c). These channels evolved in response to glacial erosion and may cut more than 500 m deep through the layers below (Stackebrandt 2009; Noack et al. 2010).

As illustrated in Fig. 4.3d the thickness of the Rupelian-clay deposits varies between 0 and 250 m across the area of Brandenburg. Thereby, the hydraulic barrier of the Rupelian-clay is not homogeneously distributed, but locally interrupted. These local interruptions of the Rupelian-clay, so-called "Rupelian windows" are linked to areas where either the Rupelian-clay was primarily not deposited, or where Quaternary channels have removed the Rupelian-clay by cutting through the older and thus also Tertiary sediments. In both cases these windows provide possible preferential pathways for intra-aquifer flow between the Quaternary groundwater system and the deeper Mesozoic aquifers. Since the available data are restricted to the area of Brandenburg and the data for the base of the Rupelian-clay are strongly limited, the thickness distribution of the Rupelian-clay shows rather the general trend without capturing local details of the topological configuration of this layer. Nevertheless, including the Rupelian-clay complex into the simulations allows assessing the regional interchange between fluids of the freshwater complexes and brines from the deep saline aquifers.

4.2.2 Modelling Approach

For the 3D heat transport simulations we utilize the commercial finite element software FEFLOW® (Diersch 2009) that is able to compute heat transfer in saturated porous media. In the simplest case, considering only heat conduction the basic equation for the energy transport which is needed to be numerically solved follows Fourrier's law as:

1. $$\rho c \frac{\partial T}{\partial t} = \overline{\nabla} \cdot (\boldsymbol{\lambda} \nabla T) + S$$

In Equation 1 *c* is the rock heat capacity, ρ is rock density, $\frac{\partial T}{\partial t}$ is temperature change per time increment, λ is rock thermal conductivity**,** ∇T is the thermal gradient, S is radiogenic heat production. Assuming that the system has reached steady state conditions ($\frac{\partial T}{\partial t}$*=0)* the solution depends only on the thermal conductivity of the rock λ and the radiogenic heat production *S*. The respective values assigned to the different model layers are chosen according to a laterally uniform dominant lithology (Table 4.1) and to results as obtained from a previous sensitivity study by Noack et al. (2012). Results of the simulations for the conductive steady state heat transport are shown in Figures 4.4b, 4.5a, 4.5c and 4.5e and will be discussed in comparison with the results from the simulations of coupled transport of fluid and heat.

For the case of coupled transport of heat and fluid, the governing partial differential equations of thermal convection are derived from Darcy's law, energy and mass conservation laws (e.g. Nield and Bejan 2006).

A linear form of the conservation equation for the linear momentum of the fluid is derived under Darcy approximation resulting in:

2. $$\mathbf{q}^f = -\mathbf{K}\left(\nabla h + \rho^r \frac{\mathbf{g}}{|\mathbf{g}|}\right)$$

In Equation 2 $\mathbf{q}^f$ is the specific discharge (Darcy's velocity), $h = h_p + z = \frac{p}{\rho^f{}_0 g} + z$ is the hydraulic head with p being pore pressure, h_p hydraulic potential, and z a reference datum, $\rho^r = \frac{\rho^f - \rho^f_0}{\rho^f_0}$ is the relative density of the fluid, **K** is the hydraulic conductivity of the porous media expressed by $\mathbf{K} = (\rho^f_0 g / \mu^f)\mathbf{k}$, with **k** is the permeability and **g** is the gravity acceleration.

According to Darcy's law (Equation 2), the fluid mass conservation reads as:

3. $$\frac{\partial[\varphi\rho^f + (1-\varphi)\rho^s]}{\partial t} + \nabla \cdot (\rho^f \mathbf{q}^f) = \varphi^f Q^f + (1-\varphi^f) Q^s$$

In Equation 3 φ is the porosity and Q^f and Q^srepresent a sink/source mass term for the fluid and the solid respectively.

If density and porosity gradients are neglected in the energy conservation law and thermal equilibrium between the solid and the fluid medium is assumed, the heat transfer equation becomes:

4. $$(\rho c)_{fs} \frac{\partial T}{\partial t} + \rho^f c^f \nabla (\mathbf{q}^f T) - \nabla (\lambda \nabla T) = S$$

where $(\rho c)_{fs} = \varphi(\rho c)_f + (1 - \varphi)(\rho c)_{fs}$ is the specific heat capacity of the system with a fluid $(\rho c)_f$ phase and a solid $(\rho c)_s$ phase for a given porosity φ. The specific heat capacity of the fluid used in the simulations is 4.2 MJ/m³*K, λ is the thermal conductivity tensor for both the fluid and the solid medium.

These balance equations (2) and (3) are coupled by closing the system specifying a proper Equation of State (EOS) for the fluid density taking into account both its pressure and temperature dependence – i.e. $\rho^f = \rho^f(p, T)$.

Table 4.1 Assigned thermal properties for geothermal modelling: for the lithological characteristics dominant lithology is mentioned first. Values for the lithologies and thermal properties are assigned for all models following earlier studies after Bayer et al. 1997. Thermal properties for the Post-Rupelian, Rupelian and Pre-Rupelian-clay after Magri et al. 2008., radiogenic heat production of Rupelian after Balling et al. 1981.

Stratigraphic Unit	Lithology	Thermal conductivity λ [W/(m*K)]	Radiogenic heat production S [W/m³]
Quaternary	Sand and Silt and Clay	1.50	0.7e-6
Tertiary-Post-Rupelian	Sand and Silt and Clay	1.50	0.7e-6
Tertiary-Rupelian-clay	Clay	1.00	0.45e-6
Tertiary-Pre_Rupelian-clay	Sand and Silt and Clay	1.90	0.3e-6
Upper Cretaceous	Limestone (Chalk)	1.90	0.3e-6
Lower Cretaceous	Clay-, sand-, and siltstone	2.00	1.40e-6
Jurassic	Clay-, sand-, silt- and marlstone	2.00	1.40e-6
Keuper	Clay-, marlstone and gypsum	2.30	1.40e-6
Muschelkalk	Limestone	1.85	0.3e-6
Buntsandstein	Silt-, sand-, claystone and evaporites	2.00	1.00e-6
Zechstein	Evaporites	3.50	0.09e-6
Basement	Clastics, volcanics, granites to granodiorites	2.50	1.5e-6

To carry out the coupled fluid and heat transport simulations a model is constructed that covers an area of 250 km in E-W and 210 km in N-S direction. This square marks the horizontal extension of the planar 2D finite element mesh of the 3D model in FEFLOW®. This 2D slice is then multiplied according to the number of geological layers within the model. Each of the generated slices has the same horizontal mesh discretisation and consists of irregular 3-noded triangular elements.

The generated model is built of 2,842,548 mesh elements and 1,546,675 nodes in total distributed to the 12 layers and 13 slices. Thus, each layer is represented by 236,879 elements and 118,975 nodes resulting in a horizontal element resolution of 0.22 km². Care has been taken to consider the structural complexity already in the horizontal mesh resolution. To obtain the thickness of each layer the z-elevations of the geological layers have been extracted from the structural model and assigned to each node of the horizontal slices by interpolating routines. During this assignment a minimum thickness of 0.1 m is automatically introduced by the software to assure continuum conditions for the solution of the equations in the finite element model where layers have de facto zero thickness. This is especially

the case where the Quaternary channels cut through the underlying layers or where diapirs break through the overlying layers. To consider nevertheless correct properties during the simulations, salt properties were assigned manually to all cover layers of minimum thickness pierced by the salt (Kaiser et al. 2011). Likewise, increased permeability is assigned manually for the Rupelian-clay in the domains of the Rupelian windows to avoid numerical artefacts induced by a 0.1 m thick low permeable Rupelian-clay layer. All layers were vertically interpolated by connecting the nodes of the corresponding elements between two consecutive slices and discretised by 6-noded triangular prisms. Hence, the vertical resolution of the model corresponds to the thickness of the geological layers. A twelfth layer has been added below the Zechstein salt closing the model downward to its base at a constant depth of - 6000 m.

According to the fluid flow and heat transport equations the numerical simulations depend on the assigned thermal conductivities and radiogenic heat production rates as well as on rock heat capacities, porosities and permeabilities. Therefore, physical parameters are assigned to the nodes of each element within the layers assuming isotropic and homogeneous conditions (Tables 4.1 and 4.2). The physical parameters depend on the respective lithology and characterise the geological and hydraulical nature of each geological unit. Rock thermal parameters, i.e. thermal conductivity and radiogenic heat production, have been already evaluated by sensitivity analyses with a previously published lithospheric scale 3D conductive model of Brandenburg, constrained by the 1300 °C isotherm (Noack et al. 2012). In their study, Noack and co-workers considered the additional influence of basal heat flow at the Moho on the thermal signature of the shallow thermal field as well as the effects of lithological variation in related rock thermal properties by testing a dataset of thermal conductivities and radiogenic heat production recently measured on rocks from wells of the NEGB (Norden and Förster 2006; Fuchs and Förster 2010). According to this previous study we use the thermal data set (thermal conductivity and radiogenic heat production) which result from the best-fit model scenario for the new conductive and coupled models of this study.

To the lowermost layer, below the Zechstein salt, we assigned averaged values of thermal conductivity, radiogenic heat production and rock heat capacity derived from the corresponding layers of the starting model. Thus, this layer represents parts of the crystalline crust. Hydraulically we consider impermeable conditions for the crustal layer since the focus is on the thermal field above the Zechstein salt for which we also assume impermeable conditions.

Table 4.2 Summary of the hydraulic characteristics for the calculated models. Porosity and heat capacity assigned to the models after Magri (2005); permeability assigned to the coupled model 2 after Magri (2005) and Magri et al. (2008); permeabilities of the coupled models 1 and 3 after Čermák et al. (1982).

Stratigraphic Unit	Permeability K [m²] Coupled Models/ Sensitivity Analysis			Porosity φ [%]	Rock heat capacity c^s[MJ/(m³*K)]
	Model 1	Model 2	Model 3		
Quaternary	1.0E-13	1.0E-12	1.0E-13	23	3.15
Tertiary-Post-Rupelian	1.0E-14	1.0E-13	1.0E-14	23	3.15
Tertiary-Rupelian-clay	1.0E-16	1.0E-15	1.0E-18	20	3.30
Tertiary-Pre-Rupelian-clay	1.0E-14	1.0E-13	1.0E-15	10	2.40
Upper Cretaceous	1.0E-13	1.0E-13	1.0E-14	10	2.40
Lower Cretaceous	1.0E-13	1.0E-13	1.0E-14	13	3.19
Jurassic	1.0E-13	1.0E-13	1.0E-14	13	3.19
Keuper	1.0E-14	1.0E-14	1.0E-14	6.0	3.19
Muschelkalk	1.0E-18	1.0E-18	1.0E-18	0.1	2.40
Buntsandstein	1.0E-14	1.0E-14	1.0E-14	4.0	3.15
Zechstein	~0	~0	~0	~0	1.81
Basement	~0	~0	~0	~0	2.46

In addition to the assigned physical properties, the results are sensitive to the applied initial and boundary conditions. The extension of the modelled area has been kept large enough to avoid any influence of the imposed side boundary conditions on the numerical results in the central domain of interest. Nevertheless, to prevent any numerical instability in the model runs lateral boundaries are considered closed to both fluid and heat flow. For the top boundary condition a fixed hydraulic head is set (Dirichlet type). Since the regional groundwater flow is driven by pressure gradients we approximate the latter by setting the hydraulic head equal to the topography on top of the Quaternary. This is calculated using a hydrostatic pressure of 0 Pa at the surface. Hence, the gradients in the topography control the groundwater flow. As surface temperature we assign a fixed value of 8°C corresponding to the average annual surface temperature in the area. Hydraulically, a no-flow boundary condition is assumed for the base of the model. For the thermal lower boundary condition we impose a non-constant temperature along the base of the model. This laterally varying temperature distribution is extracted at - 6000 m depth from the lithosphere-scale conductive thermal model of the Brandenburg region (Noack et al. 2012). Thus, the lower boundary condition enable to take into consideration heterogeneous heat input from the deeper lithosphere to the thermal budget in the calculations (Fig. 4.3e).

The initial temperature and pressure conditions are obtained from uncoupled steady-state fluid and heat simulations of the pressure and temperature field. To assure stable conditions, numerical simulations are computed letting the system equilibrating during a computing time window of 250 ka. The results obtained are not used to carry out any kind of forward modelling prediction rather they

represent pseudo steady-state conditions to be correlated to the present-day configuration of the system.
The conductive model provides insights on the background thermal field undisturbed by fluid flow. It allows assessing the interaction between the different thermal properties of the included layers (Tab. 4.1) and their feedback on the temperature field.

In the coupled models fluid and heat transport is coupled taking into account conduction as well as pressure and fluid density effects. Fluid flow is controlled both by resolved gradient in the topography - advective heat transport - and in the fluid density due to fluid temperature variations - convective heat transport.
Though a larger number of coupled numerical simulations have been evaluated we present only the results from the best-fit scenario as coupled model 1. Model results are validated by minimization of the misfit obtained with respect to an available database of measured temperature (Förster 2001; Norden et al. 2008). This database includes 81 temperature measurements (Tables 4.3, 4.4) and combines temperatures from 44 wells derived from various depth and stratigraphic levels. Figure 4.2a illustrates the lateral distribution of these wells across the model area and shows that they vary in their structural position with respect to salt structures.

A comparison of the conductive and the coupled thermal model 1 allows the identification of areas where conductive, advective and convective heat transport mechanisms are relevant. For the coupled numerical simulations we use the same thermal properties as used in the conductive model in addition to average hydraulic properties (Tables 4.1, 4.2). In addition an attempt to systematically address the influence of hydraulic properties is also carried out. Sensitivity analyses have been run to estimate the influence of variable permeabilities within individual layers on the temperature distribution (Tables 4.1, 4.2). The final coupled model 1 represents the scenario giving the best fit with observed temperatures.
Permeability for common rocks varies over more than 16 orders of magnitudes (Ingebritsen and Sanford 1998). In addition, permeability appears to be scale dependent and to vary with the methods followed for its measurements. Given the enormous space scale of the present study, and the degree of uncertainties concerning regional intra-layer variations in lithology a systematic investigation of this parameter on the modelling results has been avoided in the present manuscript. Additional phenomena as dilatational and diagenetic processes have been not considered. Despite these limitations, the simple approach adopted enable to capture first order regional effects of variation in this parameter on the resulting groundwater dynamic and temperature distribution.

Table 4.3 Observed temperatures in wells used for model validation: T at total depth (TD) of temperature log, for perturbed logs corrected temperature at TD of log and corrected bottom-hole temperatures after Förster (2001) and the respective temperatures predicted for the coupled model 1.

Well	TD of log/ depth of BHT [m]	T at TD of log [°C]	Tcorr. at TD of log [°C]	BHT corr. [± 3 °C]	BHT corr. [± 10 °C]	T of the coupled model 1 [°C]
AnsSn/Arendsee 2/60	1500	69.8				63
Chi/Chorin 1/71	3800	144.3	147			124
DaKy/Dannenwalde 102/63	1250	49.8				42
Ela/Eldena 1/74	5150	169.8	181			187
Gap/Garlipp 1/86	4580	149.7	156			164
Ggs/Gorgast 1/70	3250	120.8	124			117
Gs/Gransee 2/67	5050	181.9				177
Gür/Grüneberg 2/74	4100	157	161			147
Khs/Kahrstedt 1/85	2300	105				95
Kd/Karstädt 7/81	900	43.4	45			45
Kotz/Kotzen 1/69	4450	144.4	150			155
Kotz/Kotzen 4/74	5500	172.6	181			193
KrGs/Kraatz 1/76	4350	162	168			157
Ly/Lychen 4/76	4700	154.7	163			159
MbgOg/Meseberg 3/73	4100	148	151			145
MbgOg/Meseberg 3/73	4950				173	172
MirNs/Mirow 1/74	4400	149.2	154			133
Nn/Neuruppin 1/88	2081	78.9				68
GT NG/Neustadt-Glewe 1/88	2284	100.5				101
Ob/Oranienburg 1/68	4200	124	132			150
Pkn/Penkun 1/71	4100	142.6	144			147
Pkn/Penkun 1/71	5500				189	193
Pß/Polßen 1/74	4000	143.4	152			126
Pr/Prenzlau 1/75	4400	151.5	160			136
Pt/Pritzwalk 2/89	2145	81.1				65
RmwL/Rambow 102/64	1950	80				88
RmwL/Rambow 11A/69	4250	139.8				149
RhM/Rheinsberg 1/95	1600	66.1				58
Rhi/Rhinow 5/71	5200	179	182			181
Riu/Riebau 1/70	3500	149.5				136
Rx/Roxförde 2/62	2850	97	113			103
Sw/Salzwedel 2/64	3650	142.6	147			139
Sde/Schilde 1/69	2400	109.5	111			97
Tl/Templin 1/95	1652	69.3				75
Tuc/Tuchen 1/74	4250	139.8	147			151
Utm/Uthmöden 14/78	790			35		33
Utm/Uthmöden 14/78	950			40		37
Vet/Velten 2/90	1650	64.5				72
Wrb/Wartenberg 2/86	1749	71.9				77
Wsbg/Wesenberg 1/72	4250	145.5	149			142
Wsbg/Wesenberg 1/72	5093			184		169
Wbge/Wittenberge 7E/75	5200	171.2	181			170
Wnm/Wittenmoor 101/63	550	28.2				30
Zeh/Zehdenick 2/75	3650	139				138
Zeh/Zehdenick 1/74	4250	159.5	162			155
Zol/Zollchow 1/71	4100	149.8	161			153
ZooGs/Zootzen 1/75	5000	165	173			172

Table 4.4 Observed temperatures in wells used for model validation after Norden et al. 2008 and the respective temperatures predicted for the coupled model 1.

Well	Depth [m]	Temperature [°C]	Quality	T of the coupled model 1 [°C]
GrSk/Groß Schönebeck 3/90	2800	119.9	unperturbed	107
	3770	135.1	unperturbed	133
	4230	148.6	unperturbed	148
	4286	150.8	unperturbed	150
Gs/Gransee 2/67	4100	156.8	unperturbed	146
	4150	157.9	unperturbed	147
	4200	159	unperturbed	149
	4600	170	unperturbed	162
	4650	171.1	unperturbed	164
	4750	173.2	unperturbed	167
	4800	174.8	unperturbed	169
	5000	181	unperturbed	176
RmwL/Rambow 11/A 69	500	36.2	unperturbed	33
	750	42.3	unperturbed	41
	1700	67.6	unperturbed	69
	1950	75.2	unperturbed	76
	3200	107.3	unperturbed	113
	3450	113	unperturbed	120
	3500	114.3	unperturbed	122
Chi/Chorin 1/71	2900	126.6	slightly perturbed	97
	3650	139.8	slightly perturbed	119
Sw/Salzwedel 2/64	2850	122.6	slightly perturbed	118
	3000	126.5	slightly perturbed	122
	3150	129.2	slightly perturbed	125
	3250	131.1	slightly perturbed	127
	3350	133	slightly perturbed	130
Gap/Garlipp 1/86	3400	125	corrected	129
	3800	131	corrected	139
	3850	131.7	corrected	140
	4150	138.2	corrected	150
	4200	139.2	corrected	152
	4350	142.2	corrected	157
	4400	143.7	corrected	158
	4500	149.7	corrected	162

4.3 Results

To assess the influence of moving fluids on the regional thermal field a comparison between the undisturbed temperature field resulting from considering only conductive heat transfer and the temperature field as influenced by additional fluid transport processes is required. Therefore we first display the results from the numerical simulation of the purely conductive heat regime as well as of the coupled fluid and heat regime along a representative N-S cross section (Fig. 4.4a). From north to south, the cross section cuts the deeper basin in the north-west and the basin margin in the southwest (see Fig. 4.2a). The basin area is structured by salt diapirs and salt pillows characterized by an increased thickness as well as areas where the salt has been withdrawn. In the northern part, one major diapir pierces the overburden and reaches close to the surface. South of this diapir prominent salt rim synclines are evident in the surroundings of a smaller diapir. The rim synclines are filled with thick low conductive Pre-Rupelian-clay sediments. Further features visible on the cross-section are Quaternary channels. In the upper part of the model these Quaternary channels cut locally through the Rupelian-clay into the Pre-Rupelian-clay sediments. In contrast to the structural diversity of the basin area, the basin margin in the southwest is represented by the inverted basement crust reaching close to the surface.

Figure 4.4b displays the temperature distribution obtained from the conductive model along the N-S cross-section and illustrates characteristics of the conductive temperature field. Since no groundwater flow has been implemented, the temperature distribution reflects heat transport by diffusion alone, as due to molecules conducting kinetic energy by collision through the medium (Turcotte and Schubert 2002). The pattern of the steady state conductive field is mostly sensitive to the values of the thermal parameters adopted – i.e. thermal conductivity and radiogenic heat production of the solid medium. For this reason it is possible to assess the interaction between different thermal properties of the corresponding layers and their feedback on the temperature field. The temperature field displays nearly flat isotherms across large parts of the model area. Thermal anomalies are only located where diapirs or salt pillows are present. Within and below such structures isotherms are bent downward, whereas in the domains above major diapirs and pillows isotherms bent slightly convex upward. Higher temperatures can be observed where low conductive sediments superpose diapirs and salt pillows. This depends also on the configuration of the post-salt deposits. The Zechstein salt has a distinctly higher thermal conductivity than the surrounding sediments so that diapirs act as a "conductive chimney" efficiently transporting heat upward. This chimney effect is counteracted by a "thermal blanketing" effect by less conductive sedimentary overburden. Due to lower conductivity of the overlying sediments heat transport is reduced, thus leading to increased temperatures within this domain. For this reason conductive thermal anomalies of small-wavelength within the basin reflect the local configuration and interaction between the highly conductive Zechstein salt and the low conductive post-salt deposits.

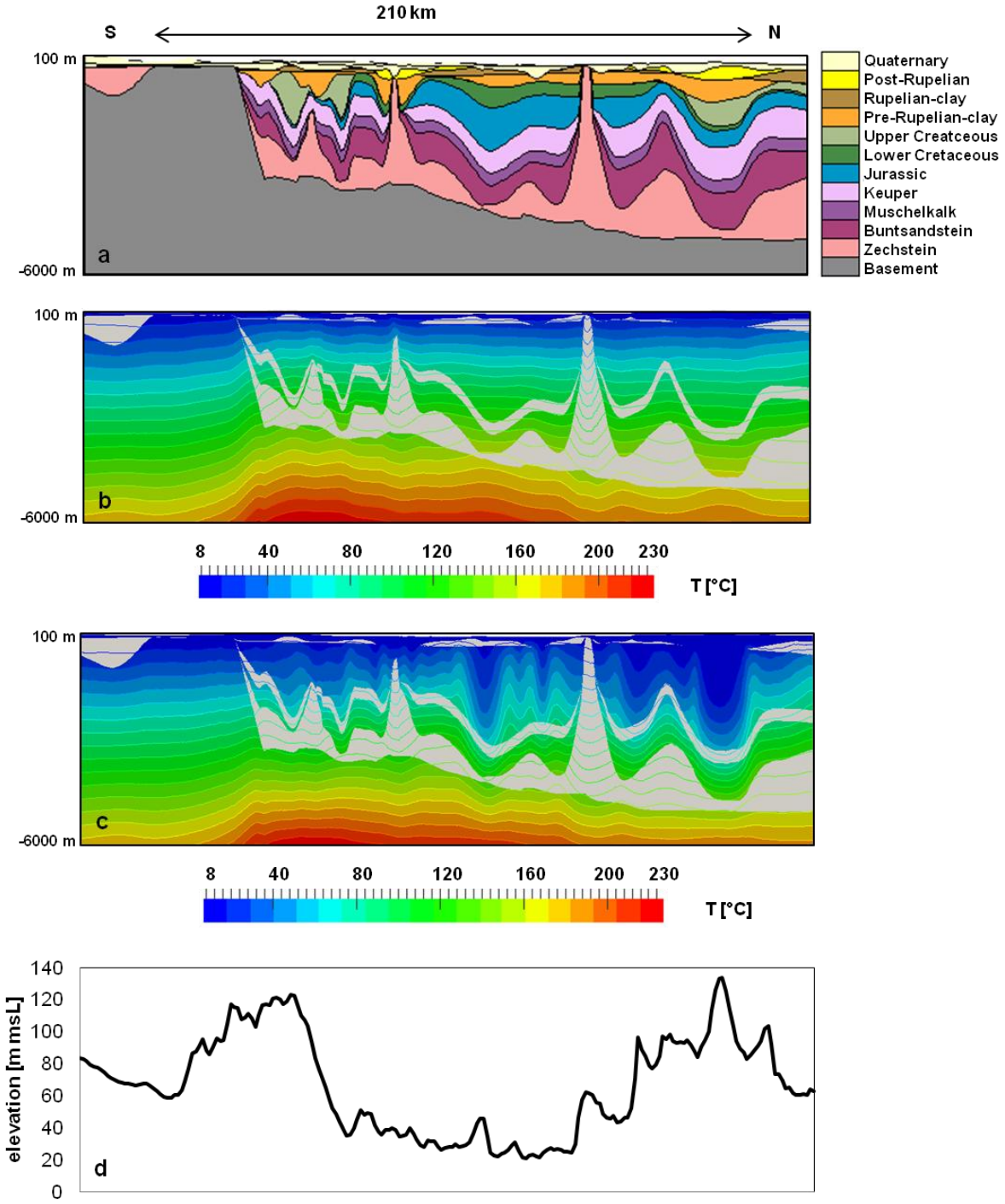

Figure 4.4a N-S cross section of the 3D structural model showing the resolution of the geological units used for the numerical simulations. Vertical exaggeration 10:1. **b** Temperature distribution for the conductive regime along the N-S cross-section with color-coded isotherms, the Zechstein salt and the Middle Triassic Muschelkalk (constant gray shaded), the Rupelian-clay on top (non-constant gray shaded line). Vertical exaggeration 10:1. **c** Numerical results for the fluid and heat regime along the E-W cross-section taking pressure driven groundwater flow and density driven fluid flow into account. The figure shows color-coded isotherms, the Zechstein salt and the Middle Triassic Muschelkalk (constant gray shaded), the Rupelian-clay on top (non-constant gray shaded line). **d** Spatial variation of the topography along the N-S cross section adopted as hydraulic head boundary condition. Vertical exaggeration: ~450:1.

In the south, where the basement is close to the surface, isotherms are bent downward thus resulting in colder temperatures compared with the central basin area. There, the Zechstein salt is absent and the highly-conductive, pre-Permian basement is nearly uncovered by low conductive sediments causing unhampered heat transport to the surface. This is reflected in lower temperatures of larger-wavelengths at the southern margin. In contrast, in the basin area, heat input from the underlying crust is stored since the lower conductivity of the sediments causes thermal blanketing and thereby higher average temperatures. These large wavelength anomalies are most obvious where small-wavelength anomalies are weakly pronounced, especially below the Zechstein salt. Thereby, the variable temperature assigned along the base of the model distinctly influences the temperature distribution (Fig. 4.3e). This is clearly visible within the basement layer in the forefront of the outcropping crust (Fig. 4.4b). Since the temperature is extracted at - 6000 m depth from a lithosphere-scale conductive thermal model of the Brandenburg region, it reflects the heat contribution of a thinned (in the north) and a thickened (in the south) upper crust enriched in radioactive decaying elements (Noack et al. 2012). Owing to the cumulative thickness of the overburden towards the basin centre this leads to higher temperatures within the crustal layer for this part of the domain.

The pattern in the temperature distribution changes if fluid flow is additionally considered (Fig. 4.4c). Since the hydraulic head is set equal to the topographic elevation for the study area (Fig. 4.4d), the regional groundwater flow as driven by pressure gradients is controlled by gradients in the topography which are characterised by recharge areas in the highlands and discharge areas in the lowlands. Thus, pressure forces act on the thermal system according to local topographic elevation and changes in the relief (Fig. 4.4d). In contrast to the temperature distribution of the conductive model, the bending of the isotherms maps the influence of the regional groundwater flow on the thermal field for the coupled model 1. The northern part of the model which belongs to the basin area is characterized by high topographic gradients (Fig. 4.1b). There, pressure forces driven by hydraulic head gradients push cold water inside the system (Fig. 4.4c). The surface water reaches a depth of more than 2000 m in these domains. This process occurs in areas where the Rupelian-clay is absent (Fig. 4.3d and 4.4c) and leads accordingly to advective cooling within the pre-Rupelian-clay aquifer. The overall net cooling effect is triggered by the choice of 8 °C as fixed temperature boundary condition at the surface and it is displayed by pronounced temperature lows far from the diapirs where the pre-Rupelian-clay aquifer is thickest. Locally, buoyancy forces may counteract forced convective forces. In the south of the major diapir, gradients in the topography are far lower than in the north and the Rupelian-clay is present over most of the area. Where the Rupelian-clay is present, the post- and pre-Rupelian-clay aquifers are hydraulically decoupled. As a consequence of this hydrogeological setting, pressure gradients are weak (Fig. 4.4d). Thus, density gradients as triggered by fluid temperature variations can induce buoyancy forces which are strong enough to activate thermal convection with rising warmer fluids from deeper parts of the system up to the base of the Rupelian-clay. At the southern part of the cross

section where the low permeable pre-Permian basement is nearly uncovered by sediments the isotherms reveal again a conductive signature.

To analyse where moving fluids are active and to illustrate the thermal and hydraulic behaviour of the geological layers we additionally compare the calculated temperature distribution of the conductive and the coupled model 1 for selected depth levels. Thereby, the conductive model is represented by figures 4.5a, 4.5c and 4.5e and the coupled model 1 by figures 4.5b, 4.5d and 4.5f.

For both models all temperature maps show an almost identical homogeneous temperature distribution for the corresponding depth levels along the southern basin margin. This rather homogeneous thermal pattern changes with increasing thickness of the overburden towards the basin centre depending on the heat transfer processes which are effective in the different domains. As a result, thermal anomalies are distinctly different for the two models. This observation holds throughout the depth levels at 1000 m depth (Fig. 4.5a and 4.5b), at 2000 m depth (Fig. 4.5c and 4.5d) and at 3000 m depth (Fig. 4.5e and 4.5f). Nevertheless, for all temperature maps a general trend is visible. In the basin area, higher temperatures are predicted for the conductive model (Fig. 4.5a, 4.5c, 4.5e).

The temperature maps at 1000 m depth (Fig. 4.5a and 4.5b) cuts structural elements above the low permeable Middle Triassic Muschelkalk layer. Temperatures between 30 and 50 °C are predicted for both models along the southern basin margin.
For the basin area the conductive model at 1000 m depth (Fig. 4.5a) shows both positive and small-wavelength thermal anomalies of 70°C and higher as well as negative thermal anomalies of limited spatial extent around 45°C according to the chimney effect as induced by major salt structures. Thereby, positive thermal anomalies are predicted for those diapirs with a significant low conductive sediment cover on their top. Diapirs which are almost uncovered by sediments are represented by localized negative thermal anomalies. Thermal anomalies of larger wavelength predicted in the northwest (negative thermal anomaly around 50°C) and in the southeast (positive thermal anomaly around 60°C) result from heat input of the underlying crust. Thereby, negative long wavelength thermal anomalies reflect the lower heat input from the thinned upper crust, whereas positive thermal anomalies result from the higher heat input of the thickened upper crust towards the basin margin (Fig. 4.4a).

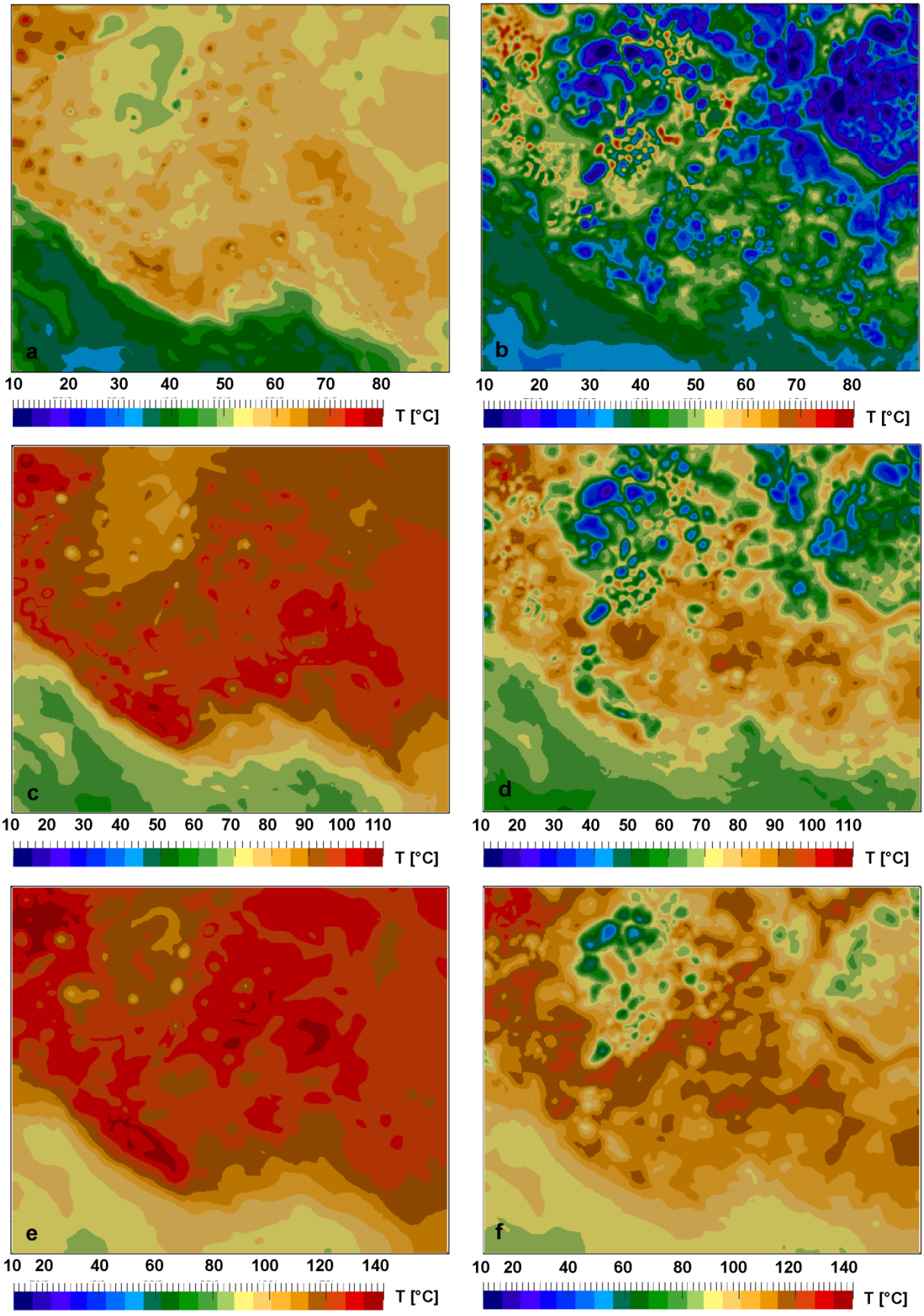

Figure 4.5 Predicted temperatures in °C extracted from the 3D thermal models at 1000 m depth (**a,b**), at 2000 m depth (**c,d**) and at 3000 m depth (**e,f**) for the conductive model (**a,c,e**) and the coupled model 1 (**b,d,f**).

Distinctly colder temperatures are predicted at 1000 m depth for the coupled model 1 (Fig. 4.5b). In the regions where the Rupelian-clay is absent lower temperatures between 10 and 30°C are predicted expressed as small-wavelength negative thermal anomalies. Based on these Rupelian windows an overall net cooling effect is introduced due to inflow of cold water from topographic highs.
In contrast to these regions characterized by advective cooling, restricted areas reveal small fields of higher thermal anomalies between 60 and 70 °C in the north-western model region. There, hot and less dense water rises due to buoyancy forces and points to the development of convective cells in the deepest part of the basin, where the thickness of the Mesozoic aquifer is largest (Kaiser et al. 2011). Furthermore, these anomalously high temperatures evolve in those regions where the low permeable Rupelian-clay is present thus preventing the inflow of cold water from above and shielding from the influence of superficial hydraulic head gradient.

The temperature maps at 2000 m depth (Fig. 4.5b and 4.5c) cut the deepest parts of the post-Rupelian aquifer and also the upper parts of the Mesozoic pre-Rupelian-clay aquifer. Almost restricted to the northern basin domain the map cuts structural elements above the Middle Triassic Muschelkalk layer (see Fig. 4.4a). At the southern basin margin, average temperatures between 50 and 70 °C are predicted by both models.
The temperature map for the conductive model (Fig. 4.5c) displays again small-wavelength warm (around 100°C) and cold (around 75°C) thermal anomalies corresponding to thickness and structural configuration of both the salt structures and their related sedimentary overburden. Large wavelength positive thermal anomalies of about 100°C are predicted for a region with increased heat input from the thickened crust (Fig. 4.4a and 4.4b). In contrast, negative large wavelength thermal anomalies of around 80°C are predicted in the northern domain where the crustal basement is thinnest.

For the coupled model 1 (Fig. 4.5d), the configuration of the Rupelian-clay and the depth position of the Middle Triassic Muschelkalk layer are of great influence for the temperature distribution (Fig. 4.3d and 4.4a). Since only parts of the northern model domain are located above the Middle Triassic Muschelkalk, a smaller region is affected by cold waters. These regions map the communication pathways between the upper post-Rupelian aquifer and the Mesozoic aquifer through the Rupelian windows at this depth level. The decrease in influence of moving fluids is also reflected in a reduced net cooling effect of local domains. This is expressed as small cold field thermal anomalies between 10 and 45 °C. Small positive t6hermal anomalies between 100 and 110°C mark again regions of thermal instabilities where warm waters rise in response to buoyancy forces.

The temperature maps at 3000 m depth (Fig. 4.5e and 4.5f) cut the deeper part of the Mesozoic pre-Rupelian-clay aquifer. Average temperatures between 80 and 100 °C are predicted for both models at the southern basin margin.

The thermal features as predicted for the conductive model do not significantly change at 3000 m depth (Fig. 4.5e). Small-wavelength temperature lows around 100 °C are located at the base of the salt structures due to the chimney effect, whereas corresponding temperature highs (around 120 °C) are predicted below rim synclines in response to the thermal blanketing effect of the salt overburden. The long-wavelength trend in the temperature distribution is expressed by temperatures between 120 and 130 °C over large areas of the basin domain.

In opposite to temperature pattern predicted for the conductive model, the coupled model 1 still shows a clear influence of moving fluids though the latter appears to be decreasing with increasing depth. Signs of advective cooling are only locally displayed for small areas above the Middle Triassic Muschelkalk layer in the northwest and northeast. Thereby, the related thermal imprint appears below Rupelian windows and deep reaching Quaternary channels as reflected in the temperature lows (see Fig. 4.3d). Corresponding temperatures range between 50 and 90°C. Due to this effect, the thermal imprint resulting from heat conduction is even more pronounced below the prominent salt rim synclines in the surroundings. However, apart from these areas the temperature pattern is affected by conduction resulting in a temperature variation between 110 and 130°C within the basin domain. Nevertheless, the comparison of both model results reveals a thermal feedback from convective heat transport of the shallow part of the upper aquifer right below the Middle Triassic Muschelkalk layer (Fig. 4.4b and 4.4c; Fig. 4.5e and 4.5f). This feedback leads to a cooling of about 10 K for respective areas compared to the conductive case.

To evaluate the temperature predictions for the conductive and the coupled model 1 we test their validity by comparison with temperature observations available from wells. For this reason we extract temperatures from both models for the horizontal coordinates and depth where observed temperatures are available (Tables 4.3, 4.4). Figure 4.6a illustrates the correlation between the temperature predictions of the conductive model (green triangles) and the coupled model 1 (blue triangles) with the observed temperatures (red triangles). To give a better illustration which model prediction is closer to the observations we plot the correlation also as a trend line. The figure indicates that the conductive model predicts too high temperatures, whereas the coupled model 1 slightly underestimates the temperature observations. Thereby, the deviation for the conductive model is highest within the shallow temperature field down to about 2000 m depth. In contrast, for the coupled model 1 approximately 70% of the model predictions show a deviation of 10 K from observations (Tables 4.3, 4.4). To give a visual impression of the distribution of these data we show the deviations between measured temperatures and model predictions by means of a histogram (Fig. 4.6b). Therefore, we subtract the temperature predictions at each coordinate from the respective temperature observations. The histogram shows the frequency of temperature deviation in non-overlapping intervals. We see that most of the temperature deviations are related to the intervals above zero. This means that despite of good correspondence between the predicted and observed temperatures, the coupled model 1 predicts

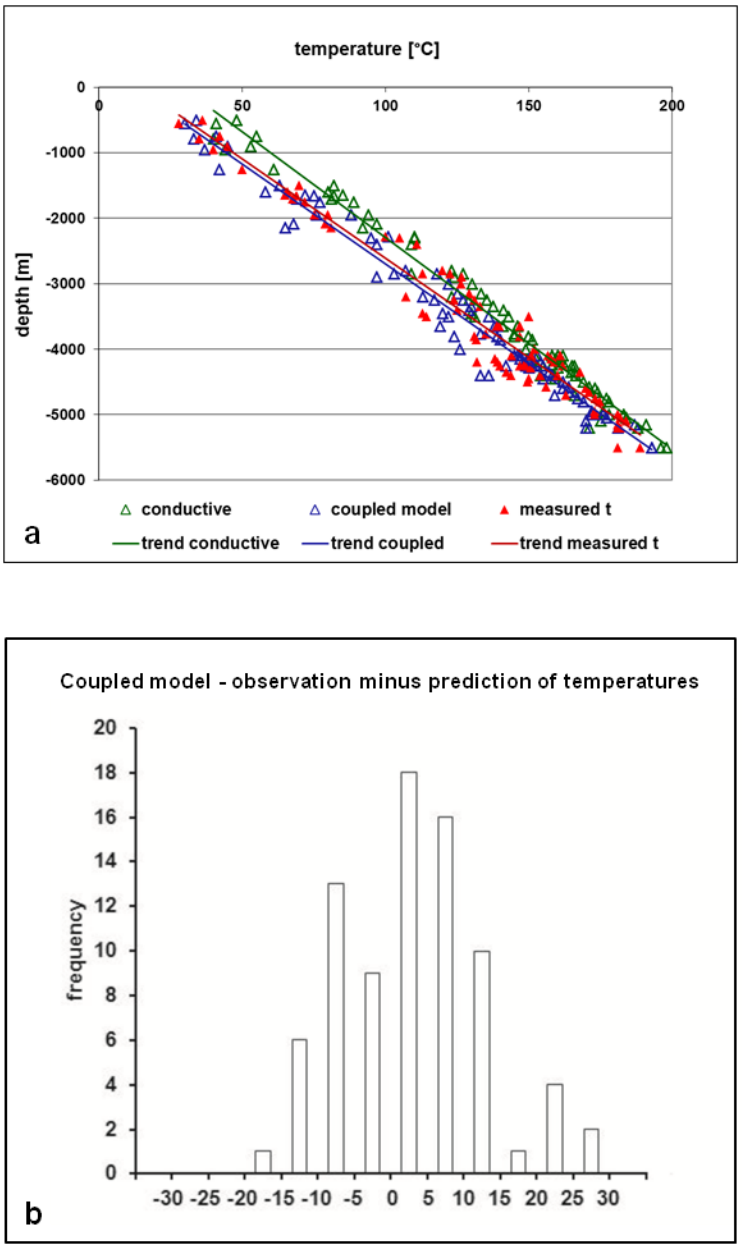

Figure 4.6a Comparison of measured and predicted temperatures: for the conductive and the coupled model 1. **b** Frequency of temperature deviation between temperature prediction and observation for the coupled model 1.

rather too low than too high temperatures. The better fit of the coupled model 1 to the observations is also reflected in a comparison of observed and modelled thermal gradients for the wells SW 2/64, RmwL 11/69, Gap 1/86 and GrSk 3/90 (Fig. 4.7).

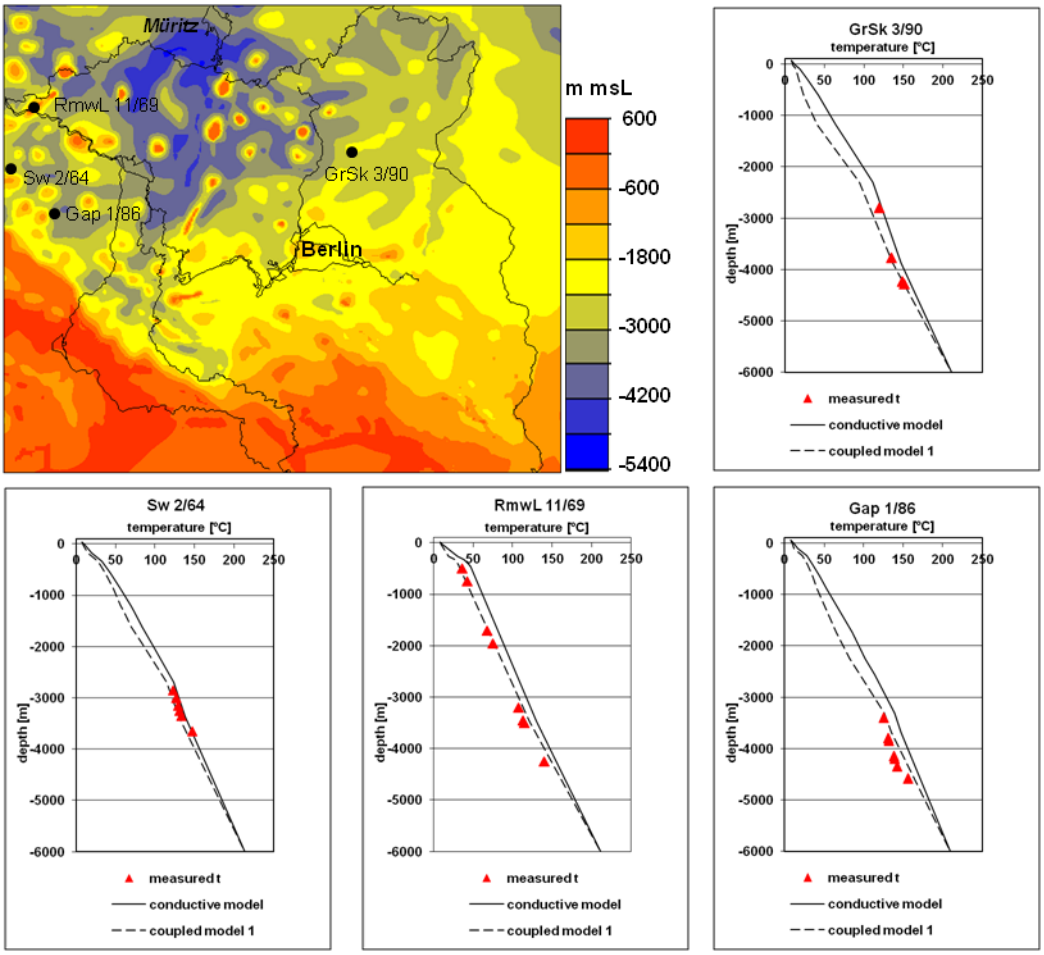

Figure 4.7 Top of the Zechstein salt with location of wells where measured temperatures to show the temperature gradients are available.

4.4 Sensitivity Analysis

The results so far indicate that motion of fluids occurs mainly above the Middle Triassic Muschelkalk where the upper aquifer is characterized by a sufficient thickness. Motion of fluids strongly depends on the lithologies of the respective layers and their associated hydraulic properties. Thereby, fluid circulation may not only depend on the thickness of the permeable layers but on their permeability as well. More precisely, fluids may distort the thermal field if the permeability is high enough (Huenges 2010). Coupled groundwater flow and heat transport analysis from other regional-scale studies in sedimentary basins for depth between 0 and 7 km infer permeabilities in the range of 10-16 to 10-12 m² (Manning and Ingebritsen 1999) and 10-18 to 10-12 m² (Ingebritsen and Sanford 1998; Neuzil 1994). To estimate to which degree variation in permeability between the aquifers controls the regional thermal field we run sensitivity analyses and compare results from three end-member scenarios (Tables 4.1, 4.2).

By observing Table 4.2, it turns out that the permeability of the Quaternary and Tertiary layers for coupled model 2 is one order higher than the values of the coupled model 1 (best fit scenario). The coupled model 2 represents a more realistic vertical distribution in permeabilities since the unconsolidated Quaternary sediments should be characterized by a higher permeability as the Mesozoic sediments due to their lower compaction. Also the permeability for the Tertiary-Post-Rupelian and the Tertiary-Pre-Rupelian-clay, both composed of sand as the main component, should not be lower than the values for the more compacted underlying clastic deposits. The permeability dataset chosen for the coupled model 2 was also used by Magri et al. (2005b) who run thermohaline simulations but did not consider the separation of the shallow aquifer by the Rupelian-clay.

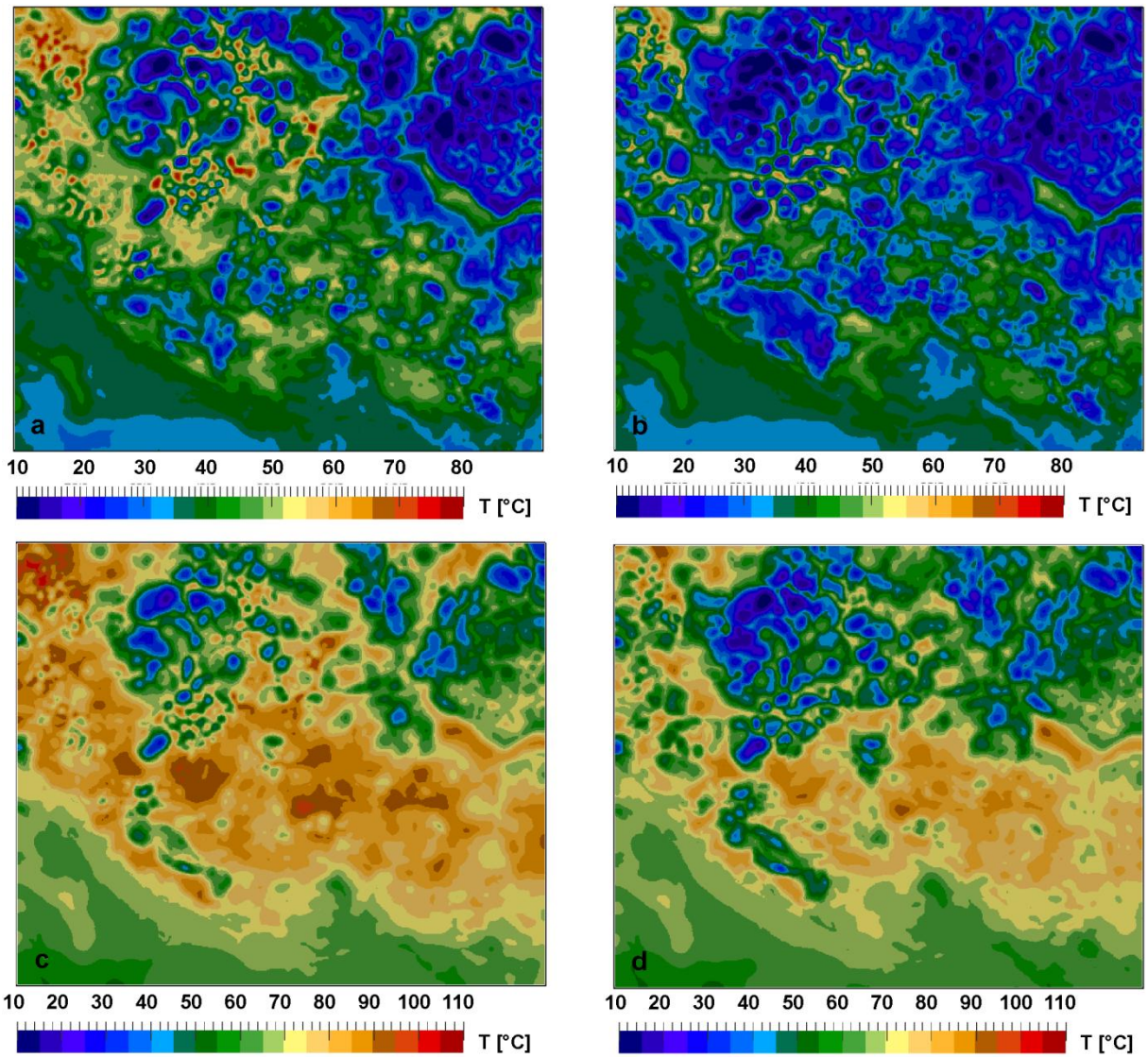

Figure 4.8 Predicted temperatures in °C extracted from the 3D thermal models at 1000 m depth (**a,b**) and at 2000 m depth (**c,d**) for the best-fit coupled model 1 (**a,c**) and for the coupled model 2 model (**b,d**).

Nevertheless, sensitivity analyses with coupled model 2 have shown that applying higher values for the permeability assigned to the Quaternary and Tertiary leads to a stronger cooling at 1000 m depth compared with the results from the coupled model 1 (Fig. 4.8a and 4.8b). This result is also valid for the thermal field at 2000 m depth (Fig. 4.8c and 4.8b). In the coupled model 3 we test the influences of a decreased permeability for the permeable layers between the Tertiary-Rupelian-clay and the Middle Triassic Muschelkalk by one order of magnitude, thus preventing the strong cooling induced by the upper boundary condition. Additionally, we set the permeability for the Rupelian-clay to the lowest magnitude for impervious clays after Čermák et al. (1982), a value equal to that of the Middle Triassic Muschelkalk formation. Sensitivity analyses have shown that such decreased permeabilities for the Pre-Rupelian-clay formations leads to rising temperatures to values close to the results from purely conductive modelling.

4.5 Discussion and Conclusion

By means of 3D numerical simulations our systematic analysis aims to investigate the shallow thermal field above the Zechstein salt in the subsurface of Brandenburg. Based on a structural and hydrological model that represents the three main aquifer complexes above the Zechstein salt separated by the low permeable Middle Triassic Muschelkalk and the important Tertiary Rupelian-clay aquitard we discuss how the main heat transport processes do interact and influence the thermal field in Brandenburg. In a second step we analyze to which degree permeabilities of the sediments play a role for fluid circulation within the aquifers. Due to the lack of hydraulic data we validate the model predictions only by means of a temperature database (Förster 2001; Norden et al. 2008).
The conductive model reflects the undisturbed thermal field for the subsurface above the Zechstein salt if heat transport by fluids is neglected. The results show that a strong lateral contrast in thermal conductivity between a conductive crystalline basement in the south and insulating thick sediments in the basin controls the regional temperature distribution. The pattern in the basin area is disturbed by local thermal anomalies in response to the chimney effect near the thermally conductive salt structures. Thus, the spatial configuration of the highly conductive Zechstein salt is the second main controlling factor for the basin-scale thermal field.

In contrast, the coupled model 1 reveals that the thermal field of the upper 2 km is strongly influenced by moving fluids driven by forced convective forces due to hydraulic pressure gradients. The depth influence of advective cooling is controlled by the depth of the shallowest aquitard and by communication pathways between the different aquifers.

Free convective thermal anomalies induced by buoyancy forces due to density gradients occur only locally where the pressure forces are weak and are controlled by the thickness and permeability of the respective permeable layers.

Summarizing, we conclude that conductive heat transport is the dominant heat transfer mechanism for the study area, whereas the thermal field in the shallow aquifer is additionally influenced by forced convective heat transfer and related advective cooling. By means of sensitivity analyses we estimate which permeabilities are effective for the model volume.
The comparison between temperature predictions and observations (Förster 2001) of the thermal models shows that the predicted temperatures of the conductive model are too high for all depth levels. The coupled model 1, using rather lower permeabilities for the less compacted succession of Quaternary and Tertiary sediments reproduces the thermal field for the area of Brandenburg best.
Down to 2 km depth, a comparison between the temperature pattern of the conductive model and the coupled model 1 reveals that the shallow temperature field is strongly affected by moving fluids. This is especially the case where the absence of the hydraulic barrier of the Rupelian-clay provides pathways between the different aquifers for fluids. However, using average hydraulic properties as assigned for coupled model 2 causes a very pronounced cooling and thus leads to an underestimation of temperature observations for this depth. This may be explained by the fixed upper thermal boundary condition of 8 °C imposed at the model surface in interaction with the structural configuration of the Quaternary and Tertiary deposits. In consequence of this hydraulic and thermal boundary condition, the mobility of fluids affects quite deep levels where the Quaternary channels cut through the Rupelian-clay. The only way to reduce this boundary effect is to assume a reduced permeability for the shallow part of the hydraulic system. A closer examination of the assigned permeabilities of the respective layers shows that the Quaternary is more permeable than the underlying deposits. Additionally, a high permeability for both, the Tertiary-Post-Rupelian and the Pre-Rupelian-clay sediments results in colder modeled temperatures than observed. Where the hydraulic head is large, cold surface water is driven by forced advection down to a depth where less permeable layers stop this process. This boundary effect is strongly reduced for the coupled model 1 if a decreased permeability for the Quaternary and Tertiary succession by 1 order of magnitude is considered to fit observed temperature in the upper 2 km. The deeper aquifer below the Middle Triassic Muschelkalk bears locally signatures of a thermal feedback from the overall lower temperatures of the depth levels influenced by cooling fluids though the regional trend is mainly controlled by heat conduction.

The observations discussed are hampered by the model simplifications. Simulation of hydrological processes for large scale models requires data that reflect the geophysical environment of the subsurface in a sufficient way. This includes hydrological and hydrogeological parameters as well as the application of reasonable boundary conditions. An upper thermal and hydraulic boundary

condition which leads to pronounced cooling is not able to reproduce adequately temperature observations. A more appropriate approach to prevent this effect may be introduced when a boundary condition based on groundwater recharge is set on the surface of the model. This should result in a more realistic temperature distribution. Nevertheless, studies in the Dutch part of the Roer Valley Graben indicate freshening of sediments within the upper 1 km of the basin fill caused by a topography driven groundwater flow system (Luijendijk et al. 2010, 2011). In addition, results from previous chemical and isotope studies by Tesmer et al. (2005) and Möller et al. (2008) revealed for the Brandenburg region that formation water have been replaced by geologically younger waters down to 700 m depth. With respect to the parameter sensitivity analysis it has to be mentioned that we address only temperature-induced density changes of the fluid, whereas salinity may also be relevant. Though there still is considerable debate on the effect of fluid salinity on the evolution or inhibition of free convection we want to mention this point for completeness. Salinity may influence fluid transport in various ways. Artemieva (1997) found that permeability of cracked granites depends on brine salinity and is less sensitive to temperature variations. Results from 2 D thermohaline simulations by Magri et al. (2008) indicate that temperature and salt concentration gradients are sensitive to hydraulic permeability, whereas some authors doubt that saline brines would rise driven by free convective forces (Kaiser et al. 2011; Cacace and Kissling 2012).

A further limitation is the simplified vertical resolution of the model. As the presence of the low permeable Rupelian-clay prevents circulation of fluids and thus heat transfer, we assume that smaller-scale lithology differences if resolved in the model structure would also influence the thermal signature. If such intercalated layers are low permeable they could prevent cold fluids to reach deep parts of the system and warm fluids to rise to shallower levels, but they could also support the increase of the temperatures below due to a lower thermal conductivity. Similar effects could arise if horizontal facies changes were resolved in the model. Anyway, the assumption of isotropic and homogeneous conditions within each layer does not reflect real aquifer conditions. Permeability is also a function of depth as presented e.g. by Manning and Ingebritsen (1999). Nevertheless, the limited stratigraphic resolution of the model enables to quantify main controlling effects on the thermal field.

Another aspect is that faults are not included in the model. Since faults provide pathways for moving fluids, regions of poor correspondence between temperature prediction and observations may be associated with hydrothermal circulation of fluids along faults which are not resolved in the model. Lampe and Person (2002) show with 2D numerical groundwater flow and heat models in their studies on advective cooling within the Upper Rhinegraben (Germany) that negative thermal anomalies develop in areas of cold recharging groundwater along the graben flanks regardless of fault permeability, whereas hot discharging groundwater near the topographic low of the graben results in positive thermal anomalies. Petitta et al. (2011) describe by means of groundwater conceptual models

in their studies on interaction between deep and shallow groundwater systems that high-salinity groundwater rises along tectonic lines and mix with shallow groundwater in the Quaternary deposits. Recently, the impact of faults and damage zones on the fluid flow and heat transport was also addressed by authors who conduct 3D numerical simulations. Cherubini et al. (2013a) focus on the impact of inclined faults on the hydrothermal field by adding simplified structural settings to synthetic models. The influence of both a major permeable fault and impermeable faults on the thermal, pressure and velocity field were also investigated for the geothermal research site Groß Schönebeck within the Brandenburg region (Cherubini et al. 2013b). Cacace et al. (2013a) present an approach to develop a model that includes a complex fault geometry and the property definition of heterogeneous fault zones and host rock via a case study in the western central Molasse Basin, southern Bavaria in Germany. According to their studies Cherubini et al. (2013a, b) find that faults may act as preferential pathways for advective heat and have a local, strong impact on the thermal field.

Our study provides basic understanding on the influence of thermal and hydraulic boundary conditions in combination with effective average transport parameters for a basin-scale model of the subsurface of Brandenburg. By means of a 3D hydrogeological model, which is representative for the sediment complexes in North Central Europe, we investigate the interaction of the heat transport processes within corresponding aquifers. In particular, the consideration of the regionally important Rupelian-clay aquitard offers new insights on the mechanisms of interchange between the shallow freshwater complexes and saline brines from the deep aquifers.

Acknowledgements

This work is part of the GeoEn project and has been funded by the German Federal Ministry of Education and Research in the program ‘‘Spitzenforschung in den neuen Ländern’’ (BMBFGrant03G767 A/B/C). We thank our colleagues from the geological surveys of Landesamt für Bergbau, Geologie und Rohstoffe Brandenburg for providing the main data to construct the refined 3D structural model of the basin fill and for fruitful discussions. Landesamt für Geologie und Bergwesen Sachsen-Anhalt and Landesamt für Umwelt, Naturschutz und Geologie Mecklenburg-Vorpommern kindly provided additional well data to complement the database of the reference structural model outside of the Brandenburg area. A huge thank to Björn Lewerenz and Björn Onno Kaiser for very helpful computational support. We also thank the anonymous reviewers for their constructive comments which greatly improved the paper. Numerical results have been visualized with the open source post-processor Para View.

5 Discussion

Heat flow measurements at the surface represent a complex signal that contains integrated effects of thermal conductivity, heat production and mantle heat flow (Davies and Davies 2010). Temperature in the Earth increases with depth at an average rate of 3 K/100 m (Beer and Hurtig 1999). This is due to a continuous basal heat input from the mantle (Huenges 2010). This heat enters the lithosphere at its base, a depth level defined by the 1300° isotherm at which partial melting of peridotite is expected to occur (Turcotte and Schubert 2002). Additionally heat is generated in the continental crust where silicic crystalline rocks are rich in radiogenic heat producing elements (Bjørlykke 2010). Thus, the crustal radiogenic heat contribution also influences the continental geotherm (Allen and Allen 2005). The heat budget can be transferred via the solid and the liquid component of the Earth system. In consequence the heat budget of the Earth may vary vertically and horizontally in response to variations of crustal composition and lithosphere thickness, but also because of the potential influence of moving fluids.
Considered as a whole these findings already point to the fact that the choice of the thermal boundary conditions, the physical properties of the rock units and the heat transport mechanism involved are the most relevant parameters for thermal modelling.

Initially two main questions have been formulated in the objectives of the thesis (section 1.1) for which the results of the thesis provide some answers.
Question 1: Is it possible to predict the regional thermal field adequately by means of thermal models which consider geological structures as well as physical processes and can these predictions be validated and considered as being more realistic than classical interpolation techniques?
Question 2: Which heat transport processes should be considered at different model scales and depths and are there processes that can be neglected?

According to the results of the thesis **Question 1** can be answered affirmatively whereby individual shares have been quantified additionally, albeit subject to certain restrictions. The first restriction is made to the heat transport process considered in the modelling approaches. The reason therefore is that several physical processes may be involved to different amounts in shaping the thermal field which leads to superposition of thermal effects. Hence, the main controlling factors impacting the thermal field of Brandenburg were assessed stepwise in this thesis by means of different modelling approaches offering improved model complexity from step to step. For the crustal-scale and the lithospheric-scale thermal models presented in chapter 2 and 3 conduction dominated heat transport is considered under the assumption that the thermal field has reached steady-state conditions in the area. If these restrictions are valid, some conclusions can be drawn from comparative thermal modelling studies of a

simpler crustal-scale model (fixed heat flow at the Moho and homogeneous crustal structure) and a higher resolved lithosphere-scale model (1300 °C at the thermal LAB and differentiated crustal structure). The resulting overall picture shows that the configuration of the lithosphere (section 5.1) and the thermal conductivities of the rock units (section 5.2) are the most influencing factors for the thermal field. Final conclusions derived from these findings are discussed in the following sections **5.1.** and **5.2.**

5.1 Configuration of the Lithosphere

The results obtained from the conductive simulations clearly show that the interaction between structural heterogeneities and the related variations in physical properties induces specific variations in the temperature distribution.
The comparison between the crustal-scale and the lithosphere-scale model indicate that the configuration of the deeper lithosphere significantly affects the shallow thermal field induced by the modified heat budget that is controlled by:

(1) The basal heat inflow from the mantle which is related to the topology of the LAB that corresponds to the 1300°C isotherm;
(2) The heat inflow which is defined by the configuration of the crystalline crust.

Accordingly, lateral variations in the temperature distribution within the shallow thermal field result from both gradients in the depth position of the LAB and the configuration of the crystalline crust. The lithosphere boundary in the lithosphere-scale model of the thesis is shallowest in the western part of the model area. According to this flat position, the lithosphere is thinnest in that region which results in a steep average thermal gradient in this domain. Additionally, in the southwestern part of the model area at the southern basin margin, the highly conductive crystalline crust close to the surface causing efficient heat transport through the lithosphere (chimney effect). This in turn results in decreased shallow temperatures in this region compared to the northerly adjacent model area which is characterized by increased temperatures according to the thermal blanketing effect of the low conductive sedimentary overburden. The overall resultant long-wavelength pattern in the temperature distribution is even more complex due to the fact that the upper crystalline crust additionally produces radiogenic heat and thus contributes to the total heat budget in areas where this layer is thick. Thus the total heat budget varies laterally due to the superposed effect of the heat input from the deeper mantle and the radiogenic heat production of the crust. The thickness of the radioactive upper crust varies from less than 6 km in the north-western part of the model to ~ 24 km in the south-east. The largest thickness (up to 30 km) is reached at the basin margin in the south-west. Consequently, in this south-western region the total heat budget is increased in the lithosphere-scale model, compared to the model

assuming a uniform crust and thus produces higher temperatures. This larger heat input results in up to 30 °C higher temperatures in 3000 m depth in that region. The temperature difference between both models is even larger towards the central model domain, where the increased thickness of the low conductive sedimentary cover causes thermal blanketing. Up to 60 °C higher temperatures are predicted by the lithosphere-scale model at 6 km depth. As the sedimentary fill is the same in both models the higher temperatures in the lithosphere-scale model have to be attributed to the contribution from the radiogenic upper crust which is thickened below the basin part of the model. In contrast, in regions where the thickness of the upper crust is reduced up to 20 °C lower temperatures are predicted by the lithosphere-scale model at the same depth than by the simpler model assuming a homogeneous crust.

The simpler crustal-scale thermal model of the thesis (chapter 2) shows a similar approach as Scheck (1997) and Bayer et al. (1997) who used a fixed temperature of 600 °C and a fixed heat flow of 25 mW/m² at the Moho respectively as lower boundary condition below a simplified crustal volume for their conductive model of the Northeast German Basin. The upgraded lithosphere-scale model as represented by chapter 3 of the thesis cannot be compared directly with model approaches of other studies. Ondrak et al. (1998) locally modified the input parameters and the lower boundary condition of the model from Bayer et al. (1997) for a high resolution model of geothermal production schemes to better fit observed temperatures. These authors calculated the temperature distribution by means of a regional model limited by a lithosphere boundary hypothesized at 90 -100 km depth. From this model they derived a constant heat flow of 60 mW/m² to constrain the basal boundary of their high resolution model. Norden et al. (2008) reproduced observed surface heat flow assuming different boundary conditions for the thickness of the thermal lithosphere along a 2D profile crossing the area of Brandenburg. The results of the thesis confirm the findings of Norden et al. (2008) in that the thermal field and the surface heat flow depend of the depth position of the LAB (lower thermal boundary condition) and of the thickness of the radiogenic crust. Cacace et al. (2010) have also stressed the importance of the consideration of the deeper lithosphere. These authors quantified the impact of different mantle configurations on the 3D thermal field for the Northeast German Basin. They showed that different topographies of the 1300 °C isotherm assigned as lower thermal boundary condition at the lithosphere-asthenosphere boundary may cause lateral temperature differences of up to 20 K at 3 km depth.

Though on larger spatial scale, also Cloetingh et al. (2010) showed how first order thermal constraints from surface heat flow and deep subsurface geophysical data sets can be used jointly to build and constrain thermal models of the lithosphere outside the coverage of well control. Moreover these authors demonstrate that the predicted first order patterns in thermal and rheological structure correlate spatially with earthquake distribution, and partitioning of deformation in Europe derived from geodetic measurements. From their findings Cloetingh et al. (2010) deduce implications for a

continent-scale exploration for geothermal resources and formulate hypotheses for both thermal and mechanical characterisation at depth. Though of a smaller spatial extent, the results of this study likewise permit characterisation for geothermal exploration and an assessment of the rheological (and mechanical) consequences of the modelled temperatures.

Considering the geological structure for geothermal exploration is not new but in consensus with studies from other basins. An example was presented by Chopra and Holgate (2005), who have generated a map of estimated temperature at a depth of 5 km in the Australian crust. Therefore the authors calculated the crustal temperature at several well locations using thermal gradients, surface temperature estimates and the depth to basement information assuming a uniform geothermal gradient of 25 °C/km for the basement rock. Though this approach is limited by a heterogeneous data distribution that produce artefacts in areas of sparse data coverage, it is in agreement with a major result from this thesis: the authors found that lowest shallow temperatures are associated with regions where the crystalline basement is near the surface (e.g. Gawler Craton, Lachlan Folt Belt), whereas regions of high shallow temperature are often associated with a thick sedimentary basin cover (e.g. Cooper-Eromanga Basin of central Australia). Chopra and Holgate conclude that the incorporation of geological information into the interpolation process can reduce interpolation artefacts where sufficient subsurface data are available.

The prominent role of the thickness of the upper crust is also documented by studies of Mareschal and Jaupart (2013) who state that crustal geotherms depend mostly on the thickness of enriched upper crustal rocks. In this context it is already known from earlier studies (Lassen et al. 2002; Bayer et al. 1997; Maystrenko and Scheck-Wenderoth 2013) that the deeper crust below the sedimentary basins of North Central Europe is heterogeneous in its structure. Mareschal and Jaupart (2013) argue that upper crustal rocks tend to have a larger heat production than the bulk crust, whereas lower crustal rocks tend to be depleted in elements producing radiogenic heat compared to the upper crust. These findings point to the fact that the assumption of a homogeneous crust underneath the basin-fill may not be justified. Instead of that, the integration of a more realistic lithosphere configuration supported by geophysical data allows to quantify the influence of a differentiated crust on the thermal field. However, to integrate a realistic configuration of the deeper lithosphere into thermal models requires that the respective geophysical information is available.

For the lithospheric model presented in chapter 3 such a database could be used to differentiate the deeper lithosphere into an additional layer for the pre-Permian, two layers for the upper and lower crystalline crust and a mantle part limited by the LAB. This database derived from a 3D structural model of the Central European Basin System (Maystrenko and Scheck-Wenderoth 2011, 2013) is consistent with seismological experiments and constrained by 3D gravity modelling. Thus, the lithospheric configuration of this model is characterized by the 1300 °C isotherm as lower boundary condition.

5.2 Influence of Physical Rock Properties

As already mentioned the configuration of both the highly conductive crust and the very radiogenic upper crust plays a role in shaping the long-wavelength pattern of the temperature distribution in shallower parts of the thermal field.
The comparative studies show furthermore, that the conductive heat transport is mainly controlled by the thermal conductivities of the rock units. These differ within the column of the lithospheric model. The reason therefore is that:

(1) Crystalline rocks of the basement are more conductive than the sediments. This is reflected in the long-wavelength pattern of the temperature distribution as already described in caption 5.1.;
(2) Variations in thermal conductivities of the sedimentary fill lead to the short-wavelength pattern of the thermal field which partly overprints the long-wavelength pattern. Therefore two factors are accountable: the configuration of the Zechstein salt and the contrast in thermal conductivities between the Zechstein salt and the other sediments.

The results show that the superposed effects of differences in thermal conductivities of basement rocks and basin fill as well as between the conductive Zechstein salt and surrounding less conductive sediments together with the structural setting of the Zechstein salt and the sediment fill are responsible for the basin wide thermal signature. This is especially the case in the north-western region of the study area where salt structures are present in the basin. There, the interaction between the highly conductive salt and the less conductive overburden creates short-wavelength anomalies in the temperature distribution of the shallow thermal field in response to the heterogeneous thickness of the Zechstein salt. Thereby, the occurrence of positive and negative short-wavelength thermal anomalies is spatially related to the salt structures and the surrounding and overlying sediments. Generally, at the bottom of salt diapirs heat is extracted and efficiently transported to the surface (chimney effect). This efficient heat transport via diapirs is counteracted where a thick less conductive overburden causes thermal blanketing above the salt structures. The latter configuration results in colder temperatures near the base of diapirs and higher temperatures in their top regions. In opposite, a thin cover of low conductive sediments on top of diapirs cannot prevent the escape of heat towards the surface so that colder temperatures develop above these salt structures. In this way the configuration of the salt cover and the overall geometry of the salt are responsible for the local thermal signature. This short-wavelength signature superposes locally the regional pattern in the temperature distribution that results from the interaction between the highly conductive crust and the low conductive sediments of the basin fill.

Such salt related thermal anomalies have been described earlier in different regional-scale and local-scale modelling studies (e.g. Yu et al. 1992; Bayer et al. 1997; Ondrak et al. 1998; Cacace et al. 2010) as well as in studies on single structures by means of measured temperatures in wells e.g. by Beer and Hurtig (1999) for the diapir Kootzen in Brandenburg and Fromme et al. (2010) for diapirs in the central part of the North German Basin. What is new in the work presented here is the quantitative assessment of the different heat components resulting from different depth levels of the lithosphere.

It is known that the thermal properties of rocks can vary laterally and a broad range of properties is documented for different lithological groups (Čermák et al. 1982; Norden and Förster 2006; Fuchs and Förster 2010; Vila et al. 2010 and Norden et al. 2012). Thus, the assignment of reliable thermal properties is a critical task in thermal modelling. The effective thermal properties thermal conductivity and radiogenic heat production for the basin fill in the conductive models of this work are derived from literature (Bayer et al. 1997). These properties are considered constant within each geological unit. The reason for this strategy was that only sparse and selective information about thermal geophysical properties is available for the whole Brandenburg region. Nevertheless, a significant horizontal variation in properties is still implemented in the models due to the thickness variation of the Zechstein salt and following general assumptions on different lithologies for the individual model layers. Compared with the overburden the thermal conductivity of the salt is up to a factor of two to three times higher than that of the other sediments. This difference causes the above described short-wavelength thermal anomalies with locally significantly elevated temperatures. Such local positive thermal anomalies may be large enough to cause oil generation and maturation as several studies confirm (e.g. Yu et al. 1992; Petersen and Lerche 1996).
Despite the mentioned simplifications the resultant temperature predictions reproduce temperature observations, derived from different structural positions (Förster 2001; Norden et al. 2008), well. Obviously, the chosen thermal properties adequately represent the overall heat budget and thermal conductivity of the main lithologies.
The temperature observations not reproduced by the lithosphere-scale conductive model indicate however, that sources of error may lay in the assigned physical properties or the assumption of lateral uniformity. On the other hand these differences may result from the influence of moving fluids a process neglected in the conductive models.

Some evidence on how to answer **Question 2** is already given in the statement(s) to question 1. To answer the question which heat transport processes should be considered at which model scale and depths and if, are there processes that can be neglected at the regional scale, models of coupled heat and fluid transport have been studied. The results show that moving fluids can exert considerable effect on the temperature distribution down to about 2 km depth caused by different mechanisms of convective heat transport. These heat transport mechanisms are of specific importance for the

temperature distribution such that those of minor influence can be neglected if the regional-scale thermal field is under consideration. Like in the case of the answer(s) to question 1, also these findings are subjected to certain restrictions. The main problem is that information on hydrogeology, boundary conditions and hydraulic permeability of the aquifers and aquitards involved are required but in most cases severely limited. Thus, the coupled model presented in chapter 4 can be seen as a first attempt to derive first-order effects of regional fluid pathways and their feed-back with heat transport.

5.3 Influence of the Coupled Fluid and Heat Transport

The final hydrogeological model additionally resolves the Tertiary succession of the basin fill by layers for the post-Rupelian, Rupelian-clay and pre-Rupelian-clay. Thereby, the prominent Cenozoic Rupelian-clay aquitard acts as a hydraulic barrier separating the Quaternary fresh water complexes from the deep Mesozoic saline aquifers due to its very low permeability. Thus, the third type of models provides additional and essential information on the 3D regional hydrogeology of the study area since relevant major aquifers and aquitards of the basin fill are considered. Moreover, the numerical simulations of the coupled fluid and heat transport were carried out with special focus on how sensitive the respective results were to assigned hydraulic permeabilities. Therefore, a range of all available permeability combinations have been tested and compared systematically with the results from the conductive simulations and observed temperatures. Finally, the results from the sensitivity study with the best-validated scenario were used to evaluate the influence of fluid flow on the thermal field.

With regard to the model restrictions mentioned above the comparative study between the numerical model which consider the pure conductive heat transfer and those that consider the coupled fluid and heat transport shows that if moving fluids are considered the shallow thermal field is controlled by:

(1) The configuration of the shallowest aquitard limiting the inflow of cold surface water (Rupelian-clay aquitard);
(2) The permeability of the aquifers and aquitards of the basin fill.

Though conduction is the dominant heat transport mechanism in the study area, heat transport via circulating fluids can play an important role for the shallow thermal field down to about 2 km depth. This is especially the case in the basin part of the model where the fluid dynamics within the sediment pile are controlled by the hydraulic interaction between aquifers and aquitards above the Zechstein salt. High hydraulic gradients generate high pressure driven forces where the Rupelian-clay is absent, thus supporting forced convective heat transfer and related advective cooling to reach greater depth of the Mesozoic aquifers. In addition, buoyancy forces due to thermally induced density gradients may

lead to the rise of warm waters in regions with low topographic gradient and where the Rupelian-clay aquitard is present. This free convection of fluids occurs only locally where the pressure forces are weak and the permeable layers reach a critical thickness. Thereby, the depth range of this influence is controlled by the permeability of the different sedimentary layers. Where the permeability of the participating layers is large enough advection of fluids may be as effective as conduction in the shallow thermal field above the Mesozoic Muschelkalk. Summarizing, the configuration of the Rupelian-clay has a first-order control and defines the regions where fluid circulation takes place within the shallower thermal field, whereas the second influencing factor is the permeability of geological units.

Groundwater research during the last years led to a growing knowledge about deeper aquifers that are dynamic systems influenced by surface processes (Hebig et al. 2012; Garven 1995; Schilling et al. 2013). Effort was also put to studies on natural free convection and mixed convection from theoretical settings (e.g. Raffensperger and Vlassopoulos 1999; Diersch and Kolditz 2002; Nield and Bejan 2006) to detect the effects in natural groundwater field settings (Van Dam et al. 2009; Kaiser et al. 2011).
The influence of moving fluids and its capability to affect the shallow temperature field have been described for different basin settings worldwide. Consistent with the results of the third study in this thesis, Lampe and Person (2002) suppose that temperatures and maturity levels observed in the northern part of the Upper Rhinegraben rift basin (Germany) are a result of an elevated heat flow and advective cooling through topography-driven fluid flow. Topography-driven flow is also found to be effective e.g. in sandstone aquifers of the intracratonic Paraná Basin, Brazil (Maynard et al. 1994) and in the Los Llanos Basin of Colombia (Villegas et al. 1994) where fresh to brackish water conditions at 1-2 km depth are known (Garven 1995). Likewise Schilling et al. (2013) state that anomalously low temperatures result from advection in shallow aquifers, especially in the north of the Perth Basin, Western Australia. Also earlier investigations in the Northeast German Basin already point to a relevant impact of fluid circulations on the thermal field. However, earlier conclusions from 2D simulations by Magri et al. (e.g. 2005a, 2008) are limited due to the 2D approach, whereas 3D simulations by Kaiser et al. (2011) are limited due to the resolution of the hydrogeological model which does not consider the Rupelian-clay aquitard for the Northeast German Basin.
That an additional advective flow component due to topography induced regional flow may have to be considered is also deduced by Cacace et al. (2013b) from differences between heat flow measurements and heat flow predicted by the lithosphere-scale conductive model of Brandenburg.
Investigations in other sedimentary basins support not only the result that groundwater flow may be affected by external advective forces due to pressure gradients (e.g. Bjørlykke et al. 1993, Maynard et al. 1994; Lampe and Person 2002), they also support the finding that internal buoyant forces in consequence to gradients in fluid density (Bjørlykke 2010, Kaiser et al. 2013) may have a local influence on the shallow thermal field. Beyond others, indications for this so-called free convection

come from resistivity measurements as e.g. from a sabkha aquifer near Abu Dhabi, United Arab Emirates (Van Dam et al. 2009). There, Van Dam and co-workers interpret imaged resistivity anomalies as caused by free convection. Schilling et al. (2013) also admit the occurrence of possible free convective effects if high average permeabilities are present.

Taken as a whole the results of the third study in the thesis clearly indicate that fluid motion, depending on the integrity of the shallowest hydraulic barrier, has a more active role in shaping the shallow thermal field than previously assumed. This is largely confirming earlier hypotheses. However, the improved hydrogeological configuration of the basin fill is more sophisticated than in previous approaches as it comprises an upgraded 3D hydrogeological configuration of the basin fill and is additionally constrained by a physically motivated lower thermal boundary condition and constrained values for the rock thermal properties – thermal conductivity and heat production derived from the conductive studies. Thus the results provide a step forward in the quantitative assessment of the individual contributions of different thermal properties at different depths, of the different heat transport mechanisms and of the influences of boundary conditions.

6 Limitations of the Method

Question 1 raised the issue whether the temperature predictions from validated models considering structure and physics are more realistic than those coming from classical interpolation techniques.
This can be answered affirmatively for the crustal-scale and the lithosphere-scale conductive models.
Both models reproduced the temperature observations well. The predicted temperature range is consistent with the general trend of published data, as for example depth-temperature maps derived from 2D interpolation of borehole measurements (Diener et al. 1984; Stackebrandt and Manhenke 2002). However, the models derive a more pronounced lateral variation in predicted temperatures compared to the published maps in response to the structural resolution of the basin fill, especially concerning the distribution of salt structures. Thereby, the more sophisticated lithosphere-scale conductive model is better in matching temperature predictions in the regions where significant additional heat input through the deeper lithosphere is added. The coupled model reproduces the temperature observations slightly better than the lithosphere-scale conductive model in some parts of the shallower thermal field. The significance of this observation is limited due to greater uncertainties. Particularly due to the lack of data on hydraulic properties and a strongly simplified assumption for the upper hydraulic boundary condition the model is not hydraulically validated. Nevertheless, the model can be used to identify areas where fluid interaction between aquifers may play a role.

Several factors need to be mentioned that may represent sources of error and thus put some limitations to the interpretation of the results of this thesis:

(1) Model Resolution

Input data:

Though being of improved resolution compared to previous models of the areas the 3D structural model of the basin fill still represents a simplified structural geometry for the area in Brandenburg based on the available base of well data, data from 2D depth and thickness maps as well as data derived from earlier 3D structural models of lower resolution. According to this database (chapter 2) the central part of the rectangular Brandenburg model is based on a better data coverage than the marginal parts of the model. Thus a higher resolution of the structural inventory and a more realistic structural distribution of its rocks (properties) is achieved in the inner parts of the model than in the marginal parts.

The configuration of the deeper lithosphere presented in chapter 3 integrates a better approximation of deeper lithosphere configuration compared to previous models. Nevertheless, a 2-layered crystalline crust still represents a strong simplification and does not account for horizontal changes in composition between crustal blocks.

Finallly, also the hydrogeological information implemented in the coupled model is strongly simplified. Although the hydrogeological model (chapter 4) comprises a higher vertical resolution of the basin fill concerning the main aquifers and aquitards above the Zechstein salt the applied configuration of the Rupelian aquitard results from a limited database that rather shows the general trend without capturing local details of the topological configuration of this layer.

Faults:

A further structural limitation is given by the fact that faults are not included in the model. This may have strong local impacts on the thermal field in regions where faults act as pathways for advective heat transport (Magri et al. 2010; Petitta et al. 2011; Cherubini et al. 2013a, b). Especially, major fault zones like the Gardelegen and Lausitz Escarpments in the southwest of Brandenburg which vertically offset the pre-Permian basement against the Permian to Cenozoic sediments may induce a pronounced, but local thermal signature depending on the permeability distribution within the faults zones (Cherubini et al. 2013 c; Cacace et al. 2013b). Barton et al. (1995) also state that particularly faults can provide permeable pathways for fluids also at great depth in the crust. As no temperature observations covering the southwestern area of Brandenburg at depths greater than 6 km were available, we refrained from assessing the influence of the large Gardelegen and Lausitz Escarpments offset on the thermal pattern. Moreover, fluid circulation via faults cutting the base of the Zechstein salt may connect the sub- and supra-salt aquifers and thus also affect the temperatures in this depth.

Furthermore not the whole lithospheric column is considered in the coupled model. This may be justified as long as only conductive heat transfer is responsible for the deeper temperature variation.

(2) Assigned Properties

Thermal Properties:

As already mentioned the effective thermal properties are derived from literature (Bayer et al. 1997) because a thermal database of measurements from the area was not available at the time when the first part of the study has been carried out. In order to get a picture of how the effects of lithology-related variations in related rock thermal properties may influence the model results a second dataset was tested that combines thermal conductivities and radiogenic heat production recently measured on rocks from wells of the Northeast German Basin (Norden and Förster 2006; Fuchs and Förster 2010) with data extrapolated to the conditions of the Northeast German Basin (Norden et al. 2008). Thereby, the measured thermal conductivities for the Mesozoic succession originate from a well near the eastern basin margin. This second dataset differs from the one used in the initial model mainly by generally higher values of thermal conductivity. The implementation of these data in the conductive modelling led to temperature predictions which did not reproduce the observed temperatures. A possible explanation for this mismatch could be that the assigned thermal conductivities for the Mesozoic layers have been derived from only one location at the basin margin, which is not representative for the entire Mesozoic model volume. These considerations may be also valid for the thermal conductivity of the Cenozoic layers. Furthermore, the measured thermal conductivities of the Mesozoic layers are related to matrix rock properties measured under ambient conditions, whereas the calculation of mean bulk conductivities requires data information on porosity and fluid content. Unfortunately, such data were not available.

Hydraulic Properties:

Like for the thermal properties only sparse and selective information about porosity and permeability was available for the whole Brandenburg region. However, in order to get first insights on the potential influences of convective heat transport in addition to conduction the applied permeabilities are derived from literature (Čermák et al. 1982; Magri et al. 2005, 2008). Given the degree of uncertainties concerning the heterogeneity of depositional sequences and the fact that permeability for rocks may vary over a few orders of magnitudes (Ingebritsen and Sanford 1998) and is also a function of depth (Manning and Ingebritsen 1999) a systematic investigation of how this parameter would influence the modelling results would be an important part for future studies.

(3) Assumptions

Lower Thermal Boundary Conditions:

Whereas the assumption of a constant heat flow at the base of the Moho as defined for the simpler crustal-scale model may not be appropriate due to the heterogeneous composition of the crust, the 1300 °C isotherm adopted for the lithosphere-scale model is in a geological sense the only physically motivated fixed lower temperature boundary in the lithosphere (Turcotte and Schubert 2002). The implementation of a differentiated crust is also a progress, though again the related data is of limited resolution and coverage. Therefore also the resultant temperature variation at 6000 m depth, extracted from the conductive lithosphere-scale model and applied as lower thermal boundary to the coupled heat and fluid transport models, may overestimate or underestimate the local temperature distribution in those parts of the model where the assigned properties of the deeper crust and lithosphere do not reflect the real crustal composition and the relevant heat budget.

Upper Hydraulic Boundary Condition:

The top hydraulic boundary condition of the coupled models should reflect the fluid and heat transport conditions for the model area adequately. Due to a lack of data, the prescribed hydraulic head for the upper boundary in these models was approximated by setting the topographic elevation as being equal to the hydraulic head. This imposes steep pressure gradients in areas with high topographic gradients. Where the shallowest hydraulic barrier – the Rupelian-clay – is absent, these overestimated gradients induce an overall net cooling effect in the system. This effect may not reflect the real hydraulic conditions for the region properly. Additionally the configuration of the Rupelian aquitard may locally overestimate the size of the Rupelian windows in response to limited data coverage. The related strong cooling effect of these two conditions could only be reduced by reducing the hydraulic permeability of the layers for the shallower part of the system. This certainly does not represent a unique solution and future work should put some effort into the choice of an improved upper hydraulic boundary condition based e.g. on groundwater recharge data.

Configuration of the Deeper Lithosphere:

The differentiated deeper crustal volume of the lithosphere-scale model is simplified in its structural composition. The configuration of the upper and lower crustal layers have been derived from seismic interpretations and 3D gravity modelling (Maystrenko and Scheck-Wenderoth 2011, 2013) and does not account for lateral variations in crustal composition. The variability of radiogenic heat production of lithological groups and its significance to lithospheric thermal modelling was in the focus of the studies by Vila et al. (2010). Vila and co-workers propose typical values of radiogenic heat production for common lithologies. They find that the largest variation in bulk radiogenic heat production corresponds to igneous rocks (from 0.1 to 3.8 $\mu W/m^3$), followed by metamorphic rocks (from 0.2 to 3.2 $\mu Wm/m^3$) and sedimentary rocks (from0.3 to 1.8 μ/Wm^3). Among others the authors remark that

implementing radiogenic heat production in modelling the thermal structure of the lithosphere requires to identify the main lithologies and their proportion on the respective layers, the consideration of the range of variability of radiogenic heat production values as well as the age of crustal domains and the integration of additional constraints to better define geometry and boundary condition of the lithosphere section. Options and limits of model validation in terms of crustal composition was also a key point for the studies of e.g. Mareschal and Jaupart (2013). In their studies on radiogenic heat production, thermal regime and evolution of continental crust the authors refer to the large spatial variations in crustal composition and heat production within a single geological province. They show that for a given crustal thickness, the Moho temperature varies within a wide range depending on surface heat flux and crustal heat production. Mareschal and Jaupart (2013) state that generic models based on a "type" crustal column cannot be used to calculate crustal geotherms. This finding is confirmed by results of the thesis in that the latter clearly demonstrate that variation in thermal properties of the basin fill may affect the temperature distribution locally whereas deeper crustal variation would lead to regional variations within the shallow thermal field.

Constant Properties within the Layers

The geological units for the basin fill are assumed to have constant average rock properties. They do not consider lithological heterogeneities inherent to depositional sequences. Thus, the assignment of vertically and laterally homogeneous and isotropic thermo-hydraulic properties for each layer may not correctly consider such locally varying lithologies. Such model limitations are not discussed without controversy. Norden and Förster (2006) point to the dependence of formation thermal conductivity on facies changes in a sedimentary basin. In this context Norden et al. (2012) distinguish twelve thermo-physical stratigraphic sedimentary units and twelve different mean rock types based on well data for the post-Permocarboniferous succession for their local-scale 3D geological model of the Altensalzwedel area, located at the western border of the Brandenburg model. The authors determined the thermal conductivity, heat capacity and porosity of the mean rock types by laboratory measurements, well-log data, analogue studies and literature data. They show e. g. that the matrix thermal conductivities of sandstones can vary from 2.4 to 5.4 W/(m*K), resulting in bulk thermal conductivities in the order of 2.1 to 3.4 W/(m*K) depending on the respective porosity. In contrast, Ollinger et al. (2010) obtained a better fit with observed temperatures for the Groß Schönebeck thermal site by assuming a non-uniform horizontal distribution of conductivities and by calculating optimized conductivities for individual wells. In case of the thesis studies the simplified homogeneous and isotropic conditions for the layers enable to capture first order regional effects of variations in permeability on the resulting groundwater dynamics and temperature distribution which can be used as a starting point to evaluate these effects in future studies.

However, due to the immature state of detailed knowledge on in situ formation characteristics and thermal conductivities of different lithologies for the sediments in the Northeast German Basin and the

uncertainties in crustal parameters a further calibration of the thermal models should be postponed to later studies that can profit of a growing number of measured properties.

Steady-state Thermal Field

Conductive: The thermal evolution of the system trough time is neglected as the aim was to arrive at a better characterisation of dominant controlling factors for the present-day thermal field. This implies that steady-state equilibrium between the present geological configuration, hydrodynamics and thermal field is assumed, which, as the last part of the study showed, was an oversimplification of the ongoing processes in the shallow aquifers.

Coupled: In agreement with the explanations above also the coupled numerical simulations represent "pseudo" steady-state conditions to be correlated with the present-day thermal configuration of the system. To assure pseudo stable numerical conditions the simulations were computed with time steps letting the system equilibrate during a computed time interval of 250 ka. Numerical stability was enforced by letting the system reaching equilibrium by means of transient simulations. The final computed result which shows no significant changes in temperatures compared to the previous time step was considered as numerically equivalent to the present-day configuration.

The simplification to consider steady-state conditions for the thermal field limits the results in that the deviation between temperature observations and predictions in the shallower thermal field can also be caused by effects of recent or ongoing changes in temperature. Majorowicz and Wybraniec (2011) suggest that the heat flow in the upper 2 km may be underestimated and thus cause also an underestimation of modelled geotherms for large regions in Europe in response to ongoing re-equilibration after the last glaciations. These authors attempt to quantify effects of past changes in surface temperature and provide a heat flow map for Europe with palaeoclimatic correction that may find consideration in future studies. These effects have not been considered in this thesis but may partially explain the overestimated temperature in the upper 2 km.

(4) Considered Heat Transport Mechanisms

In this thesis only temperature-induced fluid density changes that provoke free convective heat transport are considered in the coupled numerical simulations. In a recent study by Kaiser et al. (2013) thermohaline numerical simulations on a local-scale show amongst others the influence of density gradients induced by the combined effects of temperature and salinity variations on the thermal field. However, these authors show that thermal anomalies caused by a fully coupled thermohaline simulation are not significantly different from results of a coupled heat and fluid simulation neglecting salinity influences in areas confined by the Rupelian aquitard.

Finally, dilatational and diagenetic processes such as compaction of sediments and chemical reactions which mechanically and chemically affect the geological environment during basin evolution have

been not considered within this study. With regard to compaction-driven flow Bjørlykke (1993) points to the complex interdependencies between pressure, permeability and compaction. He proposes to use permeability distributions for modelling fluid flow since permeability is mostly determined by facies, diagenesis and the tectonic evolution of the basin. Again such level of detail was beyond the scope of this study but leaves room for future investigations.

7 Conclusions and Best-Practice Workflow

In the present thesis, the temperature distribution of the steady-state thermal field in the Brandenburg area was investigated by means of differently resolved structural models taking into account different heat transport processes. The results of these differently constrained models were compared with each other and validated by temperature measurements.
Firstly, a refined 3D structural model of the basin fill for the area of Brandenburg was built. This model of the basin fill has been modified stepwise for numerical simulations to investigate the dominant controlling factors of the thermal field. In a second step, a new database could be used to construct a more realistic and differentiated configuration of the deeper lithosphere. The integration of the full lithospheric scale in the model was accompanied by an assumed change in deeper crustal composition (2-layered crust and a mantle part) and an improved choice for the lower thermal boundary condition (1300°C isotherm). To account for the influence of fluid flow on the temperature distribution, a third type of model was constructed that combines relevant major aquifers and aquitards of the basin fill. For this basin-scale model the foregoing models provided suitable lower thermal boundary conditions and physically constrained values for the rock thermal properties. Therefore, the calculated temperature variation at 6000 m depth has been extracted from the lithosphere-scale model to prescribe a laterally varying lower thermal boundary condition of the vertically limited coupled model. Likewise, the thermal properties (thermal conductivity and radiogenic heat production) from the best-fit model scenario of the lithosphere-scale model were used as input parameters for the numerical simulations of coupled fluid and heat transport.

With respect to the initially posed questions the different numerical simulations and comparative model evaluations demonstrate the following main results:

1. 3D Models which consider (hydro)geological subsurface structures as well as physical heat transport mechanisms better reproduce the temperature distribution at depth than temperature maps resulting from classical interpolation techniques.
2. Heat conduction is the main heat transport mechanism affecting the background regional thermal field in the area. Thereby, the depth position and geometry of the upper crust and the

LAB have a first order control on the regional pattern of the temperature distribution. This influence is also reflected at shallower depth levels interesting for geothermal exploration. The long-wavelength pattern in the temperature distribution is controlled by the strong lateral contrast in thermal conductivity and radiogenic heat production between a 2-layered crystalline crust and insulating thick sediments in the basin. The short-wavelength pattern in the temperature distribution results from local thermal anomalies which occur in response to the chimney effect near the thermally conductive salt structures. Thus the second main controlling factor is the depth position and spatial configuration of the Zechstein salt.

3. Heat transport via circulating fluids can play an important role for the shallow thermal field down to 2 km depth dependent on the permeability of the sediments present at this depth.
   In particular, in regions with high hydraulic gradients where the Rupelian-clay aquitard is missing, highly permeable aquifers favour pressure driven groundwater flow to reach greater depths thus causing local cooling. There, hydraulic permeability plays a key role.
   As a relevant aquifer thickness is needed to support density-driven upward flow, free thermal convection is only of local significance thus it can be neglected in areas where aquifers are subdivided by relevant low permeable sequences.
4. To adequately assess the regional thermal field in a sedimentary basin a workflow is suggested. By means of a lithosphere-scale conductive thermal model which resolves the main geological structures of the basin fill, the deeper crust and the mantle first information on areas of cold and warm domains together with structural information is provided valuable for the assessment of areas for different subsurface utilization. Furthermore, the model provides valuable input parameters for numerical simulations of more detailed basin-scale coupled fluid and heat transport models. Such models should include relevant aquifers and aquitards of the region so that they are of higher vertical resolution than conductive models. To master the complex numerical challenges, the coupled model still need to be limited to the basin fill but may be upgraded by laterally variable heat flow or temperature distributions as lower thermal boundary condition derived from larger-scale conductive models. The resulting temperature distribution of the basin-scale coupled models can be further used to assess where advection or free convection of fluids may occur locally. In this way, prospective regions of interest for geothermal exploration can be localized. Such models then can provide valuable boundary conditions for local models of geothermal production sites.

The current model resolution is state of the art for 3D numerical simulations for both the conductive large-scale lithospheric model as well as the coupled basin-scale model. Accordingly, the results of the thesis contribute to the knowledge on hydrothermal dynamics in the basin in terms of how main impacting factors and heat transport processes influence the recent thermal field. Besides, the model predictions provide a consistent reproduction of the observed temperatures and allow temperature

predictions for the basin scale beyond the initial database. These predictions can support the localization of potential geothermal fields and thus are useful for geothermal exploration in Brandenburg. Apart from being useful for geothermal utilization these results play an important role for all other applications in the deeper subsurface for which knowledge about the temperature conditions is a pre-requisite. The results of the comparative studies show clearly that the configuration of the deeper lithosphere needs to be brought into play if the shallower thermal field is considered. Basin-scale thermal models should additionally consider the influence of moving fluids. Not at least regional basin-scale coupled models help to locate regions where fluid motion by advection or free convection may occur. In this manner these models provide valuable information in the forefront of planned geothermal production sites. The results further demonstrate that lithosphere-scale models can provide valuable input parameters for numerical simulations of the coupled fluid and heat transport. As fluid flow plays an important role in different areas on a local scale a combination between lithosphere-scale models and local basin-scale models is a recommended strategy to adequately assess potential areas for geothermal production sites.

To adequately assess regions where moving fluids influence the thermal signature future coupled models should be even of higher resolution also in horizontal direction. Though this demands a sufficiently detailed hydrogeological and thermal database which allows to represent the respective vertical and horizontal changes in facies distribution, the implementation of such data may significantly improve predictions derived from future models.

8 References

Agemar T, Schellschmidt R, Schulz R (2012) Subsurface temperature distribution in Germany. Geothermics 44: 65-77. doi: 10.1016/j.geothermics.2012.07.002

Allen PA, Allen JR (2005) Basin Analysis - Principles and Applications. Blackwell Publishing

Amante C, Eakins BW (2009) ETOPO1 1 Arc-Minute Global Relief Model: Procedures, Data Sources and Analysis. NOAA Technical Memorandum NESDIS NGDC-24, 19 pp, March 2009

Artemieva I (1997) In situ permeability of hot dry rock. In: Middleton MF (ed) Fractured reservoirs. Nordic Petroleum Technology Series, Part 1, Goteborg, pp 99-124

Balling N, Kristiansen JI, Breiner N, Poulsen KD, Rasmussen R, Saxov S (1981) Geothermal measurements and subsurface temperature modelling in Denmark. Techn. Ber. GeoSkrifter No.16: Department of Geology, Aarhus University, ISSN:0105-824X

Barton CA, Zoback MD, Moos D (1995) Fluid flow along potentially active faults in crystalline rock. Geology 23 (8):683-686. doi:10.1130/0091-7613(1995)023<0683:FFAPAF>2.3.CO;2

Bayer U, Scheck M, Koehler M (1997) Modeling of the 3D thermal field in the northeast German Basin. Geologische Rundschau 86:241-251. doi:10.1007/s005310050137

Beer H (1996) Temperaturmessungen in Tiefbohrungen - Repräsentanz und Möglichkeit einer näherungsweisen Korrektur. Brandenburgische Geowissenschaftliche Beiträge 3:28-34

Beer H, Hurtig E (1999) Das geothermische Feld in Brandenburg. Brandenburgische Geowissenschaftliche Beiträge 6:57-68

Benek R, Kramer W, McCann T, Scheck M, Negendank JFW, Korich D, Huebscher HD, Bayer U (1996) Permo-carboniferous magmatism of the Northeast German Basin. Tectonophysics 266:379-404. doi:10.1016/S0040-1951(96)00199-0

Blöcher MG, Zimmermann G, Moeck I, Brandt W, Hassanzadegan A, Magri F (2010) 3D Numerical Modeling of Hydrothermal Processes during the Lifetime of a Deep Geothermal Reservoir. Geofluids 10 (3):406-421. doi:10.1111/j.1468-8123.2010.00284.x

Bjørlykke K **(**1993) Fluid flow in sedimentary basins. In: Cloething S, Sassi W, Horvath F, Puigdefabregas C (eds) Basin Analysis and Dynamics of Sedimentary Basin Evolution. Sedimentary Geology 86:137-158

Bjørlykke K (ed) (2010) Petroleum Geoscience: From Sedimentary Environments to Rock Physics. Springer-Verlag Berlin Heidelberg

Bruns E, Ohlhorst D, Wenzel B, Köppel J (2011): Renewable Energies in Germany's Electricity Market. A Biography of the Innovation Process. Dordrecht, Heidelberg, London, New York: Springer-Verlag

BURVAL WORKING GROUP (2009) Buried Quaternary valleys - a geophysical approach. Zeitschrift der Deutschen Gesellschaft für Geowissenschaften 160 (3):237-247

Cacace M, Blöcher G, Watanabe N, Moeck I, Börsing N, Scheck-Wenderoth M, Kolditz O, Huenges E (2013a): Modelling of Fractured Carbonate Reservoirs - Outline of a novel technique via a case study from the Molasse Basin, southern Bavaria (Germany). Environ Earth Sci. 70 (8):3585-3602. doi:10.1007/s12665-013-2402-3

Cacace M, Kaiser BO, Lewerenz B, Scheck-Wenderoth M (2010) Geothermal energy in sedimentary basins: What can we learn from regional numerical models. Chemie der Erde-Geochemistry 70 (3):33-46. doi:10.1016/j.chemer.2010.05.017

Cacace M, Kissling W (2012) Hot and saline spring behaviour in the Taupo Volcanic Zone and the North-East German Basin. In: Poster, EGU General Assembly 2012, vol 14, EGU2012-1927-1

Cacace M, Scheck-Wenderoth M (2010) Modeling the thermal field and the impact of salt structures in the North East German Basin. Proceedings of the World Geothermal Congress 2010. Bali, Indonesia

Cacace M, Scheck-Wenderoth M, Noack V, Cherubini Y, Schellschmidt R (2013b) Modelling the surface heat flow distribution in the area of Brandenburg (northern Germany). Energy Procedia 40: 545-553. doi:10.1016/j.egypro.2013.08.063

Čermák VH, Huckenholz HG, Rybach L, Schmid R, Schopper JR, Schuch M, Stöffler D, Wohlenberg J (1982) Physical properties of rocks. In: Augenheister G (ed) Landolt-Börnstein, New Series. Springer, Berlin, Heidelberg, New York, pp 1-373

Cherubini Y, Cacace M, Blöcher G, Scheck-Wenderoth M (2013a): Impact of single inclined faults on the fluid flow and heat transport: results from 3D finite element simulations. Environ Earth Sci. 70 (8), 3603-3618. doi:10.1007/s12665-012-2212-z

Cherubini Y, Cacace M, Scheck-Wenderoth M, Moeck I, Lewerenz B (2013b): Controls on the deep thermal field - implications from 3D numerical simulations for the geothermal research site Groß Schönebeck. Environ Earth Sci. 70 (8), 3619-3642. doi:10.1007/s12665-013-2519-4

Cherubini Y, Cacace M, Scheck-Wenderoth M, Noack V (2013c) Influence of major faults on the 3-D coupled fluid and heat transport for the area of Brandenburg (NE German Basin) (under review Geothermal Energy Science)

Chopra P, Holgate F (2005) A GIS analysis of temperature in the Australian Crust. Proceedings of the World Geothermal Congress 2005. Antalya, Turkey

Cloetingh S, van Wees JD, Ziegler PA, Lenkey L, Beekman F, Tesauro M, Förster A, Norden B, Kaban M, Hardebol N, Bonté D, Genter A, Guillou-Frottier L, Ter Voorde M, Sokoutis D, Willingshofer E, Cornu T, Worum G (2010) Lithosphere tectonics and thermo-mechanical properties: An integrated modelling approach for Enhanced Geothermal Systems exploration in Europe, Earth-Science Reviews, 102 (3-4):159-206. doi:org/10.1016/j.earscirev.2010.05.003

Davies JH, Davies DR (2010) Earth's surface heat flux. Solid Earth, 1, 5-24. doi:10.5194/se-1-5-2010

Deming D (1994) Fluid flow and heat transport in the upper continental crust, In: Parnell J (ed) Geofluids: Origin, Migration and Evolution of Fluids in Sedimentary Basins, J. Geol. Soc. London Spec. Publ., 78, pp. 27-40

Diener I, Katzung G, Kühn P, Oelsner C, Hurtig, E, Schneider H, Zschernig J (1984) Geothermie-Atlas der Deutschen Demokratischen Republik. Zentrales Geologisches Institut, Berlin

Diersch H-JG (2002) FEFLOW finite-element subsurface flow and transport simulation system. User's Manual/Reference Manual/ White Papers, Release 5.0. WASY GmbH, Berlin

Diersch H-JG (2009) FEFLOW Finite Element Subsurface Flow & Transport Simulation System, Reference Manual. WASY GmbH Inst. for Water Resour. Plann. And Syst. Res., Berlin

Diersch H-JG, Kolditz O (2002), Variable-density flow and transport in porous media: Approaches and challenges. Adv. Water Resour. 25:899– 944

Förster A (1997) Bewertung der geothermischen Bedingungen im Ostteil des Norddeutschen Beckens. In: Hoth P, Seibt A, Kellner T, Huenges E (eds) Geothermie Report 97-1: Geowissenschaftliche Bewertungsgrundlagen zur Nutzung hydrogeothermaler Ressourcen in Norddeutschland. Scientific Technical Report STR97/15, GeoForschungsZentrum Potsdam, 20-41

Förster A (2001) Analysis of borehole temperature data in the Northeast German Basin: continuous logs versus bottom-hole temperatures. Petroleum Geoscience 7 (3):241-254

Fowler CMR (1996) The solid earth. Cambridge Universtity Press, Cambridge

Fromme K, Michalzik D, Wirth W (2010) Das geothermische Potenzial von Salzstrukturen in Norddeutschland. ZDGG 161/3, 323-333

Fuchs S, Förster A (2010) Rock thermal conductivity of Mesozoic geothermal aquifers in the Northeast German Basin. Chemie Der Erde-Geochemistry 70 (3):13-22. doi:10.1016/ j.chemer.2010.05.010.

Garven G (1995) Continental-scale groundwater flow and geologic processes. Annual Review of Earth and Planetary Sciences 23 (1), 89-117

Hebig KH, Ito N, Scheytt T, Marui A (2012): Review: Deep groundwater research with focus on Germany. Hydrogeology Journal 20 (2), 227-243. doi:10.1007/s10040-011-0815-1

Hofmeister AM (1999) Mantle values of Thermal conductivity and the Geotherm from Phonon lifetimes. Science 283: 1699-1706

Holl H-G, Moeck I, Schandelmeier H (2005) Characterisation of the tectono-sedimentary evolution of a geothermal reservoir - implications of exploitation (Southern Permian Basin, NE Germany). Proceedings World Geothermal Congress 2005, Antalya, Turkey

Hoth, K, Rusbült J, Zagora K, Beer H, Hartmann O (1993) Die tiefen Bohrungen im Zentralabschnitt der Mitteleuropäischen Senke - Dokumentation für den Zeitabschnitt 1962 - 1990. Schriftenreihe f. Geowiss. 2. Gesell. f. Geowiss., Berlin, 1-145

Huenges E (ed) (2010) Geothermal Energy Systems. WILEY-VCH, Weinheim

Hurter S, Haenel R (2002) Atlas of Geothermal Resources in Europe. EC Publication Nr. EUR17811, Luxemburg, 1-93

Hurtig E (1975) Untersuchungen zur Wärmeflußverteilung in Europa. Gerlands Beiträge zur Geophysik 84:247-260

Hurtig E, Čermák V, Haenel R, Zui V (1992) Geothermal Atlas of Europe. H Haak Verlagsgesellschaft, Gotha, 1-156

Hurtig E, Oelsner C (1979) The heat flow field on the territory of the German Democratic Republik. In: Cermak V and Rybach L (eds) Terrestrial Heat Flow in Europe. Springer, Berlin, pp 186-190

Ingebritsen S E and Sanford W E (1998) Groundwater in Geologic Processes: New York, Cambridge University Press, 341 p

Kaiser BO, Cacace M, Scheck-Wenderoth M (2013) Quaternary channels within the Northeast German Basin and their relevance on double diffusive convective transport processes: constraints from 3D thermohaline numerical simulations. Geochemistry Geophysics Geosystems 14 (8), 3156-3175. doi:10.1002/ggge.20192

Kaiser BO, Cacace M, Scheck-Wenderoth M, Lewerenz B (2011) Characterization of main heat transport processes in the Northeast German Basin: Constraints from 3-D numerical models. Geochemistry Geophysics Geosystems 12 (7). doi:10.1029/2011GC003535

Lampe C, Person M (2002) Advective cooling within sedimentary rift basins - application to the Upper Rhinegraben (Germany). Mar Petrol Geol 19:361-375

Landesamt für Umwelt, Natur und Geologie Mecklenburg-Vorpommern (2002) Lage der Quartärbasis, basierend auf der Übersichtskarte 1:500.000 - Präquartär und Quartärbasis, Güstrow

Landesamt für Geologie und Bergwesen Sachsen-Anhalt (2009) Landesbohrdatenbank URL http://www.sachsen-anhalt.de/LPSA/index.php?id=bohrdatenbank

Lassen A, Bayer U, Scheck M (2002) Deep structure of the Eastern North German Basin; possible scenarios of formation modelled and discussed on the basis of seismic and potential field data. XXVII General Assembly of the European Geophysical Society, Vol. 4, EGS, Nice, France

Littke R, Scheck-Wenderoth M, Brix MR, Nelskamp S (2008) Subsidence, inversion and evolution of the thermal field. In: Littke R, Bayer U, Gajewski D, Nelskamp S (eds) Dynamics of Complex Intracontinental Basins: The Central European Basin System. Springer Verlag, Berlin Heidelberg, 125-153

Ledru P, Frottier LG (2010) Reservoir definition. In: Huenges E (ed) Geothermal Energy Systems. WILEY-VCH, Weinheim, pp 1-36

Luijendijk E, Person M A, van Balen R, ter Voorde M (2010) The effect of topography driven groundwater flow on deep subsurface temperatures in the Roer Valley Graben (southern Netherlands). In: Abstract V13B-2361 Poster, 2010 Fall Meeting AGU, San Francisco

Luijendijk E, ter Voorde M, van Balen RT, Verweij H, Simmelink E (2011) Thermal state of the Roer Valley Graben, part of the European Cenozoic Rift System. Basin Research 23 (1), 65-82, doi: 10.1111/j.1365-2117.2010.00466.x

Magri F (2005) Mechanismus und Fluiddynamik der Salzwasserzirkulation im Norddeutschen Becken: Ergebnisse thermohaliner numerischer Simulationen. Scientific Technical Report STR05/12, GeoForschungsZentrum Potsdam

Magri F, Akar T, Gemici U, Pekdeger A (2010) Deep geothermal groundwater flow in the Seferihisar-Balcova area, Turkey: results from transient numerical simulations of coupled fluid flow and heat transport processes. Geofluids 10, 388-405

Magri F, Bayer U, Clausnitzer V, Jahnke C, Fuhrmann J, Moller P, Pekdeger A, Tesmer M, Voigt H (2005a) Deep reaching fluid flow close to convective instability in the NE German basin - results from water chemistry and numerical modelling. Tectonophysics 397:5-20. doi:10.1016/j.tecto.2004.10.006

Magri F, Bayer U, Jahnke C, Clausnitzer V, Diersch H-JG, Fuhrmann J, Möller P, Pekdeger A, Tesmer M, Voigt HJ (2005b) Fluid-dynamics driving saline water in the North East German Basin. International Journal of Earth Sciences 94 (5-6):1056-1069. doi:10.1007/s00531-005-0497-9

Magri F, Bayer U, Tesmer M, Möller P, Pekgeger A (2008) Salinization problems in the NEGB: results from thermohaline simulations. International Journal of Earth Sciences 97 (5):1075-1085

Majorowicz J, Wybraniec S (2011) New terrestrial heat flow map of Europe after regional paleoclimatic correction application. International Journal of Earth Sciences 100:881-887. doi:10.1007/s00531-010-0526-1

Manning C E, Ingebritsen S E (1999) Permeability of the continental crust: Implications of geothermal data and metamorphic systems. Reviews of Geophysics 37(1):127-150. doi: 10.1029/1998RG900002

Mareschal J-C, Jaupart C (2013) Radiogenic heat production, thermal regime and evolution of continental crust. Tectonophysics. doi:10.1016/j.tecto.2012.12.001

Maynard JB, Franca A, Medeiros L, Potter PE. (1994) Deep meteoric diagenesis in a cratonic basin: the Botucatu Sandstone aquifer of the Parana Basin, Brazil. In: Proc. SEPM Res. Conf. on Basin-wide Diagenetic Patterns: Integrated Petrologic, Geochemical, and HydrologiC, Considerations, (ed) Gregg JM, Montanez IP, Shelton KL, pp. 48-49. Tulsa: SEPM

Maystrenko Y, Bayer U, Scheck-Wenderoth M (2010) Structure and Evolution of the Central European Basin System according to 3D modeling. DGMK Research Report 577-2/2-1

Maystrenko YP, Scheck-Wenderoth M (2011) Shallow and deep controls on the thermal structure of basins – predictions from data-based large-scale 3D models. Poster, EGU General Assembly 2011, Vol. 13, EGU2011-3598

Maystrenko YP, Scheck-Wenderoth M (2013) 3D lithosphere-scale density model of the Central European Basin System and adjacent areas. Tectonophysics 601:53-77. doi:10.1016/j.tecto.2013.04.023

Moeck I, Holl H-G, Schandelmeier H (2005) 3D Lithofacies Model Building of the Rotliegend Sediments of the NE German Basin AAPG International Conference & Exhibition (Paris France 2005), CD-ROM, paper #98619

Möller P, Weise S M, Tesmer M, Dulski P, Pekdeger A, Bayer U, Magri F (2008): Salinization of groundwater in the North German Basin: results from conjoint investigation of major, trace element and multi-isotope distribution. International Journal of Earth Sciences 97, 5, 1057-1073. doi: 10.1007/s00531-007-0211-1

Mottaghy D, Pechnig R, Vogt C (2011) The geothermal project Den Haag: 3D numerical models for temperature prediction and reservoir simulation. Geothermics 40(3):199-210. doi:10.1016/j.geothermics.2011.07.001

Nield DA, Bejan A (eds) (2006) Convection in porous media. Springer, New York, 1-640.

Neuzil CE (1994) How permeable are clays and shales? Water Resources Research, 30/2, p. 145-150

Noack V, Cherubini Y, Scheck-Wenderoth M, Lewerenz B, Höding T, Simon A, Moeck I (2010) Assessment of the present-day thermal field (NE German Basin)-Inferences from 3D modelling. Chemie Der Erde-Geochemistry 70 (3): 47-62. doi:10.1016/j.chemer.2010.05.008

Noack V, Scheck-Wenderoth M, Cacace M (2012) Sensitivity of 3D thermal models to the choice of boundary conditions and thermal properties: a case study for the area of Brandenburg (NE German Basin). Environ Earth Sci. 67 (6): 1695-1711. doi:10.1007/s12665-012-1614-2

Noack V, Scheck-Wenderoth M, Cacace M, Schneider M (2013) Influence of fluid flow on the regional thermal field: results from 3D numerical modelling for the area of Brandenburg (North German Basin). Environ Earth Sci. 70 (8): 3523-3544. doi:10.1007/s12665-013-2438-4

Norden B, Förster A (2006) Thermal conductivity and radiogenic heat production of sedimentary and magmatic rocks in the Northeast German Basin. AAPG Bulletin 90:939-962

Norden B, Förster A, Balling N (2008) Heat flow and lithospheric thermal regime in the Northeast German Basin. Tectonophysics 460:215-229. doi:10.1016/j.tecto.2008.08.022

Norden B, Förster A, Behrends K, Krause K, Stecken L, Meyer R (2012) Geological 3-D model of the larger Altensalzwedel area, Germany, for temperature prognosis and reservoir simulation. Environ Earth Sci 67:511-526. doi: 10.1007/s12665-012-1709-9

Ollinger D, Baujard C, Kohl T, Moeck I (2009) 3D temperature inversion derived from deep borehole data in the Northeastern German Basin. IGET_GS_ paper_10_5Mai09_IM

Ollinger D, Baujard C, Kohl T, Moeck I (2010) Distribution of thermal conductivities in the Gross Schonebeck (Germany) test site based on 3D inversion of deep borehole data. Geothermics 39(1):46-58. doi:10.1016/j.geothermics.2009.11.004

Ondrak R, Wenderoth F, Scheck M, Bayer U (1998) Integrated geothermal modeling on different scales in the Northeast German basin. Geologische Rundschau 87(1):32-42

Person MA, Raffensperger JP, Ge S, Garven G (1996) Basin-Scale Hydrogeologic Modeling. Review of Geophysics 34(1): 61-87

Petersen K, Lerche I (1996) Temperature dependence of thermal anomalies near evolving salt structures: importance for reducing exploration risk. Geological Society

Petitta M, Primavera P, Tuccimei P, Aravena R (2011) Interaction between deep and shallow groundwater systems in areas affected by Quaternary tectonics (Central Italy): a geochemical and isotope approach. Environ Earth Sci 63:11-30. doi: 10.1007/s12665-010-0663-7

Raffensperger J P, Vlassopoulos D (1999) The potential for free and mixed convection in sedimentary basins. Hydrogeology Journal, 7(6):505-520

Scheck M (1997) Dreidimensionale Struckturmodellierung des Nordostdeutschen Beckens unter Einbeziehung von Krustenmodellen (Dissertation Thesis, Freie Universität Berlin). Scientific Technical Report STR97/10:1-126

Scheck M, Bayer U (1999) Evolution of the Northeast German Basin - inferences from a 3D structural model and subsidence analysis. Tectonophysics 313:145-169. doi:10.1016/S0040-1951(99)00194-8

Scheck M, Bayer U, Lewerenz B (2003a) Salt movements in the Northeast German Basin and its relation to major post-Permian tectonic phases - results from 3D structural modelling, backstripping and reflection seismic data. Tectonophysics 361:277-299. doi: 10.1016/S0040-1951(02)00650-9

Scheck M, Bayer U, Lewerenz B (2003b) Salt redistribution during extension and inversion inferred from 3D backstripping. Tectonophysics 373:55-73. doi: 10.1016/S0040-1951(03)00283-X

Scheck-Wenderoth M, Krzywiec P, Zühlke R, Maystrenko Y, Froitzheim N (2008a) Permian to Cretaceous Tectonics. In: McCann T (ed) The Geology of Central Europe. Volume 2: Mesozoic and Cenozoic. Geological Society of London, London, pp 999-1030

Scheck-Wenderoth M, Lamarche J (2005) Crustal memory and basin evolution in the Central European Basin System - new insights from a 3D structural model. Tectonophysics 397:132-165. doi:10.1016/j.tecto.2004.10.007

Scheck-Wenderoth M, Maystrenko Y (2008) How warm are passive continental margins? A 3-D lithosphere-scale study from the Norwegian margin. Geology 36:419-422

Scheck-Wenderoth M, Maystrenko Y, Hübscher C, Hansen M, Mazur S (2008b) Dynamics of salt basins. In: Littke R, Bayer U, Gajewski D, Nelskamp S (eds) Dynamics of Complex Intracontinental Basins. The Central European Basin System. Springer, 307-322

Schellschmidt R, Hägedorn F, Fesche H-W (1999) Das Temperaturfeld in Norddeutschland - neue Messungen, neue Karten, neue Interpretationen. Bericht Archiv-Nr. 119 563, Institut für Geowissenschaftliche Gemeinschaftsaufgaben, Hannover

Schilling O, Sheldon HA, Reid LB, Corbel S (2013) Hydrothermal models of the Perth metropolitan area, Western Australia: implications for geothermal energy. Hydrogeology Journal. doi:10.1007/s10040-012-0945-0

Schössler KS, Schwarzlose J (1959) Geophysikalische Wärmeflussmessungen. Freiberger Forsch-H. C75, Leipzig

Schulz R, Agemar T, Alten A -J, Kühne K, Maul A -A, Pester S, Wirth W (2007): Aufbau eines geothermischen Informationssystems für Deutschland. - Erdöl Erdgas Kohle 123, 2: 76-81

Schwab G (1985) Paläomobilität der Norddeutsch-Polnischen Senke, Akademie der Wissenschaften der DDR, Dissertation B, Berlin, 1-196

Smith L, Chapman D S (1983) On the Thermal Effects of Groundwater Flow. 1. Regional Scale Systems. Journal of Geophysical Research 88 (B1): 593-608

Stackebrandt W (2009) Subglacial channels of Northern Germany - a brief review. Zeitschrift der Deutschen Gesellschaft für Geowissenschaften, 160 (3):203-210

Stackebrandt W, Ludwig AO, Ataficzuk S (2001) Base of Quaternary deposits of the Baltic Sea depression and adjacent areas (map 2). Brandenburgische Geowiss. Beitr., 8(1):13-19

Stackebrandt W, Manhenke V (eds) (2002) Atlas zur Geologie von Brandenburg im Maßstab 1:1 000 000. Landesamt für Geowissenschaften und Rohstoffe, Kleinmachnow

Stackebrandt W, Manhenke V (eds) (2010) Atlas zur Geologie von Brandenburg im Maßstab 1:1 000 000. Landesamt für Geowissenschaften und Rohstoffe, Kleinmachnow

Tesmer M, Otto R, Pekdeger A, Möller P, Bayer U, Magri F, Fuhrmann J, Enchery G, Jahnke C, Voigt H (2005) Migration paths and hydrochemical processes of groundwater salinization in different aquifer systems of the North German Basin., Dynamics of the Central European Basin System: DFG-SPP 1135; 4th Rundgespräch, 30th November - 2nd December, Eringerfeld, Germany, pp 123-126

Turcotte DL, Schubert G (2002) Geodynamics (2nd edition). Cambridge University Press, Cambridge

Van Dam RL, Simmons CT, Hyndman DW, Wood WW (2009) Natural free convection in porous media: First field documentation in groundwater, Geophys. Res. Lett. 36, L11403. doi:10.1029/2008GL036906

Vila M, Fernández M, Jiménez-Munt I (2010): Radiogenic heat production variability of some common lithological groups and its significance to lithospheric thermal modeling. Tectonophysics 490:152-164. doi:10.1016/j.tecto.2010.05.003

Villegas ME, Bachu S, Ramon JC, Underschultz JR. (1994) Flow of formation waters in the Llanos Basin, Colombia. Am. Assoc. Petrol. Geol. Bull. 78:1843-1862

Vosteen HD, Rath V, Schmitd-Mumm A, Clauser C (2004) The thermal regime of the Northeastern-German Basin from 2-D inversion. Tectonophysics 386:81-95. doi:10.1016/j.tecto.2004.05.004

Yousafzai A, Eckstein Y, Dahl PS (2010) Hydrochemical signatures of deep groundwater circulation in a part of the Himalayan foreland basin. Environ Earth Sci 59:1079-1098. doi: 10.1007/s12665-009-0099-0

Yu Z, Lerche I, Lowrie A (1992) Thermal impact of salt: Simulation of thermal anomalies in the gulf of Mexico. Pure and Applied Geophysics 138 (2):181-192

Ziegler PA (1990) Geological Atlas of Western and Central Europe. Shell Internationale Petroleum Maatschappij B. V., New York, 1-239

Appendix 1 Governing Equations

The system of flow equation with variable fluid density (ρ^f) and viscosity (μ^f) is given by (a) the mass conservation of the fluid:

$$\frac{\partial(\varepsilon\rho^f)}{\partial t} + \nabla\cdot(\rho^f \mathbf{q}^f) = \rho^f Q_\rho \qquad (2)$$

where

ε	porosity
ρ^f	mass density of the fluid
$\mathbf{q}^f$	specific discharge (Darcy's velocity)
Q_ρ	the sink/source mass term

and by (b) the generalised Darcy's law:

$$\mathbf{q}^f = -\mathbf{K}\left(\nabla h + \frac{\rho^f - \rho_0^f}{\rho_0^f}\frac{\mathbf{g}}{g}\right) \qquad (3)$$

where

$\mathbf{K}$ is the hydraulic conductivity tensor of the porous media given by $\mathbf{K} = \frac{\rho_0^f g}{\mu^f}\mathbf{k}$, with $\mathbf{k}$ permeability tensor, and $\mathbf{g}$ is the gravity acceleration).

Equation 3 is written in terms of hydraulic head rather than pressure as primary variable to conform to the mathematical formulation used in FEFLOW®. Under assumption of thermal equilibrium between the porous medium and the fluid and if density and porosity gradients are neglected in the energy conservation law, the following heat transfer equation results:

$$(\rho c)_{fs}\frac{\partial T}{\partial t} + \rho^f c^f \nabla\cdot(\mathbf{q}^f T) - \nabla\cdot(\boldsymbol{\lambda}\nabla) = Q_T \qquad (4)$$

with $(\rho c)_{fs}$ being the specific heat capacity of the fluid (f) plus solid (s) phase system as

$$(\rho c)_{fs} = \left[\varepsilon\rho^f c^f + (1-\varepsilon)\rho^s c^s\right] \qquad (5)$$

Q_T is the heat source function, and $\boldsymbol{\lambda}$ being the equivalent thermal conductivity tensor of the fluid and porous medium. It incorporates dispersion effects in the fluid and heat transport for both the solid and fluid phase as:

$$\boldsymbol{\lambda} = \rho^f c^f \left[\alpha_T \sqrt{\left(q_i^f q_i^f\right)} \mathbf{I} + (\alpha_L - \alpha_T) \frac{q_i^f q_i^f}{\sqrt{\left(q_i^f q_i^f\right)}} \right] + \\ + \left[\varepsilon \boldsymbol{\lambda}_{cond}^f + (1-\varepsilon) \boldsymbol{\lambda}_{cond}^s \right] \mathbf{I} \quad (6)$$

where α_L and α_T are respectively the longitudinal and transversal dispersion lengths, $\boldsymbol{\lambda}_{cond}^f$ and $\boldsymbol{\lambda}_{cond}^s$ the thermal conductivity of the fluid and solid phase, and $\mathbf{I}$ is the unit matrix). The set of these balance equations are coupled by proper equations of state establishing the dependence of the fluid density and viscosity on the primary variables. In FEFLOW® the fluid density is expressed as a linear polynomial function of temperature and pressure as:

$$\rho^f = \rho_0^f \left[1 - \bar{\beta}(T - T_0) + \bar{\gamma}(h - h_0) \right] \quad (7)$$

where $\bar{\beta} = \frac{1}{\rho^f} \frac{\partial \rho^f}{\partial T}\Big|_p$ is the thermal expansion coefficient at constant pressure condition, and $\bar{\gamma} = \frac{1}{\rho^f} \frac{\partial \rho^f}{\partial h}\Big| T$ is the coefficient of fluid compressibility at constant temperature condition.

Taking into account both coefficients $\bar{\beta}$ and $\bar{\gamma}$ constant may become inappropriate for geothermal applications where a larger temperature range has to be considered. To improve the relationship (Eq. 7) a 6th order polynomial $\rho = \rho(T)$ was introduced into FEFLOW® defining β as a nonlinear variable thermal expansion $\beta = \beta(T)$ (Diersch 2002) valid for temperatures from 0 to 100 °C.

Considering wider ranges of pressure and temperatures require variable thermal fluid expansion $\bar{\beta}$ and fluid compressibility $\bar{\gamma}$ within the state of equation of density (7). In order to reproduce the fluid density for this wider range both coefficients has been approximated for $\rho_{sat} < \rho \leq 100$ MPa and for temperature $0 \leq T \leq 350$ °C by Magri (2005).

The dependence of the fluid dynamic viscosity on the temperature as implemented in FEFLOW® follows the empirical polynomial expression (Diersch 2002):

$$\mu^f = \frac{1 + 0.7063\varsigma - 0.04832\varsigma^3}{\mu_0} \quad (8)$$

with $\varsigma = \frac{(T - 150)}{100}$, and μ_0 the reference viscosity obtained from Eq. 6 when $T = T_0 = 150$°C.

Appendix 2 List of Publications Related to this Thesis

Chapter 2

Noack V, Cherubini Y, Scheck-Wenderoth M, Lewerenz B, Höding T, Simon A, Moeck I (2010) Assessment of the present-day thermal field (NE German Basin)-Inferences from 3D modelling. Chemie Der Erde-Geochemistry 70 (S3):47-62. doi:10.1016/j.chemer.2010.05.008

Chapter 3

Noack V, Scheck-Wenderoth M, Cacace M (2012) Sensitivity of 3D thermal models to the choice of boundary conditions and thermal properties: a case study for the area of Brandenburg (NE German Basin). Environ Earth Sci. 67 (6), 1695-1711. doi: 10.1007/s12665-012-1614-2

Chapter 4

Noack V, Scheck-Wenderoth M, Cacace M, Schneider M (2013) Influence of fluid flow on the regional thermal field: results from 3D numerical modelling for the area of Brandenburg (North German Basin). Environ Earth Sci. 70 (8), 3523-3544. doi: 10.1007/s12665-013-2438-4